SCUOLA DOTTORALE IN BIOLOGIA MOLECOLARE
CELLULARE E AMBIENTALE

SEZIONE MOLECOLARE E CELLULARE

XXXI CICLO

Modulation of telomere stability and radiation sensitivity in *in vitro* and *in vivo* systems.

Modulazione della stabilità telomerica e della sensibilità alle radiazioni in sistemi *in vivo* ed *in vitro*

PhD Student
Daniela Muoio

Tutor
Prof. Antonio Antoccia

Coordinator
Prof. Paolo Mariottini

INDEX

ABBREVIATIONS

T-loop: *Telomeric loop*
ALT: *Alternative Lengthening of Telomere*
TMM: *Telomere Maintenance Mechanism*
TRF1: *Repeat-Binding Factor 1*
TRF2: *Repeat-Binding Factor 2*
DSBs: *Double-Strand Break*s
BFB: *Breakage-Fusion-Bridge*
CIN: *Chromosome Instability*
DDR: *DNA Damage Response*
53BP1: *53 Binding Protein 1*
γH2AX: *phosphorylation of H2AX*
TIFs: *Telomere-dysfunction induced foci*
ChIP: *Chromatin Immunoprecipitation*
G4: *G-quadruplex*
GSCs: *Glioma Stem Cells*
CRISPR: *Clustered Regularly Interspaced Short Palindromic Repeats*
BLM: *Bloom Syndrome Protein*
WRN: *Werner Syndrome ATP-dependent Helicase*

Riassunto

La radioterapia rappresenta il trattamento standard di una vasta gamma di tumori. Le radiazioni uccidono le cellule mediante la formazione di lesioni irreparabili nel genoma, quali rotture a doppio filamento del DNA. Tuttavia, la radioterapia convenzionale, che coinvolge l'uso di radiazioni ionizzanti (RI), in combinazione o meno con chemioterapia, non è sufficiente ad aumentare la sopravvivenza complessiva di pazienti affetti da tumori radioresistenti, quali ad esempio il Glioblastoma multiforme (GBM) (glioma di IV grado secondo la WHO). Il GBM è il più comune e letale tra i tumori cerebrali primari maligni negli adulti. Il trattamento convenzionale include la resezione chirurgica massimale seguita da trattamento con radiazioni in combinazione con l'uso del chemioterapeutico temozolomide (TMZ), con l'obiettivo di uccidere le rimanenti cellule tumorali. Sfortunatamente, le recidive dopo trattamento solo molto frequenti, e l'esito della malattia rimane nefasto. L'inefficacia della radioterapia rende necessario studiare i possibili meccanismi responsabili della radioresistenza, per permettere il successo dei trattamenti. La radioresistenza delle cellule tumorali può essere attribuita a diversi meccanismi. È stata proposta una correlazione tra radiosensibilità e disfunzionalità telomerica. I telomeri sono strutture nucleoproteiche situate alle estremità dei cromosomi lineari eucariotici, consistono di ripetizioni in tandem della sequenza non codificante TTAGGG. Il loro ruolo primario è proteggere le estremità naturali dei cromosomi, e quindi mantenere la stabilità genomica. I meccanismi coinvolti nel mantenimento e nella funzionalità del telomero rappresentano promettenti target per lo sviluppo di molecole selettive per le terapie antitumorali. Inoltre, data la natura ripetitive delle loro sequenze ricche in guanina, i telomeri tendono a riorganizzarsi in inusuali conformazioni del DNA, quali i G-quadruplex (G4). L'obiettivo di questo lavoro è testare diversi composti in grado di stabilizzare i G4 telomerici, per indurre una perturbazione dell'architettura del telomero. Proteine coinvolte nelle funzioni e nel mantenimento del telomero partecipano inoltre anche alla risposta al danno al DNA. Miriamo difatti ad interferire con i meccanismi di risposta al danno, per sensibilizzare le cellule al danno indotto da radiazioni ionizzanti. Per prima cosa abbiamo valutato l'efficacia biologica di tre differenti derivati del naftalene dimide (NDI) (C1, C2 e C6), nell'inibire la proliferazione nella linea cellulare di GBM, U251MG e in fibroblasti umani primari, AG01522, comparando con l'effetto di RHPS4, un ligando del G4 precedentemente dimostratosi in

grado di bersagliare i telomeri e indurre radiosensibilizzazione. Tutti i ligandi del G4 utilizzati hanno mostrato un forte effetto citotossico sulle cellule tumorali, con valori calcolati per la concentrazione inibente il 50% della crescita nel range del nanomolare, e tutti mostrano una ridotta citotossicità nella linea cellulare normale, facendo di questi composti ottimi candidati per lo studio di ipotetici effetti radiosensibilizzanti in correlazione al telomero. Tuttavia, nell'effettuare un pannello di esperimenti con lo scopo di studiare gli effetti telomerici dei ligandi, quali l'analisi della lunghezza telomerica, l'induzione di foci telomerici disfunzionali e l'analisi dei livelli delle proteine shelterine, abbiamo notato come gli NDI causassero solamente una lieve disfunzionalità telomerica, contrariamente a RHPS4. Infatti, nel trattamento combinato delle cellule tumorali con agenti stabilizzanti i G4 e radiazioni ionizzanti (RI), gli NDI non sono riusciti a migliorare gli effetti delle radiazioni nelle cellule di GBM. I risultati ottenuti dalle curve di sopravvivenza e dal saggio di crescita a lungo termine (in cellule trattate per 5 giorni e irraggiate con una dose di 6 Gy di raggi X), hanno confermato RHPS4 come unico ligando in grado di dare un effetto sinergico nel trattamento combinato. I dati sull'induzione di risposta al danno al DNA dopo irraggiamento, ottenuti tramite l'analisi dei foci di danno indotti da RI, confermano come gli NDI non influenzino la riparazione del DNA, in contrapposizione con RHPS4. Questi risultati ci hanno spinto a studiare altri possibili target dei ligandi dei G4, per scoprire le ragioni di un comportamento così diverso nel sensibilizzare le cellule alle RI. Abbiamo testato i livelli di proteine codificate da geni coinvolti nella riparazione del DNA, nello stress replicativo (SR) e nella regolazione del ciclo cellulare, che presentano putativi G4 nelle loro sequenze. Tra tutti i target testati, abbiamo trovato alcune variazioni molto interessanti. La risposta al danno al DNA mediata da ATR-CHK1 è considerata il principale pathway di risposta allo SR, mediante la regolazione dei checkpoint della fase S. Entrambi i ligandi, NDI e RHPS4, modulano i livelli di ATR e CHK1 fosforilati. Un meccanismo comune proposto coinvolge la possibilità che i ligandi del G4 inducano SR. In linea con questa osservazione troviamo la modulazione di altre proteine coinvolte nella regolazione e progressione del ciclo cellulare, come le cicline A e E per gli NDI, PCNA e CDK2 per RHPS4. Questi risultati suggeriscono come la presenza di G4 stabilizzati nelle sequenze genomiche possa costituire un impedimento fisico alla corretta progressione della forca replicativa, inducendo così una perturbazione del ciclo cellulare. Abbiamo confermato gli effetti deleteri sul ciclo cellulare, mediante lo studio

dell'incorporazione dell'analogo BrdU durante la fase S, nelle cellule dopo 5 giorni di trattamento. I dati ottenuti confermano un forte rallentamento della fase S per tutti i ligandi, ma RHPS4 è l'unico capace di bloccare persistentemente le cellule persino 48 ore dopo la rimozione della sostanza. Abbiamo confermato così gli effetti radiosesibilizzanti di RHPS4 *in vitro* nelle cellule radioresistenti di GBM, mediante il bersaglio e la disfunzionalizzazione del telomero. Abbiamo deciso di spingerci oltre e mostrate come la combinazione della somministrazione di RHPS4 (10mg/kg/die per 5 giorni) e l'esposizione alle RI (10 Gy in singola dose) fosse altrettanto efficace *in vivo*, bloccando la crescita del tumore nei topi, come valutato fino a 65 giorni in modelli xenograft eterotopici. La riduzione del volume del tumore e il controllo del tumore a lungo termine osservati nei topi esposti a trattamento combinato, hanno suggerito il targeting sia della massa tumorale differenziata che del compartimento delle cellule staminali. Diversi studi si sono focalizzati sulla validazione delle Cellule Staminali Cancerose (CSC), che si ritiene essere responsabili della progressione a lungo termine del tumore e delle recidive. Per dissezionare il meccanismo di azione di RHPS4 nelle cellule differenziate versus le staminali tumorali, sono stati effettuati esperimenti *in vitro*, in neurosfere rappresentati le staminali, derivate dalle U251MG, e in 4 linee staminali ben caratterizzate, derivate da paziente. Curiosamente, in entrambi i modelli, il singolo trattamento con RHPS4 è stato in grado di ridurre fortemente la proliferazione cellulare, ma inaspettatamente, il trattamento combinato con le RI non ha determinato nessun incremento dell'effetto. La mancanza di radiosensibilizzazione è supportata dalla resistenza telomerica a RHPS4 delle staminali, osservata nella totale mancanza di aberrazioni cromosomiche derivanti dal telomero. Il meccanismo attraverso il quale RHPS4 colpisce il compartimento staminale rimane da elucidare ma, interessante è notare come il trattamento con RHPS4 determini una forte riduzione dei livelli proteici e dell'espressione genica di RAD51 e CHK1. Ipotizziamo che RHPS4 inibisca la crescita delle cellule staminali mediante il targeting diretto o indiretto di geni coinvolti nella risposta allo SR e nella ricombinazione omologa. Questo determina una risposta deficitaria allo SR, che aumenta la resa dello stallo della forca replicativa in caso di G4 stabilizzati. Uno dei meccanismi proposti per la risoluzione delle forche replicative in stallo è l'inversione della forca, mediato dalla proteina della ricombinazione omologa RAD51. La forca stallata viene processata da una endonucleasi, ed esposta come una rottura a doppio filamento del DNA, che attiva la ricombinazione mediata da RAD51. Tuttavia, nelle

cellule staminali tumorali di glioma, RHPS4 induce una deplezione di RAD51e CHK1, determinando l'impossibilità di avviare il processo di reversione della forca e risoluzione dello stallo replicativo, portando al collasso della forca e induzione di danno al DNA, ancor prima che sia apprezzabile l'effetto genotossico delle radiazioni ionizzanti. Tuttavia i soli effetti sulla proliferazione rimangono molto alti anche nella componente staminale, rendendo RHPS4 un buon candidato per futuri approcci terapeutici. Per chiarire ulteriormente le conseguenze di RHPS4 sullo SR, abbiamo deciso di utilizzare un approccio genomico per silenziare una RecQ elicasi, BLM, coinvolta nello svolgimento dei G4 telomerici alle forche replicative stallate. La stabilizzazione dei G4 potrebbe aumentare lo SR in assenza di componenti necessarie alla loro risoluzione, quali BLM, anche se ulteriore sperimentazione è ad oggi necessaria per chiarirne l'effetto. Complessivamente i nostri dati indicano come i ligandi dei G4 siano potenti agenti antiproliferativi nelle cellule tumorali differenziate, e come alcuni di essi siano anche agenti radiosensibilizzanti, mediante il targeting del telomero, e possano inoltre inibire la proliferazione della componente staminale tumorale, indipendentemente dai telomeri.

Summary

Radiotherapy (RT) is one of the standard treatments of a wide range of cancers. Cells killing by radiation is based on production of unrepairable lesions involving DNA double-strand breaks (DSBs). Nevertheless, conventional RT, which involves ionizing radiation (IR), with or without the combination of chemotherapy, is not sufficient to increase the overall survival of patients suffering from radioresistant tumors such as glioblastoma multiforme (GBM) (WHO grade IV glioma). GBM is one of the most common and lethal primary malignant brain tumors in adults. Standard treatment includes maximal surgical resection followed by concurrent radiation and chemotherapy with temozolomide (TMZ), with the aim to kill the remain tumor cells. Unfortunately, recurrences after treatment are very frequent, and the outcome remain very poor. Failure of radiotherapy make necessary to investigate possible mechanisms responsible for resistance, to enable the success of treatments. Radioresistance in cancer cells could be ascribed to several possible mechanisms. It has been proposed a correlation between radiosensitivity and telomere dysfunction. Telomeres are nucleoprotein complex situated at the end of the linear eukaryotic chromosomes that consists of tandem

repeats of TTAGGG non-coding sequences. Their primary role is to protect the natural ends of chromosomes, and thus to maintain genome stability. Mechanisms involved in telomere maintenance and function are promising targets for the development of selective molecules for cancer therapy. Furthermore, due to the repetitive nature of their guanine-rich sequences, telomeres tend to rearrange in unusual DNA conformations such as G-quadruplex (G4). We aim with this work to test different compounds proposed to target and stabilize telomeric G4s, to induce telomere architecture disruption. Proteins involved in telomere function and maintenance are also involved in DNA damage response (DDR). We indeed aim to interfere with DDR mechanisms, to sensitize cells to the damage induced by IR. We first evaluated the biological effectiveness of three different naphthalene diimide (NDI) derivatives (C1, C2 and C6) as inhibitors of cell proliferation in U251MG glioblastoma (GBM) cells and human primary fibroblast (AG01522), in comparison to RHPS4, a G4-ligand that already proved its ability to target telomeres and to induce radiosensitization. All the G4 ligands used, showed a strong cytotoxic effect on the cancer cell line, with calculated IC_{50} in the range of nanomolar, and exerted a lower cytotoxicity in the normal cell line, making all the compounds good candidates to investigate any hypothetic telomeric-related radiation sensitizer role. However, when we performed a panel of experiments aimed to investigate telomeric effects of the ligands, such as telomere length analysis, induction of telomere dysfunctional foci (TIF) and shelterin proteins analysis, we noticed that NDIs caused only mild telomere dysfunction, contrary to RHPS4. Indeed, in the combined treatment of cancer cells with G4s stabilizing compounds and IR, NDIs failed to enhance the effects of IR in GBM cells. Only RHPS4 showed a synergist effect, as obtained from survival curves and long-term growth assays, after 5 days of treatment and reaching 6 Gy of X-rays irradiation. Data from the induction of DDR after irradiation, by the analysis of the IR-induced foci (IRIF), confirmed that NDIs did not affect DNA repair in contrast to RHPS4. Those results prompt us to study other possible target of G4s ligands to uncover the reasons of such different behavior in sensitize cells to IR. We tested the amounts of proteins encoded by genes involved in DNA repair, replication stress (RS) and cell cycle regulation, harboring putative G4s within their sequences. Among all the targets tested, we found some very interesting variations. The ATR-CHK1 mediated DNA damage response is thought to be the main RS responsive pathway that mediates cellular DNA damage checkpoint responses in S-phase. Both ligands, NDIs and RHPS4,

modulate the levels of pATR and pCHK1. One proposed shared mechanism is the possibility that G4 compounds induced RS. In line with this observation, we found modulation of other proteins involved in cell cycle progression and checkpoint, such as cyclin A and E for NDIs, and PCNA and CDK2 for RHPS4. Those results suggested that the presence of stabilized G4s within genomic sequences could physically impede the correct progression of replication fork, thus inducing cell cycle perturbation. We confirmed the detrimental effects in cell cycle, studying the incorporation of BrdU analog during S-phase, in cells treated for 5 days. Data confirmed a strong delay in S-phase for all the ligands, but RHPS4 was the only one able to block persistently cells even 48 h after ligand washout. We therefore confirmed RHPS4 *in vitro* radiosensitizing effect in GBM radioresistant cells through the targeting and dysfunctionalization of telomeres. We decided to go further and show that the combination of RHPS4 administration (10mg/kg/die for 5 days) and IR (10 Gy X-rays in a single dose) exposure was very effective also *in vivo*, blocking tumor growth in mice as evaluated up to 65 days in a heterotopic xenograft model. The reduction of tumor volume and the long-term tumor control observed in mice exposed to combined treatment suggested the targeting of both the bulk differentiated tumor mass and stem cell compartment. Several studies have been focused on the validation of Cancer Stem Cells (CSCs) which are believed to be responsible of the long-term progression, and recurrence of the tumor. To dissect the RHPS4 mechanism of action in differentiated vs cancer stem cells, *in vitro* experiments were performed in stem-like neurospheres derived from U251MG and in four well-characterized patient-derived GSCs. Interestingly, in both systems, RHPS4 alone was able to strongly reduce cell proliferation but, unexpectedly, combined treatment with IR did not determine any increased effect. The lacking of the radiosensitization was supported by the GSCs telomeric-resistance to RHPS4 observed as the total absence of telomere-involving chromosomal aberrations. The mechanism by which RHPS4 targets the stem compartment remains to be elucidated but, interestingly, RHPS4 treatment determined a strong reduction of RAD51 and CHK1 protein level and gene expression. We propose that RHPS4 inhibits stem cell growth by the direct or indirect targeting of genes involved in RS response and Homologous Recombination (HR). This determines a deficient RS response that increases the yield of replication fork stall in case of stabilized G4. A mechanism proposed for the resolution of stalled replication forks is the replication fork reversal, which is prompted by the

activity of the HR protein RAD51. The most accepted mechanism indicates that an endonuclease cleaves DNA at stalled fork and determines the formation of a one-ended DSB that in turn activates RAD51-mediated recombination. However, in GSCs, the concomitant RHPS4-induced depletion of RAD51 and CHK1 determines the failure in reversal of the stalled replication fork leading, in turn, to collapse and DSB induction, even before the genotoxic effect of IR is appreciable. Nonetheless, the proliferation effects remain very high even in the stem component, making RHPS4 a good candidate for therapeutic approaches. To finally further clarify the RHPS4 RS consequences, we decided to target, with a genomic approach, a RecQ helicase, BLM, involved in the unwinding of G4 at telomeric stalled replication fork. G4 stabilization could enhance the RS in absence of players needed for the unwinding, such as BLM, even if we need further experiments to clarify the effect. Overall, our data indicate that G4-ligands are powerful antiproliferative in tumor-differentiated cells, and some ligands are also radiosensitizer through telomere targeting, and could inhibit GSCs proliferation in a telomere-independent manner.

INTRODUCTION

1. CANCER AND RADIOTHERAPY

The major effort of large part of the biomedical research in the last years is to try to unravel the principles behind one of the greatest evil of our time: cancer. Indeed, tumor malignancy remains one of the main leading causes of death globally (**fig.1**). Despite remarkable progress has been made in understanding cancer development and treatments, the clinical outcome remains very low, making necessary to go further in the discover of new therapeutic strategies.

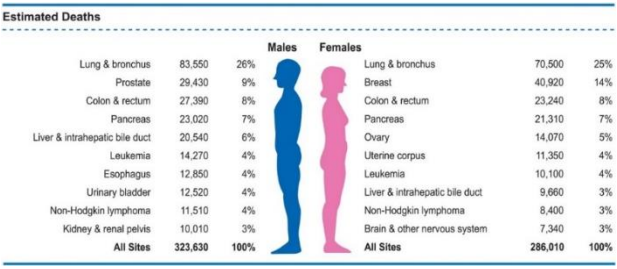

Figure 1: Ten leading cancer types estimated deaths by sex, United States, 2018 (Modified from Siegel, Miller, & Jemal, 2018)

Cancer treatment modalities include surgery for tissue removal, chemotherapy, immunotherapy, hormonal therapy and radiation therapy [2]. Among all the strategies, radiotherapy remains one of the useful tools to improve the course of the illness, with a 50% of people subject to the treatment every day, and with the 40% of possibility of being successful [3]. However, human individuals exhibit important differences in their sensitivity to radiations. This work deals with the possibility to combine radiotherapy with the use of specific molecules targeting the natural ends of chromosomes, the telomeres, to induce a specific response that aims to increase the sensibility to radiation therapy.

1.1 RADIOTHERAPY PRINCIPLES

In 1895, Wilhelm Conrad Röntgen from Germany discovered X-rays and the diagnostic potential of it was immediately appreciated, but it took almost 100 years, to fully understand the value of radiation in cancer therapy [2]. Radiation is a physical agent used with the aim to interfere with malignant cells viability. Usually radiations used in the treatment of

tumors are ionizing radiations (IR) which are energy propagations, through electromagnetic waves or particle flux, able to form ions (electrically charged particles) and deposit the energy from this event in the cells of the tissue it passes through. This deposited energy can kill cancer cells or cause genetic changes resulting in cancer cell death [4]. High-energy radiation damages genetic material (DNA) of cells and thus blocks their ability to divide and proliferate further [5]. Among all forms of DNA damage induced by radiations (SSBs, DBSs, DNA-protein crosslink and complex damage), the most toxic are DSBs, since they are responsible for structural chromosomal aberrations [6]. Although radiations damage both normal and cancer cells, the goal of radiotherapy is to maximize the effect only on cancer cells (**fig. 2**), taking in consideration several physical parameters.

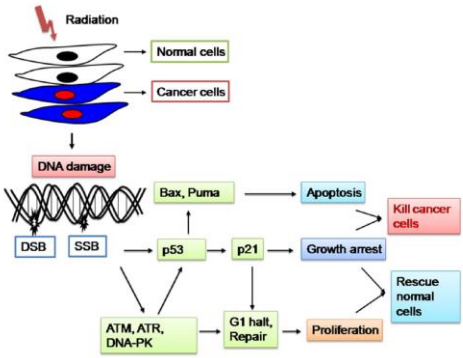

Figure 2: Radiation damages the DNA causing single strand breaks (SSB) or double strand breaks (DSB) in cells, thus blocking their ability to divide and proliferate further. Mechanisms involved in the decrease of radiosensitivity of the fast doubling cancer cells, while increasing radioresistant of the slow doubling normal cell benefits the cancer patients [7]

However, efficacy of radiotherapy rely also on the impaired DNA damage response of cancer cells, and their ability to proliferate more rapidly, with the S phase as a vulnerable time for DNA-damage exposure [5]. The major types of IR are alpha particles, beta particles, X-rays, and gamma rays. X- and gamma rays are more penetrating. The radiation biological effectiveness (RBE) of radiotherapy is driven by the differences in dose and Linear Energy Transfer (LET, the amount of energy that an ionizing particle transfers to the material traversed per unit distance) among all the radiation types. When X- and γ-rays (which are low-LET radiations) are absorbed by cells or tissues, they interact with atoms or molecules,

especially water which makes up 80% of the cell, to produce free radicals (e.g. hydroxyl, superoxide radicals) and other reactive oxygen species (ROS), which finally induce a DNA damage [4] [8]. Once cancer cells are damaged, they have to cope with the event, and if the damage is not repaired properly, it leads to the death of cancer cells. The biological response is actually more complex, and radiotherapy can kill cancer cell in a variety of ways. The DNA of cancer cells repairs more slowly. Growing evidence suggests that various signaling pathways including the DNA repair response pathways, show redundancy in normal cells. Cancer cells have various mutations that cause the loss of this redundancy and therefore, targeting the DNA damage response pathways in the cancer cell can induce cell death [7,9]. In case of DNA DSBs occurrence, there are two major enzymatic types of DNA DSBs repair modes: the homologous recombination (HR) repair, which plays a more prominent role during meiosis and when sister chromatids are available during the late S and G_2 phases [10] and the non-homologous end-joining (NHEJ), which is more important during G_1 phase. It is generally believed that HR plays a more important role than NHEJ in mitotically replicating cells, since HR mainly repairs DSBs in late S and G_2-M. [11]. As already told, many damage response players in cancer cells are impaired, thus DSBs are not correctly rejoined, and the free strands of broken chromosomes, which are sticky, are misrepaired, and joined between different chromosomes. Thus, chromosomal aberrations, as well numerical aberration for the loss of genetic material, could arise in cancer cells. Structural aberrations can be produced in every moment of the cell cycle, whilst numerical disorders are usually produced during the cellular division in mitosis, for incorrect segregation in anaphase [12,13]. Finally, unrepaired DSBs can result in permanent cell cycle arrest, induction of apoptosis, or mitotic cell death caused by loss of genomic material [14].

1.2 RADIOTHERAPY IN GLIOBASTOMA MULTIFORME: NOT ALWAYS A SUCCESFUL STRATEGY

It is important to consider inherent differences in sensitivity to IR to assert the success of cancer radiotherapy. Indeed, it is well established that there is considerable variation in sensitivity to IR among both cancer patients and healthy individuals, and that radiation sensitivity can contribute significantly to the clinical outcomes of radiotherapy. Furthermore, for a lot of cancers, radiotherapy is just a palliative, since after the treatment, residual “resistant” cells remain viable and continue to propagate [15], giving rise to tumor recurrences. Malignant astrocytic gliomas including

the most common subtype, glioblastoma multiforme (GBM) (WHO grade IV glioma), are the most common and lethal intracranial tumors. These tumors exhibit a devastating malignant progression characterized by widespread invasion throughout the brain [16,17]. Despite the variety of modern therapies against GBM, it is still a deadly disease with extremely poor prognosis. Patients usually have a median survival of approximately 14 to 18 months from the diagnosis [18–20]. Only few patients reaching long-term survival status of 2.5 years and less than 5% of patients survive 5 years post diagnosis [19]. Several new therapies have been developed in the last decades to improve overall survival (OS). However, those improvements did not change the deadly destiny of GBM patients. Current treatment for patients with newly diagnosed GBM includes maximal safe resection followed by concurrent radiation therapy and adjuvant chemotherapy (chemo-RT) with temozolomide (TMZ), a monofunctional alkylating agent [21]. Radiation therapy, following surgical resection, has the aim to kill the remain tumor cells. The treatment constitutes of fractionated involved-field radiation therapy (IFRT) (2 Gy per day, 5 days a week, for a total dose of 60 Gy), which recently replaced the standard whole brain radiation therapy to offer maximal treatment of the tumor while minimizing radiation to normal brain tissue [21]. Median OS is estimated to be 14.6 months with RT alone [22]. Still, at least 50% of GBM patients are resistant to TMZ treatment due to either an overexpression of methylguanin-DNA-methyltransferase (MGMT), which is an enzyme responsible for initiating DNA repair against alkylating chemotherapeutic agents such as TMZ, or a methylation of the promoter site stifling protein expression [23]. Over the last years, innovative studies on hadrontherapy with carbon ions gave interesting results in GBM treatment management [24–26]. The advantage of this approach is a higher RBE, because it is more likely that ions interact with the target molecule, the DNA, and lead to a more complex DNA damage. Therefore, ions cause “direct” effect of irradiated cells, and are less influenced by the presence of oxygen [27], since low oxygen availability decreases the efficacy of radiation and adversely affects the prognosis of patients with cancer, making tumor hypoxia a marker of radiation sensitivity [9]. Nonetheless, the high cost of hadrontherapy, made this approach unlikely in current treatments. Analysis of the causes of failure of radiotherapy to improve the quality of survival, have uncover some of the possible mechanism of radioresistance of GBM cells.

1.3 RADIORESISTANCE: THE GLIOMA Cancer Stem Cells (CSCs) MODEL

Recent discoveries in cancer biology have suggested new mechanisms of resistance and recurrence after radiation therapy. Tumor heterogeneity has long been recognized as a cause of failure of radiotherapy, with a sub-population of cancer cells that exhibit stem-cell properties and are responsible for treatments resistance and recurrence [28]. Evidences of Cancer Stem Cells were first shown in human acute myeloid leukemia (AML). $CD34^{+}/CD38^{-}$ cancer initiating cells isolated from AML formed tumors *in vivo* when transplanted into nude mice [29]. In 2002 we had the first evidence of "stem-like" cells within glioma: glioma stem cells were in fact capable of forming clones under culture conditions used for normal stem cells, and also were capable to differentiate in astrocytic and neural lineages [30]. Two different models have been proposed to elucidate the acquisition of intra-tumor heterogeneity in established malignancies. The stochastic model postulates that all somatic cells have the potential to initiate neoplasms and maintain tumor growth/survival via the random acquisition of gene mutations [31,32]. In this model, tumor heterogeneity would result from genetic changes occurring during the process of clonal tumor expansion [33,34]. Opposite to that there is the hierarchical model: this theory proposes the existence within the tumor of a cell hierarchy with varying extent of proliferation, differentiation capability and in vivo tumorigenicity, with a subset of tumorigenic Cancer Stem Cells (CSCs) at the apex. The small subset of clonal cells, precisely CSCs that in case of gliomas are very similar to normal Neural Stem Cells (NSCs), are responsible for the expansion and cellular differentiation of tumors [35–37]. CSCs share with stem cells certain properties, including the ability to self-renew either symmetrically, generating two daughters CSCs, or asymmetrically, generating one CSC and one cell with a certain degree of differentiation, propagating the pool of differentiated cells within the tumor, without losing the population of cells with tumorigenic potential [35,38].The origin of Glioma Stem Cells remains elusive, as they can arise either from NSCs or differentiated glia cells via genetic alterations which enables transformation [39] (**fig. 3**).

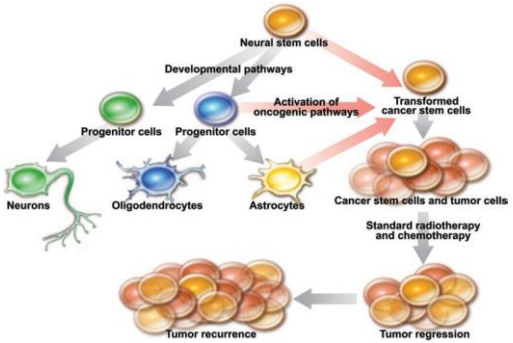

Figure 3: Cancer stem cells may be transformed from neural stem cells or progenitor cells or from glial cells. Radiation and chemotherapy may eradiate most of tumor cells but be ineffective on the population of radioresistant and chemoresistant cancer stem cells, respectively [40]

After the initial discover of Glioma Stem Cells (GSCs) in 2002, another milestone was the discovery of the expression of the transmembrane glycoprotein CD133 (Prominin-1) on the surface of those initiating cells. Indeed, $CD133^+$ cells are able to form serially transplantable xenograft to recapitulate the pathology of patient tumor [36]. Previous reports suggested that tumorigenic cells in glioblastoma are confined into the $CD133^+$ population [41]. However, these findings have been revisited in light of recent studies showing that $CD133^-$ cells isolated from human and mouse gliomas are also tumorigenic [42,43]. Xenograft studies with cells that differs in CD133 expression have confirmed how the two types have different tumorigenic potential and sensibility to therapies [44,45], making CD133 expression a significant prognostic factors for glioma patients [46]. Since their discovery, GSCs are now identified by the presence of stem cell markers, such as the already mentioned CD133. Among all the markers uncover, we can find SOX2 [47], SALL2, POU3F2, OLIG2 [48], MYC [49], BMP4, BMI1, NESTIN [50], STAT3 [51], CD44 [44], OCT4, Musashi1 [52] and Nanog [53,54]. The GSCs population is radioresistant, and could be the cause of recurrence after radiation therapy. This could be ascribed to the ability of the staminal component of the tumor to survive DNA damage thanks to an enhanced DNA damage response (DDR) (contrary to "normal" cancer cells): multiple DNA repair pathways show cumulative effect on GSCs radiosensitivity with enhanced cell cycle checkpoint activation [55,56]. The DDR include ATM and ATR pathways, which maintain genomic integrity by activating cell-cycle checkpoints and DNA repair mechanisms. The MRN (MRE11–RAD50–NBS1) complex has key roles

in sensing and processing DSBs as well as activating ATM and ATR. In response to DSBs induced by radiation, the activation of ATM, Chk2, and Rad17 are indeed higher in GSCs than the matched non-stem tumor cells [45]. Analysis of glioblastoma clinical samples has revealed high levels of p-ATM, p-CHK1, p-CHK2, which are also players involved in the DSBs damage response induced by radiations, and PARP1, which facilitates repair of radiation-induced single-strand breaks, compared with normal brain tissue [57,58]. CD133-expressing glioma ($CD133^+$) cells survive ionizing radiation in increased proportions relative to most tumour cells, which lack CD133 ($CD133^-$). Thus, enrichment of CD133 cells is crucial in glioma recurrence after radiotherapy. The better survival of $CD133^+$ cells is associated to preferential activation of the G_2/M DNA-damage checkpoint response and increased DNA repair capacity compared with normal cells [45]. However, recent data show a lack of association between CD133 expression and the radioresistant phenotype of GSCs [59]. In GSCs it's established that the DNA repair mechanism preferentially activated is Homologous Recombination (HR), and one player involved in HR that seems crucial in the radioresistance is RAD51 [60]. Indeed, the targeting of RAD51 may be a relevant way of sensitize GSCs to radiation: the use of small RAD51 inhibitors or siRNA silencing the expression of the protein cause a significant decrease of cell survival after IR, because of the reduced DNA repair capability which leads to cell death [61–63]. Currently, the targeting of GSCs are object of extensive research, with the aim to improve the response to radiation therapy and to prevent the possibility of recurrence.

1.4 IMPROVING RADIOTHERAPY

Despite the improvement of the therapeutic approach of GBM, the ability to deliver an efficient radiotherapy has still limitations. A better knowledge of the hallmarks of cancer and of the pathways involved in radiation response, provide the opportunity to design molecular therapies to increase the effectiveness of radiotherapy. The combination of different therapies to enhance the effects of radiation on cancer cells has given interesting results over the last decades. We already mentioned how the first-line adjuvant therapy for glioblastomas consists of treatment with the alkylating agent TMZ and concurrent radiotherapy [64]. Another target is the tumor vasculature, essential for tumor growth. GBM is in fact characterized by sustained angiogenesis [65]. Vascular normalization via anti-VEGF (vascular endothelial growth factor) has been proposed as a mechanism to radiosensitize cancer cells [66]. Bevacizumab (Avastin, BEV)

is a humanized monoclonal antibody that binds to and inhibits the activity of VEGF. In preclinical models, BEV has been shown to exhibit activity against GBM both alone and in combination with RT and TMZ. [67–69]. Molecular profiling of glioma has revealed signaling pathways driving the malignant behavior of tumors. Specific targeting of these pathways, in combination with radiotherapy, has shown synergy in preclinical models. To date, several genetic alterations in those pathways are reported in GBMs, including epidermal growth factor receptor (EGFR) amplification, CDKN2A loss, phosphatase and tensin homolog (PTEN) loss, and so forth. Among these various alterations, several alterations deregulate players involving the RTK/PI3K/Akt/mTOR pathway [70], which is one of the most amenable pathway to pharmacologic intervention [18]. To date, some small-molecule inhibitors of EGFR introduced in clinical trial include gefitinib, erlotinib, and nimotuzumab. However, the results, in combination with RT and TMZ, were disappointing [71,72]. In addition, we discussed above the importance of GSCs in failure of RT: tumors surviving radiations are enriched in glioma initiating cells, which are very radioresistant, and are able to recapitulate the tumor itself. Selectively targeting of GSCs population rather than the bulk of the tumor could be the strategy to radiosensitize gliomas. One intriguing factor involved in cancer progression is the role of the last part of linear chromosomes: telomeres. Maintenance of the telomeres in the tumor cells is an essential step towards cancer cell immortality, since enable repeated cell division [73].

2. TELOMERE

It is known for a long time that chromosomes termini need a special protection to avoid the accidental “erosion”, enzymatic or not, of genetic information. During the same years, in the 1930s, Barbara McClintock and Herman Muller assumed independently the existence of specialized structures at chromosomes ends, named “telomeres” (from Greek, telo = end and mere = part), with the function of distinguish and protect chromosome termini from DNA double-strand breaks (DSBs) repair systems [74]. Since then, extensive research has been made to unravel the composition, structure and function of telomeres.

2.1 TELOMERE STRUCTURE

The key aspect of any living organism is to maintain genome integrity of every cell, thus avoiding any mutation or process, which could lead to genome instability and eventually tumor transformation. One player in

protecting cell integrity are indeed telomeres, nucleoprotein structures situated at the end of linear eukaryotic chromosomes [75,76]. Linear chromosomes have to face two important problems: to enable the replication machinery to replicate the last part of the chromosome, and to protect the natural ends from being recognized as DNA double-strand breaks (DSBs) [77]. Telomeres have specific structural features to achieve both of these tasks. Telomeric DNA consists of tandem repeats of the G-rich TTAGGG non-coding hexanucleotide that in humans varies in length in a range between 5 to 15 kb [78,79], while in other organisms telomeric repeats length can differ: for instance in the mouse *mus musculus* is several times higher [80]. Telomeres end with a 3' single-stranded G-rich overhang (G-tail), which is able to form a higher-order chromatin structure that physically protect the 3'-end of chromosomes, called T-loop [81]. The G-tail folds back and invades the double stranded region of the telomere, forming a D-loop (displacement loop), which stabilize the whole T-loop [82,83]. To assure the correct formation of this protective loop a minimal number of intact repetitions is required, thus the T-loop formation is affected by the length of the telomere [81] (**fig. 4**)

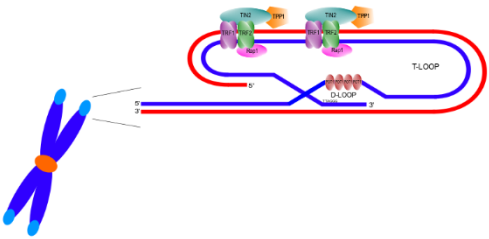

Figure 4: Schematic representation of a putative telomeric capping structure, the T-loop. The single-stranded G-rich overhang at the 3' end is able to invade and anneal with part of the duplex telomeric DNA, thereby forming a D-loop, remodeling the DNA into a final form of a circle, the T-loop. Three factors are required for the correct formation of the cap: minimal length of the TTAGGG repeats, integrity of the 3'-overhang and specific telomere-binding proteins.

Telomeres, with the T-loop formation, prevent the ends of linear chromosomes from being recognized, since the end is "tucked in" and hidden from the DNA repair processes and checkpoint activation [79,81].

2.1.1 TELOMERIC G-QUADRUPLEX

A very notable property of telomeres is their ability to form *in vitro* DNA secondary structure called G-quadruplex (G4). Formation of G4 is possible since telomeric sequences are rich in guanine at the 3'-tail [84] (**fig.**

5). The evidence of high-order structures in guanine-rich nucleic acids was determinate by fibre diffraction [85] and biophysical studies based on the fact that tetrads of guanines interacts via Hoogsteen hydrogen bonds (in which each guanine base makes two hydrogen bonds with its neighbor using different hydrogen-bonding positions to the canonical Watson–Crick base pairing) [86–88], forming the basic structural motif of G4, the G-quartet [89]. Those tetrads are then able to stack on one another, forming the final four-stranded helical G4 structures, which are stabilized by the presence of monovalent cations such as Na^+ and K^+ [90]. G4 are very polymorphic and can be present in different topologies, based on the orientation of the strand (parallel or antiparallel) or if they are intra- or inter-molecularly folded. They can also display difference in the number of stacked G-quartets, in the glycosidic conformations of the guanines, and different types of loops connecting the G-strands (lateral, diagonal and propeller) [91,92]. Direct evidence of the presence of G4 at telomeres came more than 10 years ago form studies that target telomeres in *Stylonychia* with a specific antibody against G4 [93,94]. G4 at telomeres could have a regulatory function, since they might act as a telomeric capping structure, protecting from telomere elongation by telomerase [95]. However, recently G4 are being involved in other important process like DNA replication and gene expression [96]. As a matter of fact, telomeres are not the only region of the genome able to form those secondary structures. Different bioinformatics studies suggested that there are ~370 000 regions in the human genome that can potentially form G4 [97,98], giving more biological importance to those type of structure in different pathways, not just in telomere homeostasis.

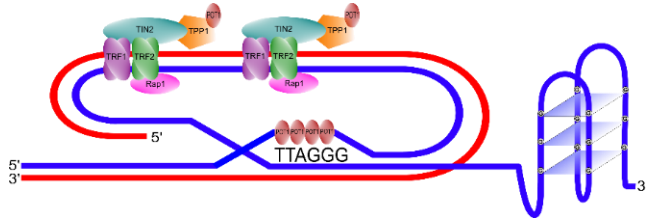

Figure 5: Telomeric DNA has the ability to fold over itself, forming what is called the T-loop. Furthermore, telomeric sequences are rich in guanine and are able to form intramolecular secondary structures called G-quadruplex (G4).

2.2 TELOMERIC PROTEINS

Telomere length homeostasis is essential for its function, and for the formation of the cap, through the T-loop. The regulation of telomere

length and the T-loop formation relies on several telomeric interacting proteins [76,79], that are divided in two classes: those that are telomere-specific and proteins that are primarily involved in the DNA repair pathways. The central component of telomere maintenance is a six-subunits complex called telosome or Shelterin [79,99]. The first mammalian telomeric shelterin protein to be discovered was TRF1, isolated by its in vitro specificity for the double stranded TTAGGG repeats [100,101]. TRF1, together with its paralog TRF2, binds the duplex part of the telomeric DNA due to the presence of multiple TTAGGG repeats recognition domain: the SANT/Myb-type domain has indeed high binding specificity for the half site 5'-YTAGGGTTR-3' in telomeric double-stranded DNA (dsDNA) [79]. TRF1 and TRF2 are both extremely abundant and ubiquitously expressed, with no variation during the cell cycle [99]. TRF1 acts as a negative regulator for telomere length, blocking the access to chromosomes termini to telomerase, an RNA-polymerase that synthetize telomeric DNA sequences [102]. TRF1 can also stimulate the folding of telomeres in vivo, bringing to the final formation of the T-loop [79], and because of this is crucial for the T-loop presence and for the negative regulation of telomere length. Its overexpression leads to an acceleration of telomere shortening [103]. TRF2 has the important role to dismiss the DNA damage signaling at the natural end of chromosomes, and this is achieved with the inhibition of the ATM signaling and NHEJ, not only thanks to the close structure of the telomeres, but also with a direct inhibitions of the kinase itself by TRF2 [104]. POT1 is the third shelterin component with a strong telomeric sequence specificity, thanks to the OB-fold domain which binds the 5'-TAGGGTTAG-3' sequence of single-stranded G-overhangs [105]. POT1 is able to protect telomere ends from ATR-dependent DNA damage response, control 5'-end resection at telomere termini, and regulate telomerase-dependent telomere elongation [76]. Rap1 is the binding partner of TRF2, and depends on this shelterin for its telomere localization [99]. Rap1 seems to be necessary to repress homologous recombination (HR) at telomeres [106]. Other components of the telosome are TPP1, that interacts with POT1 and with the last member, TIN2, which is the central component of the complex. In fact is able to bind also TRF1 and TRF2, and its disruption leads to a decrease telomere localization of all shelterin components [76]. All the six proteins of the shelterin have specific roles to allow cells to protect the natural ends of the chromosome to not be recognized as DNA damage (**fig. 6**).

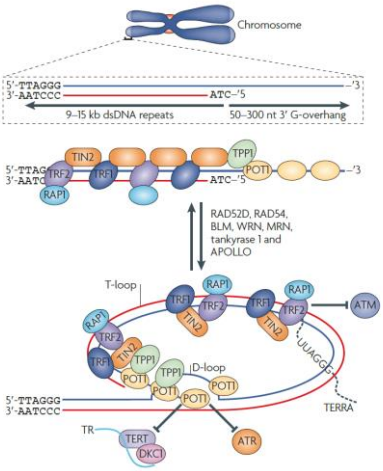

Figure 6: Human telomeres are protected by the Shelterin complex, consisting of TRF1, TRF2, RAP1, TIN2, TPP1 and POT1, covering the double- and single-stranded repeats. Many other factors are able to interact with Shelterin component, transiently and usually in a cell cycle-dependent manner, with the aim to help to the formation of the T-loop and the protection of the natural ends. Telomeric repeats also bind RNA called TERRA, which could be involved in protection mechanisms [107].

2.3 TELOMERE FUNCTION: SENESCENCE, APOPTOSIS AND GENOMIC INSTABILITY

The linearity of eukaryotic chromosome creates one other major problem in cells other than not to be recognized as DNA double strand breaks. The DNA replication machinery is not able to copy the extreme ends of chromosome, often referred as the "end-replication problem" [108,109]. In fact, at every replication cycle, DNA polymerase replicates the genome in 5' to 3' direction by extending polynucleotides chains. The mechanism of DNA replication differs for the leading and the lagging DNA strands. The leading strand is replicated continuously, contrary to the lagging strand. Because there is no template for the "last" Okazaki fragment beyond the 5' end of the chromosome, one strand cannot be synthesized to its very end. The "end replication problem" predicts the progressive reduction of chromosomal DNA at the 3' ends during multiple cell cycles [109]. This results, in almost all normal cells, in a progressive telomere shortening with ongoing cell divisions, which initially do not affect cell function, until a subset of telomeres reach a critically shortened length that induce a DNA damage signaling which, at the end, induce to replicative senescence [110]. It is estimated that telomere loss consists of

100-200 bp per division in most human cells [111]. Cells indeed can only undergoes to a certain number of cell division, and telomers mark the lifespan of the cells [112]. The consequence of telomeres progressive shortening, due to the end-replication problem, which causes the reproductive limit of normal cells, is the entrance, once telomeres reach a critical length, in a phase of permanent growth arrest called replicative senescence or mortality stage I [113,114]. Senescence cells are stuck in the G_0, acquired an enlarged morphology and express senescence-associated genes [115], which are indicators of an activated DNA damage response. This mechanism could prevent any consequences due to an unstable chromosomal asset, potentially leading to tumorigenesis [116]. However, telomere presence in senescent cells, even if shorter, is needed for cell viability: in fact, in case of excessive telomere impairment, cells activate the proper pathways to lead eventually to apoptosis [117], such as the ATM-p53 and pRb pathways [118]. During senescence, if any of those cell cycle regulators are mutated or do not work properly, cells could escape the replicative senescence and continue to divide even in the presence of critically short telomeres. Deregulated cell proliferation leads to a further telomere shortening, until the cell undergoes a crisis state due to telomere dysfunction, known also as mortality stage II [119,120]. This phase is characterized by genomic instability and massive cell death [121]. Even if cells have all the aforementioned mechanisms to escape to genome instability due to the presence of short telomeres, in rare cases this is not enough (**fig. 7**).

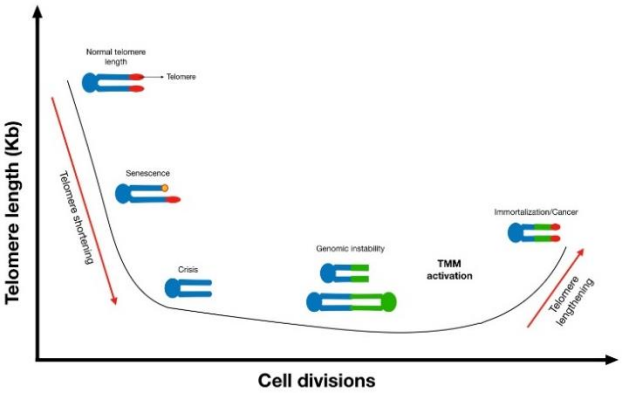

Figure 7: Telomere shortening in normal cells and during tumor transformation.

The danger caused by excessive telomere loss is linked to the impossibility for very short sequences to arrange in a T-loop. In such condition telomere are no longer able to form the cap and the natural end of chromosomes became sticky and are recognized as DNA DSBs [104,122]. This led to the fusion of telomeres of different chromosomes, with the genesis of abnormal chromosomes with more than one functional centromere (dicentric). Those could form anaphase bridges during mitosis that are often broken once sister chromatid segregates, with the occurrence of the so-called "break-fusion-break" cycle (**fig. 8**), which results in reproductive death [123,124]. The aberrations linked with telomeric shortening are reported to increase the level of genomic instability since, even if the cases are rare, the breakages could result in a high rate accumulation of karyotypic aberrations during several cell cycles, condition known as chromosome instability (CIN), which is typical of many cancers [120,125]. Cancer cells can escape the crisis phase, acquired CIN and this could drive oncogenesis, and ultimately genomic instability due to short telomeres could lead to the random activation of mechanisms of maintenance of telomere length [78,126].

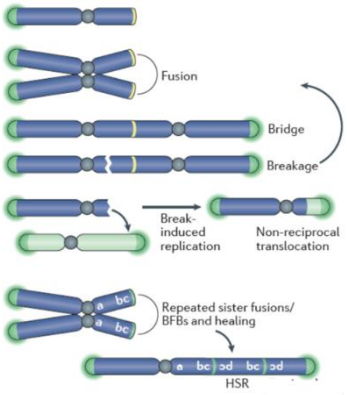

Figure 8: Breakage-fusion-bridge (BFB) cycles can lead to telomere fusion and generation of dicentric chromosome. During mitosis (in anaphase) the mitotic spindle pulls the dicentric chromosomes towards opposite poles, generating anaphase bridges. This can potentially happen repeatedly during cell division. Broken chromosomes can be repaired by break-induce replication, yielding a non-reciprocal translocation. If BFB cycles occur between sister chromatids can results in regional amplification and the genesis of a homogeneously staining region (HSR), if chromosomes are stained (Modified from Maciejowski & de Lange, 2017)

2.4 TELOMERE MAINTENANCE MECHANISMS: TELOMERASE AND ALT (Alternative Lengthening of Telomeres)

All eukaryotes have a specific enzyme involved in the task of solving the end-replication problem and counteract telomeric erosion: the telomerase. Biochemical evidence for telomerase came from a series of experiments carried out by Blackburn and Greider, when they investigated how telomeres are replicated and what caused the sequence addition seen in *Tetrahymena*, yeast and trypanosomes [127]. Telomerase adds TTAGGG repeats onto pre-existent telomeres [128], and consists of two essentials components: a reverse transcriptase catalytic subunit knows as Tert (Telomerase Reverse Transcriptase) and an RNA subunit or Terc (Telomerase RNA component), which constitutes the template (CAAUCCCAAUC) for telomeric DNA synthesis [129,130] (**fig. 9**). The ribonucleoprotein dyskerin (encoded by the *DKC1* gene on the X chromosome) is required for proper folding and stability of telomerase RNA [131].

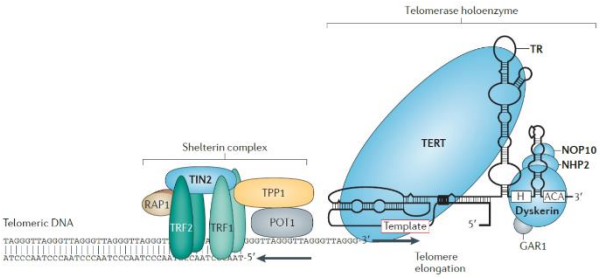

Figure 9: The telomerase enzyme complex comprises TERT (the reverse transcriptase) and TR (the essential RNA component that contains a template for telomere repeat addition). TR contains a 3′ H/ACA box motif that binds the dyskerin protein, which is part of a larger dyskerin complex that also consists of NHP2, NOP10 and GAR1 (Modified from Armanios & Blackburn, 2012).

Telomerase is normally downregulated during human development through the silencing of *TERT* gene, in the vast majority of cells, and is expressed in a small number of normal cell types, such as the germline cells and some proliferating somatic adult progenitor cells [133]. Moreover, in normal somatic cells, also the expression of *TERC* is maintained in low levels. This repression of telomerase in somatic cells and the resulting telomere programmed shortening represent a tumor suppressor pathway that limits tumor cells outgrow. Thereby, telomere erosion at each cell division lead to three different fates, as we already discuss above:

proliferative senescence, apoptosis or continued proliferation accompanied by genomic instability [134]. In the last scenario (called crisis), the increasing instability due to telomere dysfunction is counteract by the activation of cell cycle arrest pathways, to stop those potential cancer cells to initiate tumorigenesis [120,135]. Although most cells succumb to telomere crisis, it can happen that rare "survivors" reactivate telomerase, which prevents telomere exhaustion and allows viability of cells that show genomic instability, leading eventually to cell immortalization and cancer [135]. Telomerase reactivation is in fact one of the requirements proposed for malignant transformation, and is often achieved through mutation in the *TERT* promoter [136,137], although it is not the only mechanism by which telomerase activity is restored. However, in many cancers, how telomerase is upregulated is yet to be known. More than 85-90% of human cancers escape telomere crisis due to telomerase activity [138], but a significant minority of cancers, 10-15%, use an alternative telomere maintenance system that lead to exit crisis in a telomerase-independent way, referred to as alternative lengthening of telomeres (ALT) [139], and it tends to be most prevalent in tumors of mesenchymal origin [140]. Even if we still lack precise information about the molecular mechanisms of ALT, experimental evidences indicated that ALT relies on homologous recombination-mediated DNA copying to counteract telomere shortening [141–143]. Mounting evidences indicate the potential coexistence of telomerase activity and ALT in cancer cells, making both mechanisms interesting targets for cancer therapies.

2.5 TELOMERE AND IONIZING RADIATIONS

A major factor in the failure of radiotherapy is inherent or induced cellular radioresistance. This is a characteristic of many different tumor types which is also retained in cultured cells. Radioresistance could arise in cancer cells by several possible mechanisms. Among the possibilities, differences in the amount of initial DNA damage related to chromatin conformation and capacity to repair DNA DSBs generally are considered the principal causes. Furthermore, a correlation between radiosensitivity/resistance and telomere dysfunctions /telomere length has been postulated [4,144–146]. This relationship between telomere function and the sensitivity to IR was assessed in rare human recessive genetic syndromes characterized by chromosomal instability, clinical radiosensitivity and telomere maintenance defects. Indeed, patients affected by Ataxia-telangiectasia (AT), Nijmegen Breakage Syndrome (NBS), Ataxia-telangiectasia-like disorder (ATLD) and Fanconi Anemia

(FA) group D, in spite of the different clinical signs, all show peripheral blood lymphocytes carrying critically short telomeres [147–150]. Studies on 11 primary fibroblast cell lines with different genetic defects correlate the radiation response to the rate of telomere shortening [151]. Furthermore, telomere loss lead to an enhanced genomic instability, with increased end-to-end chromosome fusions and bridges, due to the loss of the capping function of telomeres [152]. Several genes involved in telomere maintenance are also linked to the DDR [153], and therefore proteins involved in the damage response are physically associated with telomeres. In particular, proteins such as those of the MRN complex (MRE11, NBN, and RAD50), DNA-PKcs, Ku70/80, ATM and ATR are sequestered on telomeric chromatin by TRF2, some of them apparently in a cell cycle dependent manner [154,155], while others seem to associate directly with telomeric chromatin. Telomeric modifications following ionizing radiations could actually alter the kinetics of DNA damage repair, which is directly involved in the repair of radiation-induced DSBs, thus this leads to additional chromosomal aberrations originating from telomeres-DSB rearrangements [156]. However, the molecular basis of the correlation between telomere shortening and radiosensitivity remains unclear. Only when was possible to study the deficiency of telomerase in TERC$^{-/-}$ mouse, it started to be clear that is the length of telomere, rather than telomerase itself, the determinant of an enhanced radiosensitivity [157,158]. Corroborating this relationship is the evidence of a 7-8 fold reduction in telomere length observed in radiosensitive murine lymphoma cells L5178YS compared with the radioresistant parental cells L5178Y, possessing 7 kb and 48 kb, respectively [159]. On the contrary, analysis of Large Cell Lymphomas (LCLs) established from 33 radiosensitive cancer patients, showed how a subset of them had abnormally long telomeres, even longer than telomeres observed in 18 LCLs from individual with normal tissue response after radiotherapy [160]. Other than studies in normal human cells, human tumor cell lines show a reduced clonogenic potential in correlation with elongated telomers [161]. A study on different human carcinoma cell lines reported a significant negative correlation between telomere length and radiosensitivity [162]. It is clear from these conflicting results that further investigations are needed to clarify the link between telomeres and IR. However, since the importance of the link between telomere function and radiosensitivity, it is appealing to use chemical approaches to interfere with telomere biology to sensitize cancer cells to IR.

2.6 TELOMERE AND TELOMERE MAINTENANCE MECHANISMS (TMM) IN CANCER THERAPIES

Increasing evidence on the importance of telomeres and telomerase in cancer cells (as we reported previously), support the fact that in the last years there was a growing effort in discover new ways to target telomeres as anti-cancer therapies. The theory of carcinogenesis suggested that the unlimited proliferative potential is needed for the development of malignant tumors, since cancer cells have to be immortal. Therefore, the reactivation of TMMs is an essential step in cell transformation, and the possibility to interfere with telomerase expression or function became at first a useful strategy in many cancer therapies, as telomerase is reactivated in the 90% of tumors [163]. However, a small percentage of cancers do not rely exclusively on telomerase, and many of the telomerase target-strategy developed to these days have shown no improvements in overall survival in recent clinical trials [164]. Hence, other strategies to target telomeres are needed.

2.6.1 TELOMERASE AND TELOSOME TARGETING

Therapeutics inhibiting telomerase work by a variety of mechanisms. Several compounds, as nucleoside analogs and non-nucleoside compounds, have been created with the aim to interfere with telomerase catalytic activity [165]. Nucleoside analogs are chain-terminators during nucleotide polymerization of reverse transcriptase and were among the first drugs to be tested for their ability to inhibit telomerase [166,167]. For example, treatments with 3'-azido-2',3'-dideoxythymidine (AZT), even though is not specific for telomerase, prove to efficiently inhibit enzyme activity and to induce telomere shortening [168], and several others compounds have been proven to also have antiproliferative and antitumor effects. Among the non-nucleoside compounds the small-molecule BIBR1532 is one of the most potent selective non-competitive pharmacological inhibitors targeting the telomerase core components [169,170]. Another strategy in targeting the telomerase is to interfere with the expression of the enzyme's core subunits (i.e. hTR and hTERT or hTERC) using antisense-based approaches. Antisense oligonucleotides (AS-ODNs) are chemically modified short single-stranded DNA (ssDNA), able to block mRNA translation thanks to their sequence complementary to the sense RNA. Among AS-ODN, the most promising molecule is the GRN163L oligo (entered in clinical trial as Imetelstat®). GRN163L is a lipid- based conjugate of the first-generation oligonucleotide GRN163 [171]. GRN163L inhibits the biochemical activity

of telomerase through the binding to the telomeric template of hTERC, blocking telomere access to telomerase and thereby acting like a conventional pharmaceutical drug. Imetelstat proves to also efficiently target glioma tumor-initiating cells [172]. Catalytic RNAs such as ribozymes as well as small interfering RNAs (siRNAs), which are the terminal effectors of the RNA interference pathway, have been also used as antisense-based strategies [163]. Various siRNAs have different efficiency in suppressing telomerase expression, and this method has been largely employed to inhibit telomerase activity either by targeting *TERT* or *TERC*. To date, however, among all the strategies and the compounds, only GRN163L have enter successfully the clinical trials on diverse types of tumors including myeloma, tumors of the breast, lung, brain and central nervous system [163,165]. Telosome consists as a physical cap that protect natural ends of chromosomes to be recognized as DNA DSBs, thus prevent the activation of the DNA damage checkpoints. Deprotected chromosomes indeed show the typical markers of an activated DNA damage response, localized at uncapped telomeres, such as 53BP1, γH2AX, Mre11, and the phosphorylated form of ATM, forming cytological structures referred to as telomere dysfunction-induced foci (TIF) [173]. The most important player in the capping role of telomeres are shelterin proteins, such as TRF2, and depletion of this protein leads to telomere dysfunction with chromosome instability, induction of DNA damage, and eventually to cell death caused by the severe phenotype [79]. In many tumors, overexpression of TRF2 induce carcinogenesis. Inhibition of TRF2 indeed, in cancer models, proves that in fact telomere dysfunction has a role in sustain cancer progression and also that TRF2 inhibition could have an inhibitory effect in cancer cell growth [174,175]. TRF2 is not the only shelterin protein which is target as a possible way to induce telomeric dysfunction in cancer cells: TRF1 and POT1 are also important component of the telosome, and depletion of one of this two could also lead to a strong reduction of proliferation in cancer cells. This approach allows to reduce telomere length and impede in an indirect way also the action of telomerase [176,177].

2.6.2 G-QUADRUPLEX TARGETING

G4 seem to act as negative regulators of telomere extension *in vivo*, and therefore they are object of interest for the design of new anti-cancer agents, since telomerase is upregulated in 85% of human cancers [178]. Indeed, there is increasingly evidence that long-term application of G4 stabilizing ligands to telomerase-positive cell lines leads to telomere

shortening, senescence and apoptosis consistent with impairment of telomerase function [179]. Other than that, the cellular response to G4 targeting suggests that there is also a direct and more rapid involvement of telomere itself [180] inducing the depletion of proteins involved in telomere capping (e.g. POT1 and TRF1) because of the physical encumbrance of the G4, finally leading to telomere dysfunction. For this reason, G4 targeting is attractive also in ALT positive tumors. Many small aromatic molecules with binding specificity for telomeric G4 have been described. The first compound to be defined to induce telomerase inhibition via G4 interaction was a 2,6-diamidoanthraquinone [181], and since then many others have reported efficacy in different cancer types. Some of those telomeric G4 ligands, such as BRACO-19, Telomestatin, RHPS4 and derivatives of naphatalene diimides (NDIs) are able to induce antitumoral effects as single treatment, but also to enhance the genotoxic effects of other therapeutic strategies such as IR. Among those compound, RHPS4 is very effective in cancer growth inhibition as single agents [182,183], but different works showed that is able to synergistically enhance the effects of chemicals such as Bleomycin and Campotothecin [184]. Furthermore, RHPS4 is able also to target cancer stem cells within the tumor, not only the differentiated population, probably through different pathways of telomeric targeting [185]. Other than RHPS4, only few other telomeric G4 ligands were investigated in combination with IR. A telomeric ligand called TAC proves to significantly increase the frequency of chromosomal aberrations in GBM cells, when combined with IR [186], proving for the first time the possibility to couple the exposure to telomeric G4 ligands to radiosensitize glioma cells. The mechanisms involved in this process through telomere G4 stabilization is still unclear, even if other works on RHPS4 clarify the involvement of telomere structure in chromosomal aberrations caused by G4 ligands after IR [187]. It was proved that RHPS4 can also impair the progression of replication fork at telomeres, which is usually counteracted in cancer cells by the overexpression of several helicases (BLM, WRN and RTEL1), with the aim to resolve the G4 structures which impede correct telomere replication [188]. Nonetheless, G4 ligands are able also to induce a response that is affected by the region of the genome whereas the stabilized G4 is present (since telomeres are not the only G4-forming sequences). Indeed, stabilized G4 in oncogene promoters or in gene transcripts (such as messenger RNA), may modulate target gene expression [189–191], making G4 compounds strategically useful in cancer treatments.

AIM OF THE STUDY

Ionizing radiations (IR) has become an important and fundamental component of diagnosis and treatment in the management of many tumors. Despite radiotherapy is able to interfere with viability of cancer cells, new developments are needed for those tumors that are not responsive to the treatment, such as aggressive gliomas. The rate of tumor recurrence and the overall survival of patients diagnosed with gliomas, make necessary to investigate new approaches to improve the prognosis. Radiotherapy represents a valid therapeutic tool, based on the ability to induce DNA damage on cancer cells, which are incapable to repair properly, leading finally to cancer cell death. Since gliomas seem to be not responsive to radiations, due to cell population heterogeneity within the tumor, and the enhanced DNA damage response, our hypothesis is to target instead telomeres, the last part of linear chromosomes. Telomeres play a key role in the maintenance of genome stability. We aim, with this work, to investigate the radiation-sensitizer role of dysfunctional telomeres in a radioresistant cancer model. We also investigate the response of glioma stem cells to our approach, since cancer stem cells represent the component of the tumor responsible for resistance to therapies, and recurrence. For our purpose, we performed the following analyses:

1) We induced telomere dysfunction via the stabilization of DNA secondary structure within the telomere, called G4. To this end, we tested the telomeric effects of different G4 telomeric stabilizing ligands, RHPS4 and three derivatives of naphthalene diimides (NDIs), as single treatment in glioblastoma multiforme cells.
2) We investigated the correlation between telomere destabilization induced by G4 ligands and the radiation response in glioma cells
3) Considering the different type of biological response to the different chemical used for telomeric-G4 stabilization, and the corresponding different radiosesitization, and given that G4 are present also in other regions of the genome, it was interesting to analyze the possible modulation of other genomic targets.
4) Among all the molecules, G4 ligand RHPS4 was able to inhibit cell growth *in vitro* in GBM cells, inducing damage mainly at telomeric region and this led to a synergistic sensitization to IR. We decided to go further and investigate the *in vivo* efficiency of RHPS4 and IR combined treatment in immunodeficient mice xenograft tumors derived from U251MG cell.

5) Glioma are very heterogeneous tumors characterized by a strong resistance to chemo- and radiotherapy. Since the discovery of a population within the tumor, with characteristics of stem cells, and with a tumorigenic potential, we decided to focus our attention on the telomeric dysfunctionalization only in glioma stem cells, and their consequent response to IR.
6) Finally, we try to understand if the presence of stabilized G4 within the telomere could also induce replication stress, due to the impediment to normal progression of the replication fork. Since helicases are proposed to resolve those G4 at telomere in normal conditions, we try to knockout the RecQ helicase BLM via CRISPR/Cas9 and to evaluate the replication stress at telomere induced by G4 ligand in such conditions.

RESULTS

RHPS4 and NDI derivatives cytotoxic activity on GBM as single treatment

In the first step of our project, we comparatively evaluated the cytotoxic activity of three naphtalene diimide (NDI) derivatives (H-NDI-Tyr, H-NDI-NMe2, and tetra-NDI-NMe2, thereafter named C1, C2 and C6) with respect to an acridine derivative, RHPS4 (which already have shown a potent inhibitor effect on GBM cell growth in a previous work [187]) (**fig. 10**) in an *in vitro* GBM cell line (U251MG) and in normal human primary fibroblasts (AG01522). Specifically, 120 h (5 days) exposure to increasing concentrations (ranging from 0.01 to 1 µM) of NDIs or RHPS4, resulted in a remarkable and concentration-dependent inhibition of cell growth. In particular, the NDI derivatives exerted a superior cytotoxic effect in GBM cells compared to RHPS4, as revealed by the nanomolar values of IC_{25} and IC_{50} (i.e., concentrations of compounds leading to 25% and 50% inhibition of cell proliferation, respectively), calculated from the dose-response curves (**fig. 11**; **Table 1**). In addition, the NDI derivatives exerted a lower cytotoxic effect on AG01522 normal primary fibroblasts, used as a control, compared to U251MG, thus suggesting that a good therapeutic window for this class of compounds could exist (**Table 1**).

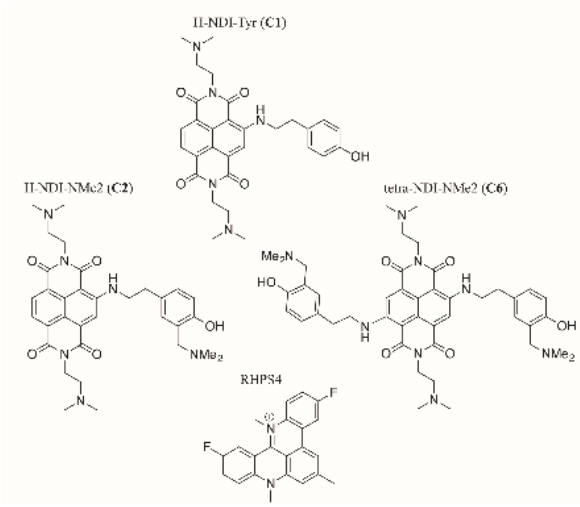

Figure 10: Chemical structures of the three NDI derivatives (C1, C2 and C6) and RHPS4

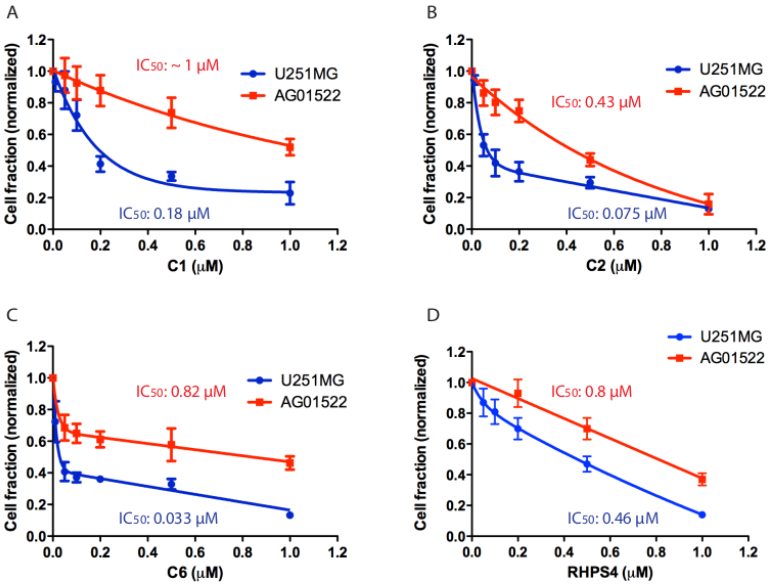

Figure 11: Effect of increasing concentrations of NDIs and RHPS4 on the proliferation of U251MG and AG01522 cells as determined after 120 h of exposure to ligands. (A–D) Both NDIs and RHPS4 displayed a higher effectiveness in growth inhibition in glioma cells (blue line) than in normal primary fibroblasts (red line). Data have been reported as cell fraction with respect to untreated cells and represent mean values ± SD (n = 4). The IC_{50} values have been reported on each graph (blue and red IC_{50} values for U251MG and AG01522, respectively).

	C1	*C2*	*C6*	*RHPS4*
U251MG IC_{50} (μm)	0.180 (0.050)	0.075 (0.008)	0.033 (0.006)	0.460 (0.060)
U251MG IC_{25} (μM)	0.090 (0.010)	0.028 (0.004)	0.007 (0.009)	0.160 (0.040)
AG01522 IC_{50} (μm)	1.020 (0.220)	0.430 (0.050)	0.820 (0.090)	0.800 (0.090)
AG01522 IC_{25} (μM)	0.490 (0.050)	0.200 (0.030)	0.340 (0.030)	0.450 (0.060)

Table 1: IC_{50} and IC_{25} values for NDIs and RHPS4 as evaluated after 120 h in AG01522 and U251MG. Standard deviations were reported in brackets.

Evaluation of G4 ligand-dependent induction of telomeric alterations

Due to their G4-binding activity, the capability of NDIs to induce perturbations in telomere length or architecture was comparatively evaluated with respect to RHPS4, which is already known to preferentially induce telomeric G4 stabilization [187]. Primarily, we investigated their capability to affect telomere length using centromere-calibrated quantitative fluorescence in situ hybridization (Q-FISH) (**fig. 12**). To this aim, after 120 h of G4 ligands treatment, U251MG and

AG01522 cells were subjected to metaphase spreads followed by co-staining with the whole telomeric peptide nucleic acid (PNA) probe and chromosome 2 centromeric specific probe. The mean basal values of telomere length were 3.6 and 11.4 T/C% in untreated U251MG and AG01522, respectively (**figure S1**). Distributions of telomere lengths were clustered in six different groups to compare their frequency, with particular attention to the fraction of very short telomeres (< 5 T/C%). No telomere shortening was observed in cells exposed to NDIs and RHPS4 (both cell lines were treated using the IC_{50} calculated for U251MG) as assessed after 120 h of treatment (**fig 13A, B**).

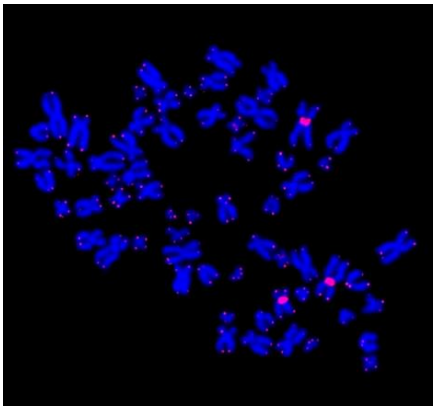

Figure 12: Representative image of a U251MG metaphase spread stained with telomeric and centromere 2 PNA probes (RED) and counterstained with DAPI (BLUE) (Magnification 639).

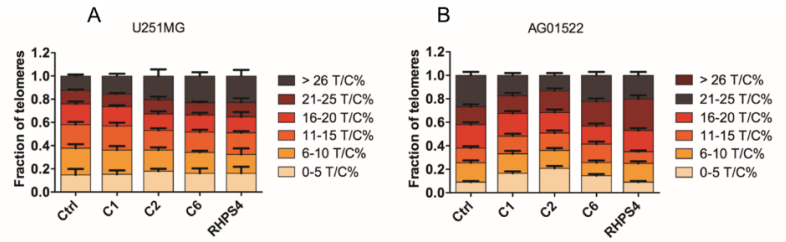

Figure 13: (A, B) Quantification of telomere length in U251MG and AG01522 cells, respectively. Telomeres length was grouped in 6 different classes (0–5, 6–10, 11–15, 16–20, 21–25 and ≥ 26 T/C%) for both U251MG (A) and AG01522 (B). Data have been reported as fraction of the total number of telomeres analyzed and represent mean values ± SD (n = 2).

In order to verify the capability of NDIs to induce telomere dysfunctions, the occurrence of telomeric-localized DNA damage was first investigated after the exposure of GBM cells to both IC_{25} and IC_{50} using a co-immunofluorescence with primary antibodies against DNA damage protein 53BP1 and the shelterin component TRF1, that specifically localize at telomeres. Notably, U251MG cells showed a dose-dependent induction of DNA damage, which was at least in part localized at telomeric level, as evidenced by the co-localization of 53BP1 with the telomere-associated factor TRF1 (**fig. 14A**). Conversely, telomeric DNA damage induced by RHPS4 was about two times higher than that induced by NDIs at both tested concentrations (**fig. 14B**). On the other hand, no DNA damage induction (both at genomic and telomeric level) was observed in AG01522 cells treated with a concentration of the compounds corresponding to the IC_{50} obtained in U251MG cells (**fig. 14C**).

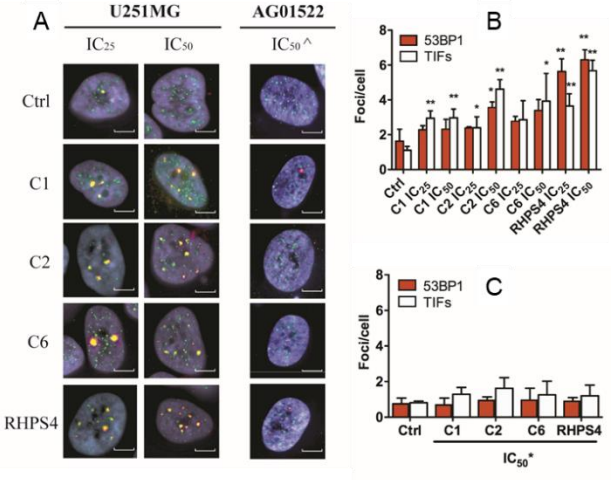

Figure 14: (A) Representative image of U251MG and AG01522 cells stained with antibodies against 53BP1 (red dots) and TRF1 (green dots) to determine TIFs. Scale bars, 5 µm. (B,C) Quantification of 53BP1 foci (red columns) and TIFs (white columns) in U251MG and AG01522 cells, respectively. U251MG cells were treated with both IC_{25} and IC_{50} of the diverse ligands used, whereas AG01522 were treated only with the higher concentration tested for U251MG (IC_{50}^). Data have been reported as number of foci per cell and represent mean values ± SD (n = 2). $*P < 0.05$, $**P < 0.01$, $***P < 0.001$ (Student's t-test)

To further analyze the effect of NDIs on proteins involved in telomere stability and damage, we investigated the binding of the shelterin proteins TRF2 and POT1, and the recruitment of γH2AX at telomeres, by

Chromatin Immunoprecipitation (ChIP) (**fig. 15A**). Results showed a significant ($P < 0.05$) decrease of POT1 for all the NDIs analyzed and a significant diminution in TRF2 levels ($P < 0.05$) only for RHPS4 (**fig. 15B**). Furthermore, data obtained from the analysis of γH2AX at telomeres demonstrated a mild (though not significant) increase in telomeric DNA damage with the three NDIs; a significantly ($P < 0.05$) higher enrichment in telomeric chromatin upon γH2AX immunoprecipitation was appreciable only in RHPS4-treated cells (**fig. 15B**), thus indicating that the acridine derivative had a greater specificity for telomeric G4s than NDIs.

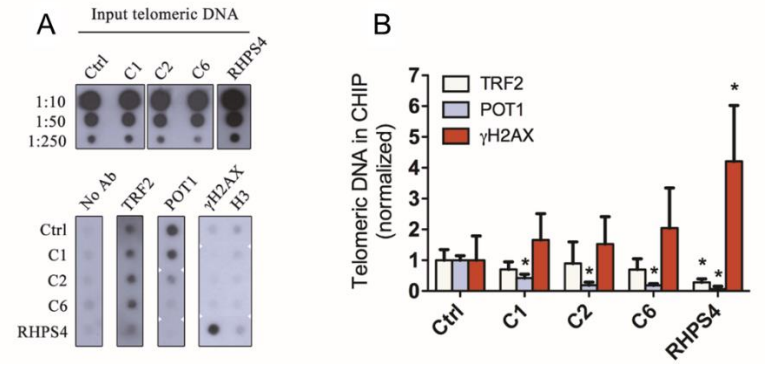

Figure 15: (A) Representative ChIP experiments showing the abundance at telomere of POT1, TRF2 and γH2AX (normalized on the telomeric amount of histone H3) in U251MG untreated cells (Ctrl) and following treatment with C1, C2, C6 and RHPS4. (B) Quantification of telomeric DNA amounts after ChIP. Data have been reported as fold-increase in telomeric DNA in treated with respect to untreated (Ctrl) cells, (n = 3). **P* < 0.05, ***P* < 0.01, ****P* < 0.001 (Student's t-test).

Overall, these findings would suggest that, as previously reported [191], other "off-telomere" targets might account for the biological effects exerted by the NDIs. Moreover, to assess whether the NDIs treatment affects telomerase function, *hTert* gene expression through qRT-PCR and telomerase activity via TRAP assay were evaluated. Although it was previously reported that C2 was able to reduce *hTert* expression and telomerase activity in SKMel-5 melanoma and H69 lung cancer cell lines [191], no data are available in the literature regarding the other NDIs. Results indicated that, among NDIs only C1 and C2 were able to reduce *hTert* expression and telomerase activity (*hTert* expression was reduced by the 30% and 50% and telomerase activity was reduced by the 50% and 70% after C1 and C2, respectively), whereas C6 did not (**fig. 16A, B**). On the

other hand, RHPS4-treated samples showed a 40% reduction of *hTert* expression and a 50% reduction in telomerase activity confirming previously published data [182].

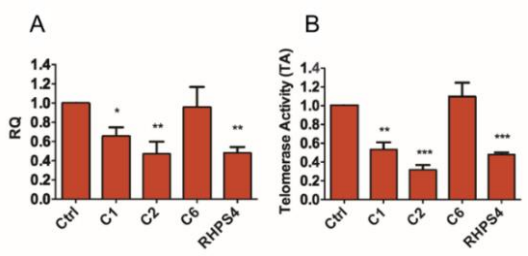

Figure 16: (A) Quantification of *hTert* mRNA expression levels. Data have been reported as relative quantity (RQ) with respect to untreated cells according to $2^{-\Delta\Delta Ct}$ method and represent mean values ± SD (n = 2). (B) Quantification of telomerase activity (TA) in response to G4-ligands. Data have been reported as relative TA with respect to untreated (Ctrl) cells and represent mean values ± SD (n = 3). **P* < 0.05, ***P* < 0.01, ****P* < 0.001 (Student's t-test)

Interestingly, the exposure of GBM cells to RHPS4 resulted also in a remarkable increase in the amounts of PIN2/TERF1 Interacting Telomerase Inhibitor 1 (PINX1) protein (**fig. 17A, B**), a potent endogenous telomerase inhibitor that plays a pivotal role in telomere length maintenance and chromosome stability [192,193]. Conversely, PINX1 levels were not significantly affected by NDIs treatment (**fig. 17A, B**). These data suggest that RHPS4 have a higher capability to induce telomere dysfunction respect to NDIs.

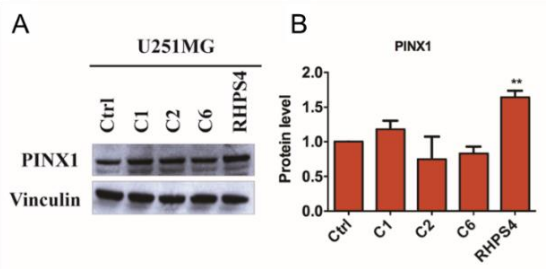

Figure 17: (A) Representative western immunoblotting showing PINX1 protein amounts in untreated (Ctrl) and G4 ligand-treated U251MG cells. Vinculin was used to ensure for equal protein loading. Cropped image of the selected protein has been shown. (B) Quantification of PINX1 protein amounts in cells treated with either NDIs or RHPS4. Data have been reported as relative protein levels with respect of untreated (Ctrl) cells and represent mean values ± SD (n = 3). **P* < 0.05, ***P* < 0.01, ****P* < 0.001 (Student's t-test).

NDIs and RHPS4 combined treatment with X-rays

To investigate G4 ligands radiosensitizing effect on U251MG cells surviving fraction (SF) experiments were performed. In contrast to RHPS4, that shows a potent radiosensitizing effect on GBM cells [187,194] NDIs did not increase cell killing up to 6 Gy of X-rays (**fig. 18A**). Data were also confirmed performing long-term growth assays. The heat map in Figure (**fig. 18B**) indicates that RHPS4 in combination with 4 Gy of X-rays strongly impaired cell proliferation [evaluated over 21 days as cumulative population doubling level (cPDL)] and the combined effect is much greater than that reported for X-rays and RHPS4 in a single treatment. Conversely, NDIs did not enhance the effect of X-rays in terms of inhibition of cell proliferation (**fig. 18B**).

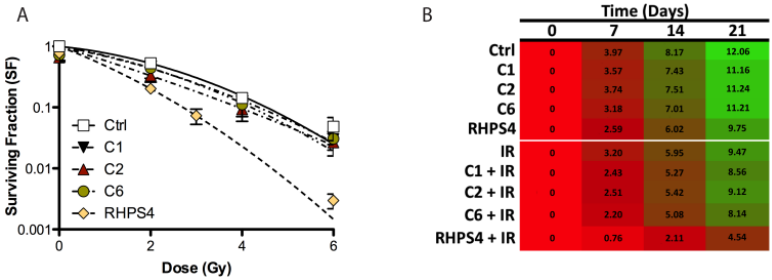

Figure 18: (A) Cell survival experiments in cells treated with NDIs (black, red and green symbols for C1, C2 and C6, respectively) and RHPS4 (yellow lozenges) and exposed to increasing doses of radiation (0–6 Gy). Data have been reported as the SF with respect to non-irradiated cells (0 Gy) and represent mean values ± SD (n = 3). (B) Quantification of the cPDL after 7, 14 and 21 days from the exposure to 4 Gy X-ray in untreated, NDI- and RHPS4-treated cells. The heat-map indicates the progressive increase in cumulative population doublings (red to green color-change).

Further experiments were performed to evaluate DNA repair proficiency after X-ray exposure in the presence or absence of NDIs and RHPS4. Co-immunofluorescence using antibodies directed against the DNA damage markers 53BP1 and γH2AX allowed the analysis of the IR-induced foci (IRIF) that consist in 53BP1 and γH2AX colocalization dots. Data indicated that NDIs did not affect DNA repair in contrast to RHPS4 that interferes with the DNA damage response [187] (**fig. 19A-C**). Of note, GBM cells exposed to all the tested ligands were characterized by an increased remaining fraction of γH2AX foci after 6 h, probably due to ligand-dependent, replication stress-mediated DNA damage (**fig. 19B**).

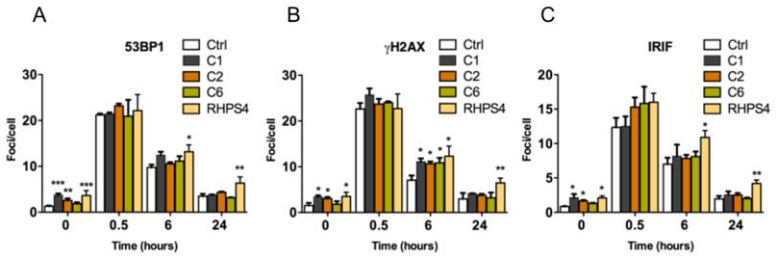

Figure 19: (A-C) Quantification of 53BP1, γH2AX and IRIF foci at different time points from the exposure to 1 Gy of X-rays in samples pretreated or not with either NDIs or RHPS4. Data have been reported as the number of foci per cell and represent mean values ± SD (n = 2). **P* < 0.05, ***P* < 0.01, ****P* < 0.001. Student's t-test. IRIF, ionizing radiations induced foci.

Analysis of a panel of possible off-target genes harboring putative G4-forming sites

Since G4 ligands give a different response to IR treatment, we decided to investigate the possible targeting of other regions harboring G4 structures, such as oncogenes or players involved in cell cycle regulation, DNA damage response and cell transformation. Analysis of proteins levels of oncogenes (KIT, MYC, and BCL2), previously reported to be targeted by C2 ligand [191,195], was performed. Data indicated a slight modulation of *Kit* and *Myc* as also confirmed by gene expression (**fig. 20A-C**). On the other side, protein level of the oncogene *Bcl2* indicated a significant decrease after the exposure to the drugs, with the ligand C1 inducing the strongest effect (32.1% reduction in protein level compared to untreated cells). Interestingly, RHPS4 induced an opposite effect, with a significant upregulation of BCL2 level (**fig. 20A-C**). Gene expression levels were assessed for all the ligands and confirmed the dissimilar modulation of *Bcl2* expression, highlighting the significant RHPS4-mediated increase of *Bcl2* transcript levels (6-fold increase on control level) (**fig. 20C**).

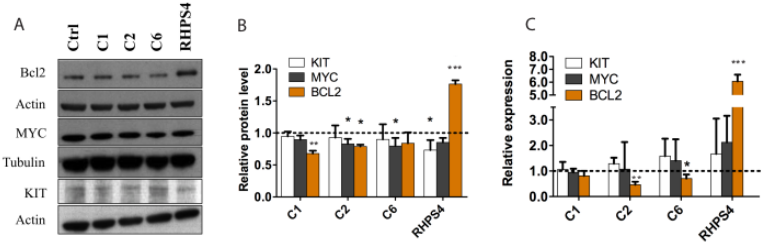

Figure 20: (A) Representative western immunoblotting showing BCL2, MYC and KIT protein amounts in untreated (Ctrl) and G4 ligand-treated U251MG cells. β-actin and c-tubulin was used to ensure for equal protein loading. Cropped image of the selected protein has been shown. (B) Quantification of BCL2, MYC and KIT protein amounts after C1, C2, C6 and RHPS4 treatment. Data have been reported as relative protein levels with respect to untreated cells and represent mean values ± SD (n = 3). (C) Quantification of *Bcl2*, *Myc* and *Kit* mRNA expression in response to either NDIs or RHPS4. Data ha ve been reported as relative quantity with respect to untreated cells, according to the $2^{-\Delta\Delta Ct}$ method, and represent mean values ± SD (n = 2). **P* < 0.05, ***P* < 0.01, ****P* < 0.001. Student's t-test.

With the aim to investigate whether NDIs modulate DNA repair proteins we tested a selected panel of players of the DDR. Most of the protein tested did not show any significant modulation in response to G4 ligands, whereas 53BP1 and γH2AX increase was reported for RHPS4 (data not shown), confirming immunofluorescence data. However, among DDR proteins we found an interesting increase of phospho-ATR (thr1989) levels irrespective of the compound used. Subsequent analysis of the main ATR downstream effector CHK1 in its phosphorylated form (ser345) indicated a strong activation in particular after NDIs treatment (**fig. 21A, D**). Specifically, NDIs were more effective in the phosphorylation of CHK1 whereas higher level of pATR were found in response to RHPS4. Of note, RHPS4 was also able to reduce basal level of CHK1, however this not seems to impact on its phosphorylation. The involvement of ATR and CHK1 suggests the induction of replication stress, likely due to the stall of the replication fork. To investigate the possible occurrence of cell cycle defects, a panel of proteins involved in cell cycle regulation and progression was analyzed (**fig. 21B, C**). NDIs treated-cells showed a distinguished modulation in Cyclin E, required for the transition from G1 to the S-phase, with the ligand C6 showing the strongest up-regulation. C2 ligand, instead, showed a significant overexpression of Cyclin A compared to controls (**fig. 21E**). NDIs, but not RHPS4, were able to upregulate the levels of p21/CDKN1A (**fig. 21F**). RHPS4 reduced both CDK2 and Proliferating Cell Nuclear Antigen (PCNA) up to the 50% and

40% of control level, respectively. Of note, the latter proteins were not significantly affected by NDIs treatment (**fig. 21E, F**).

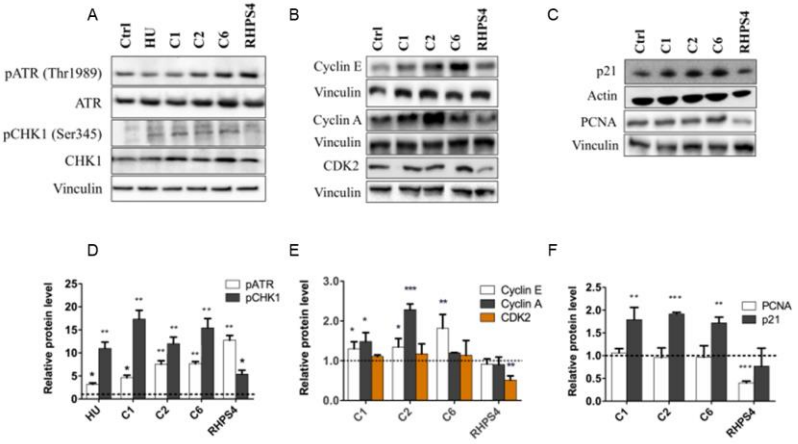

Figure 21: (A-C) Representative western immunoblotting showing pATR, pCHK1, cyclin E, cyclin A, CDK2, PCNA and p21/CDKN1A protein amounts in untreated (Ctrl) and G4-ligand-treated cells. b-actin, Tubulin and Vinculin were used to ensure for equal protein loading. Cropped images of selected proteins have been shown. Hydroxyurea (HU) in panel A and D was used as internal control for ATR and CHK1 activation. (D-F) Quantification of the amounts of proteins shown in panels A-C. Data (mean values ± SD, n = 3) have been reported as relative protein levels with respect to untreated cells. $*P < 0.05$, $**P < 0.01$, $***P < 0.001$ (Student's t-test).

NDIs and RHPS4 effects on cell-cycle progression

On the basis of our biochemical data, the possible occurrence of cell-cycle perturbations in G4 ligand-treated cells was investigated by bromodeoxyuridine (BrdU) pulse and chase experiments, by doing a wash out of G4-ligands after 120 h of treatment and following BrdU incorporation at several timepoints. In controls, at 6-8 h after BrdU washout, a fraction of labelled cells reentered in G_1 (**fig. 22A**); on the contrary, NDI and RHPS4 treated cells showed a delay in the cell cycle progression as evidenced by the appearence of BrdU-positive cells in G_1 phase only at 24 h. In addition, untreated cells re-entered in the S-phase (as BrdU- positive cells) after 24 h from release, whereas for NDI- and RHPS4-treated samples this population was not detected (**fig. 22A**). This data suggests that cells that were in S-phase at the time of the treatment escaped from G_2-M and remain arrested in the following G_1-phase without moving on to S-phase. To determine how persistent was the G_1

blockage observed, we performed a BrdU pulse and fix experiment after 48 h from drugs washout. Data indicated that, differently from NDIs-treated samples that re-entered cell cycle as shown by the high percentage of BrdU-labeled cells, RHPS4-treated cells remained totally blocked (**fig. 22B**).

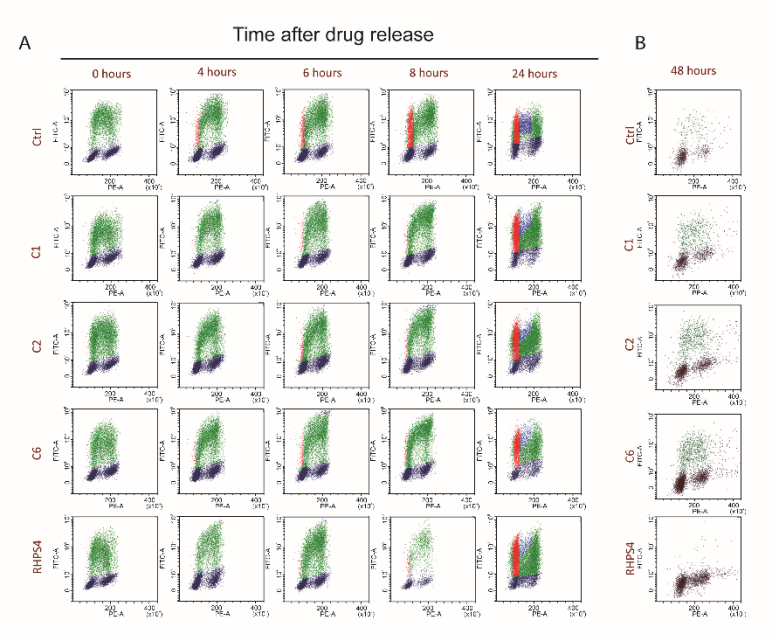

Figure 22: Detailed analysis of cell cycle progression after NDIs or RHPS4 treatment. (A) Assessment of BrdU incorporating cells over time upon a pulse and chase experiments within the first 24 h. BrdU incorporating-cells in S-phase were indicated in green; G1 cells that have incorporated BrdU in previous S-phase were depicted in red. (B) BrdU-positive cells after a 48 wash out from the G4 ligand treatment and following a 30 min BrdU pulse. BrdU incorporating cells were depicted in green

With the aim to clarify the progression in M-phase, we tested the status of phospho-Histone-H3 (p-H3) that is phosphorylated at serine 10 during mitosis [196]. To dissect the delay of cell cycle progression after NDIs treatment, we designed a gating strategy based on p-H3 signal vs. DNA content (**fig. 23A**). Data indicated that only RHPS4 displayed a significant reduction of p-H3 positive cells compared to controls, confirming the general picture of its higher potential to block cell cycle also after drug release (**fig. 23B**). Moreover, we designed a box marker on p-H3 positive cells with a DNA content 4N and a contiguous box with a reduced (<4N)

DNA content. This last box represents cells displaying premature chromosome condensation (PCC) (also known as premature mitosis). With this cytometric approach we noticed that after 24 h C2 and C6 caused an increase of cells in PCC condition and a further increase of sub-G_1 population (**fig. 23C**) that was not detected after C1 and RHPS4 treatment (**fig. 23C**).

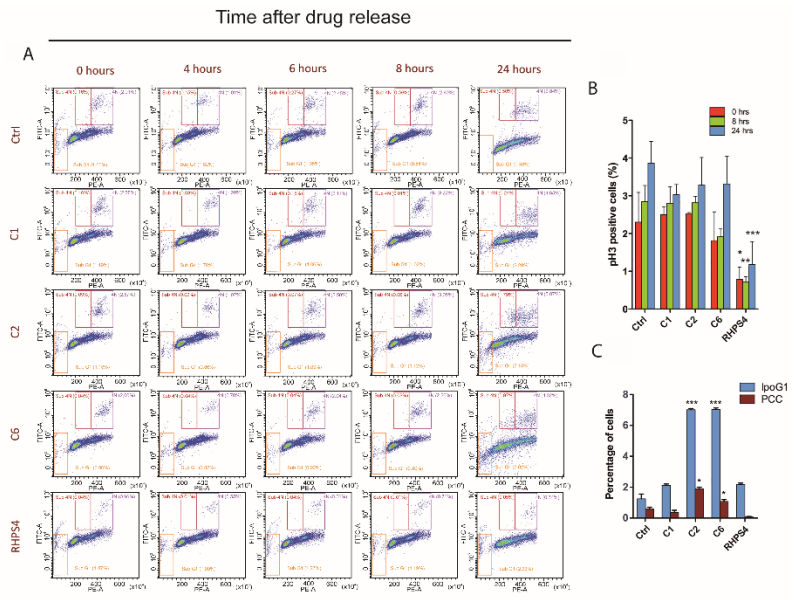

Figure 23: (A) Analysis of M-phase by the flow cytometric assessment of p-H3. (B) Quantification of p-H3-positive cells. Data have been reported as percentage of cells stained positive for p-H3 over time (0–24 h) in untreated and G4 ligand-treated cells and represent mean values ± SD (n = 2). (C) Quantification of PCC and apoptosis induction in cells treated with the tested G4-ligands. Data have been reported as percentage of cells showing PCC or residing in sub-G1 and represent mean values ± SD (n = 2). $*P < 0.05$, $**P < 0.01$, $***P < 0.001$ (Student's t-test).

RHPS4 combined treatment with IR in *in vivo* U251MG-derived tumors

The detailed characterization of the cellular effects of the three NDIs and RHPS4 clarify to us how different molecules have different potential to target G4s within telomeric sequences. Indeed, NDIs and RHPS4 behave differently. Contrary to NDIs, we confirmed RHPS4 as a highly potent and specific G4 ligand, which binds and stabilizes telomeric G4s leading

to the block of the replication forks at telomeres and consequently to telomere dysfunctionalization. Therefore, telomeres are recognized as DNA DSBs, leading to damage response, and impairment of cancer cell growth. We proved the effective correlation between telomeric effects and radiation response, confirming the synergic capability of this compound to sensitize radioresistant U251MG to IR. Consequently, we decide to test the radiosensitization capability of RHPS4 also *in vivo*, using mice heterotopic xenograft derived from U251MG cells (in collaboration with Mariateresa Mancuso Lab, ENEA, Rome). Glioblastoma cells were injected subcutaneously into the flank of CD1 nude female mice. Animals were randomized in four groups as summarized in **figure 24**.

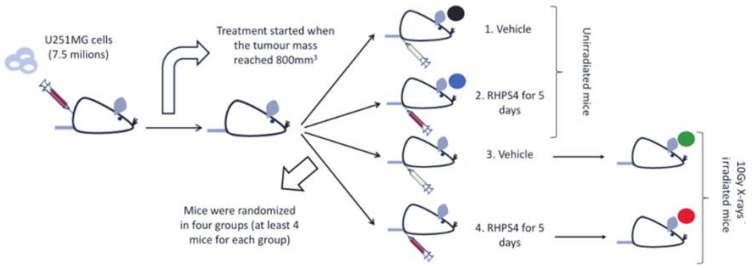

Figure 24: Graphical representation of the *in vivo* experimental plan. U251MG cell xenografted mice were randomized in four groups: Vehicle, RHPS4, Vehicle + 10Gy and RHPS4 + 10Gy. RHPS4 (10 mg/kg per day) or PBS (vehicle) were administered through intravenous injection for 5 days, then mice were irradiated with a single dose of 10Gy of X-rays.

Tumors in the control group (Vehicle) grew rapidly (**fig. 25A**); after 20 days, in fact, the tumor average size is 2.4-fold greater than the beginning. The growth kinetics of tumors in mice treated with RHPS4 for 5 days was comparable to that observed in the vehicle group, with a final tumor growth inhibition (TGI) of 1.9% (**fig. 25A, B**). In the first 30 days of experiment, irradiation alone (Vehicle + 10Gy group) significantly inhibited the tumor growth compared with control group; afterward, a slight but constant regrowth of tumor mass was recorded until the end of the experiment (**fig. 25A, B**). Nevertheless, the final value of TGI was 66.7%, approaching an acceptable significance level (**fig. 25C**; P = 0.0516). When mice were treated with RHPS4 followed by irradiation (RHPS4 + 10 Gy group), a striking block in the tumor growth was observed. At all time-points examined, the tumor dimension was

significantly reduced when compared to other groups (**fig. 25A, B**), indicating that this combination synergistically inhibited tumor growth in comparison with single treatments (RHPS4 or x-rays alone). Furthermore, the final value of TGI obtained in this group (TGI%= 122.1%) clearly indicate that double treatment caused regression of tumors far below the starting volume and, importantly, no tumor re-growth was observed during the 65-days post-treatment observation period.

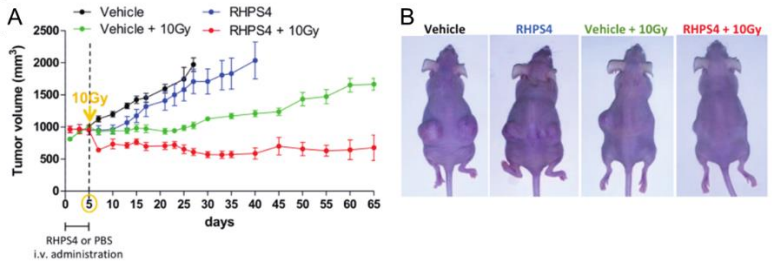

C

Treatment group *vs* Vehicle	Number of tumors	TGI (%)	P value *t*-test treated group *vs* Vehicle
RHPS4	10	1,9	0,5710
Vehicle + 10Gy	8	66,7	0,0516
RHPS4 + 10Gy	4	122,1	P<0,0001

Figure 25: (A) The graph shows the tumor growth kinetic relative to each treated group started when tumor mass reached 800 mm^3 in volume. (B) Representative images of U251MG cell xenografted mice 65 days post-treatment with a clear regression of tumor mass in the combined treatment group (RHPS4 + 10 Gy). In panel C is shown the tumor growth inhibition (TGI%) of treated tumors for each experimental group compared with vehicle group.

Characterization of stem-like cells derived from U251MG

To assess whether stem cell compartment was specifically targeted by RHPS4 we isolated U251MG stem-like cells (U251MG-SC-sph), growing as suspending spheres enriched with stemness characteristic, form the parental U251MG total cell line (from now on referred as U251MG-Adh) (**fig. 26**).

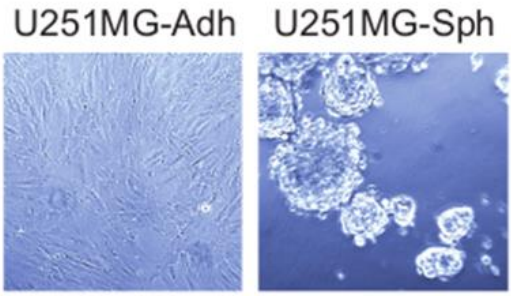

Figure 26: Representative figures of adherent U251MG cells and spheres derived from the same cell line.

In order to determine the immunophenotype of U251MG cells (U251MG-adh) and derived U251MG stem-like neurospheres (U251MG-SC-sph) specific markers of stem cells and differentiated cells were examined. Analysis of CD133, CD44, Sox2, Nestin and GFAP expression was performed through immunofluorescence, western blotting or relative qPCR experiments. Although all the two types of cells exhibited a lack of immunoreactivity for CD133, U251MG-SC-Sph cells showed higher expression of Nestin at the protein and RNA levels compared with that of U251MG-Adh cells (**fig. 27A-D**). Sox2 and CD44 levels were comparable in both cell types (**fig. 27A, B** and **C**). Notably, U251MG cells under the two culture conditions exhibited distinguishing immunoreactivity for GFAP, that is a marker of differentiated neural cell type. Compared with U251MG-SC-Sph cells, U251-Adh cells showed statistically significant immunoreactivity for GFAP (**fig. 27D**).

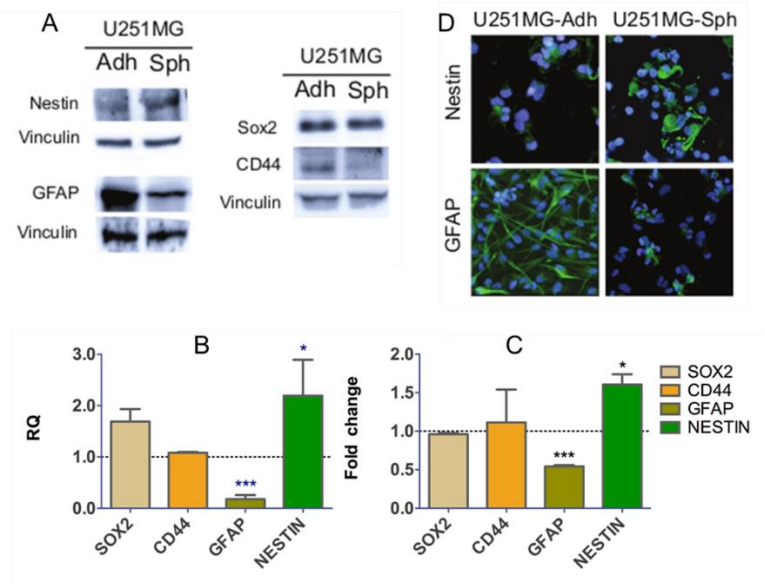

Figure 27: (A) Representatives Western immunoblotting showing levels of NESTIN, SOX2, CD44 and GFAP in U251MG-Ahd and -Sph cells. (B) Relative quantity of mRNA levels and (C) densitometric analysis of protein bands revealed a significant reduction of GFAP and a significant increase of NESTIN in U251MG-Sph compared to U251MG-Adh. (D) Images of immunofluorescence versus NESTIN and GFAP confirmed Western blot data. Data have been reported as relative quantity with respect to U21MG-Adh cells and represent mean values ± SD (n = 2). *$P < 0.05$, **$P < 0.01$, ***$P < 0.001$ (Student's t-test).

In addition, a cytogenetic and biochemical analysis of U251MG-adh and U251MG-SC-sph was performed in order to evaluate the overall genomic stability, telomeric length, telomere fragility and telomerase activity in the two cell types. Although we did not found differences in cell ploidy (modal number is about 65 in both cell types) (**fig. 28A, B**), mFISH staining revealed that chromosomal rearrangements were more frequent in U251MG-adh than in U251MG-SC-Sph cells (**fig. 28C**). Although in both cell types we found 4 conserved derivative chromosomes that were present in more than 90% of the cell observed (derivative chromosomes are described in **fig. 28C**), U251MG-adh cells displayed a significantly higher number of de novo randomic rearrangements than observed in U251MG-SC-sph.

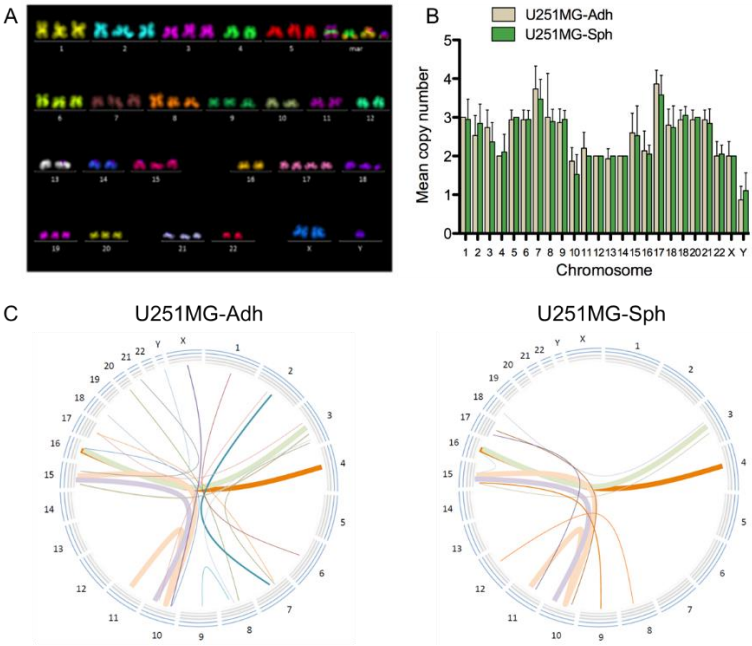

Figure 28: (A) Most common karyogram observed in U251MG-Adh cells. Derivative chromosomes are indicated as mar and involved chromosomes 11-10-15, 10-15, 16-4 and 16-3. (B) Ploidy of U251MG-Adh and -Sph was completely over-imposable, whereas as shown in circos graphs (C) chromosomal exchange frequency are very higher U251MG-Adh than in U251MG-Sph. Data represent mean values ± SD (n = 2)

Analysis of telomere length and telomerase activity showed that telomere metabolism was differently regulated in U251MG-Adh and U251MG-SC-sph. Telomere length measurement showed significantly longer telomeres in stem-like cells when compared to their differentiated counterpart (9.1 and 5.6 T/C%, respectively) (**fig. 29A, B** and **C**). As previously reported [188] RHPS4 induces telomere doublets that are double or discontinuous telomere signals at the chromatid end. In some cases, the multiple signals were spatially separated from the chromatid terminus, as if the telomeric DNA had failed to condense or was broken [197]. We refer to these various abnormal telomeric patterns as fragile telomeres. Longer telomeres in spheroid were also coupled with higher telomere fragility as demonstrated by the higher frequency of telomere doublets per chromosome (**fig. 29D**). The two cell types displayed also different levels

of telomerase activity (TA). Indeed, U251MG-adh cells showed a three-fold higher TA than U251MG-SC-sph (**fig. 29E**).

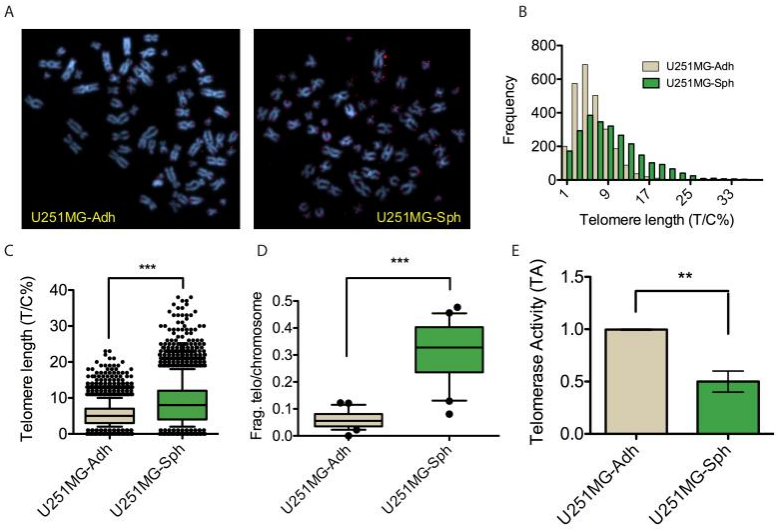

Figure 29: (A) Representative image of metaphase spreads of U251-Adh and -Sph stained with telomeric and centromere 2 PNA probes (RED) and counterstained with DAPI (BLUE) (Magnification 639). (B) Telomere length distributions in U251MG-Sph cells compared to -Adh cells. Telomere length was expressed as the ratio between the fluorescence of each telomere signal and the fluorescence of the centromere of chromosome 2, used as a reference. (C) The mean basal values of telomere length were showed as T/C% in U251MG-Adh and U251MG-Sph, respectively. (D) Increased telomeric fragility induced in U251MG-Sph cells respect to -Adh cells, quantified by the presence of telomeric defects in metaphase cells (doublets at telomeres). (E) Quantification of telomerase activity (TA) in U251-Sph cells. Data have been reported as relative TA with respect to U251MG-Adh cells and represent mean values ± SD (n = 2). * $P < 0.05$, ** $P < 0.01$, *** $P < 0.001$ (Student's t-test).

RHPS4 treatment and growth inhibition in U251MG staminal component without IR radiosensitization

To investigate the RHPS4 ability to inhibit cell proliferation in the stem cell-like neurospheres and the effects of the combined treatment with IRs, we treated the cells with different concentrations of the G4 stabilizing agent and after 120 h, we proceed to expose cells to 10 Gy of X-rays and let the cells growth for additional 120 h. We then measured the number of the spheres (we considered only spheres >2800 μm^2) and the area of each sphere. Data from the neurospheres assay showed that 10 days after treatment, RHPS4 was able to reduce in a linear dose-dependent manner ($R^2 = 0.93$) both number and size of spheres (**fig. 30A**), with the maximum

effect observed at the concentration of 1 μM, where we found a 60% reduction in spheres number and about 70% reduction in spheres size (**fig. 30B, C**). However, no radiosensitization was observed when samples were exposed to 10 Gy of X-rays (**fig. 30B, C** and **D**).

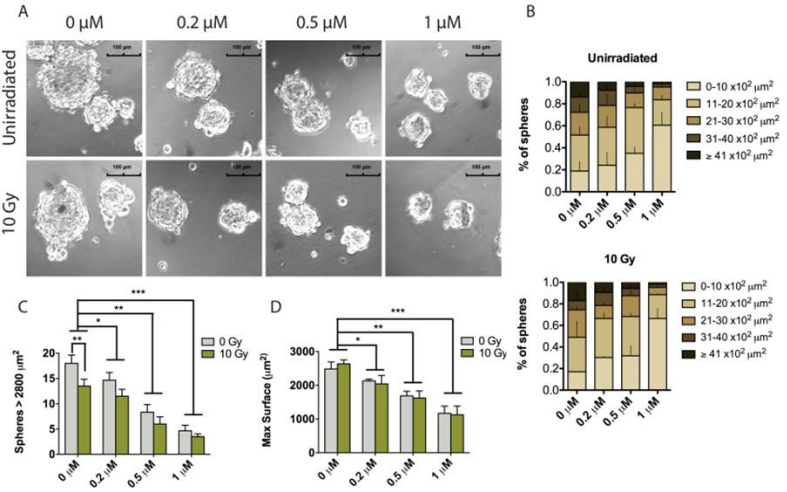

Figure 30: (A) Images of U251MG-derived neurospheres treated with increasing concentrations of RHPS4 (0.2-1 μM for 120 h) and then exposed to 10 Gy of X-rays. (B) Neurospheres maximal surface was automatically calculated by IS-Capture software after manual surrounding of each sphere. Maximal surface data were grouped in 5 different classes (0-10, 11-20, 21-30, 31-40 and ≥ $41*10^2$ μm²) for both unirradiated and 10 Gy-exposed U251MH-Sph cells. Data have been reported as percentage of the total number of spheres analyzed and represent mean values ± s.d. (n=3). (C, D) Spheres number and max surface in samples exposed to RHPS4 and IR were shown, respectively. Data represent mean values ± s.d. (n=3). * $P < 0.05$, ** $P < 0.01$, *** $P < 0.001$ (Student's t-test).

Since RHPS4 treatment was promising in inhibit proliferation of the stem-like cells derived from the total U251MG line, even if we show lack of radiosensitization, we decide to go even further and test RHSP4 also in Glioma Stem Cells (GSCs) derived from patient biopsy (kindly characterized and provided from Lucia Ricci-Vitiani lab, Istituto Superiore di Sanità, Rome). In agreement with neurospheres data, RHPS4 was also able to reduce drastically cell proliferation in vitro in four different patient-derived GSC lines. Although confirming that GSCs are more resistant to drug treatments compared to differentiated cancer cells [46,198], in all of the GSC lines analyzed RHPS4 inhibited cell growth in a dose- and time-dependent manner (**fig. 31A**). The IC_{25} values calculated

after 4 days of treatment were: 0.7 μM for GSC#1; 0.8 μM for GSC#61; 0.5 μM for GSC#83; 1.2 μM for GSC#163 whereas IC_{25} for U251MG was 0.16 μM. Based on these results, we investigated if RHPS4 exposure could enhance GSCs sensitivity to ionizing radiations. Therefore, GSCs were treated with IC_{25} doses of RHPS4 for 4 days and then exposed to single dose of γ-rays (10 Gy), selected as the closest to the maximum tolerated dose for adult brain and optic pathways on unfractionated radiosurgery [199]. Evaluation of cell viability 72h and 168h after irradiation showed that combined treatment was not able to improve GSCs sensitivity to ionizing radiation. We observed the same results even treating GSCs with lower doses of RHPS4 (IC_{25}) (**fig. 31B, C**).

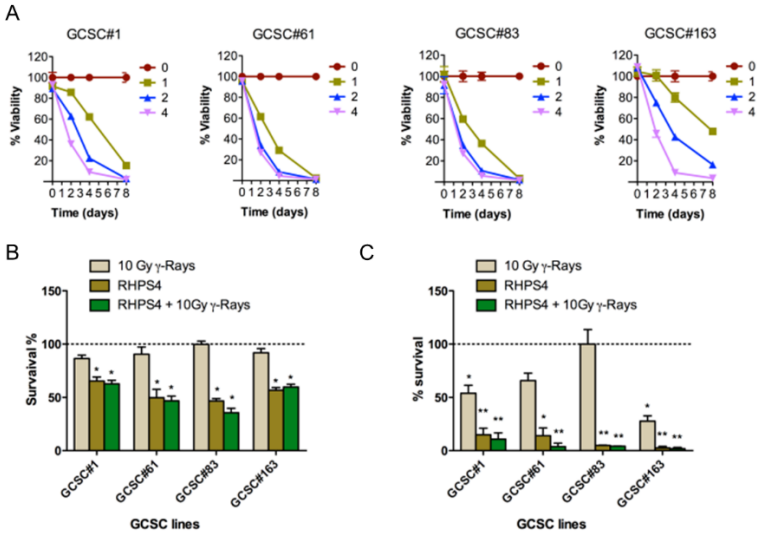

Figure 31: (A) Cell viability of GSCs from patients treated with RHPS4 (1, 2, 3 and 4 μM) and followed for 8 days. Data represent mean values ± s.d. (n=2). Effect of RHPS4 and γ-rays combined treatment on cell growth in GSCs from patients. Cell growth was evaluated after 72 (B) and 168 h (C) from irradiation. Combined treatment was performed treating cells with IC_{25} calculated at 96 h and then exposing them to 10 Gy γ-rays. Data represent mean values ± s.d. (n=2). * $P < 0.05$, ** $P < 0.01$, *** $P < 0.001$ (Student's t-test).

RHPS4 telomere-mediated effects in U251MG-derived neurospheres and patient-derived GSCs

RHPS4 radiosensitization of GBM cells is mainly driven by telomere dysfunction [187]. In order to understand whether the lack of

radiosensitization observed in stem cells may be ascribed to a telomeric resistance to RHPS4 we performed a cytogenetic telomeric analysis in order to evaluate telomere-mediated chromosomal aberrations and/or telomere length modulation in both U251MG-Sph and patient derived-GSCs. In general, results indicated that, in contrast to U251MG-Adh, both the stem cell models did not respond to RHSP4 at telomeric levels. In detail, differently from adherent U251MG, stem-like spheres and GSCs did not show any induction of dicentric chromosomes or telomeric fusions suggesting the capacity to bypass stabilized G4 structures at telomeres (**fig. 32A, B**). Accordingly, with the high genetic and karyotypic complexity of GBM cells, we found near-to-tetraploid modal number in three out of four untreated patient derived cell lines (**figure S2-A**) and, moreover, we observed the clonal presence of dicentric chromosomes in lines 1, 61 and 83 and telomeric fusions in line 61. Analysis of fragile telomeres (**fig. 32C**) confirmed the different telomeric response of differentiated and cancer stem cells to RHPS4. In particular, we found a significant induction of fragile telomeres in U251MG-Adh cells with frequencies two-fold higher in RHPS4 treated cells than in untreated controls (**fig. 32D**). On the other hand, U251MG-SC-Sph and GSCs from patients did not display any increase in telomeric fragility confirming the lack of telomeric effect of the ligand in GSC (**fig. 32D**). Moreover, telomere lengths were analyzed using centromere-calibrated Q-FISH [200,201]. As general information regarding telomere lengths in GSCs we found a very heterogeneous telomere length ranging from 4 to 15 T/C%. In particular, as expected for RHPS4 short treatment duration (5 days) [183,187], none of the analyzed cell lines showed neither mean telomere length modulation nor the enrichment of shortest telomeres **figure S2-B,C**).

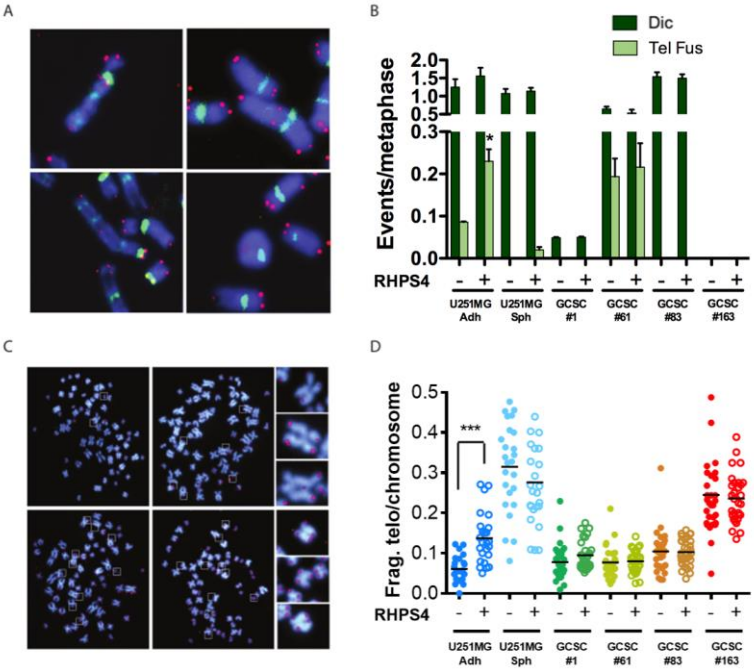

Figure 32: (A) Representative images of telomere fusions involved in the formation of dicentric, tricentric and ring chromosomes observed in the U251MG-Adh cell line treated with 0.5 μM RHPS4 for 120 h. (B) Frequency of classical dicentrics (dic) and dicentrics generated from telomere fusions (tel fus) in the U251MG derived cell lines and in GSCs lines from patients. Data represent mean values ± s.d. (n=2). (C) Representative images of U251MG-Adh cells in which are present several fragile telomeres (surrounded by boxes). Some of them were enlarged on the right side of the figure. (D) Frequency of fragile telomeres per chromosome in the U251MG derived cell lines and in GSCs lines obtained from patients treated or not with RHPS4. Data represent the frequency of each metaphase scored and black bars denotes mean values (n=2). $P < 0.05$, ** $P < 0.01$, *** $P < 0.001$ (Student's t-test).

RHPS4 induces the reduction of RAD51 and CHK1

The absence of telomere-involving chromosomal aberrations led us to investigate additional RHPS4 targets able to explain the potent proliferation inhibition observed in Cancer Stem Cells. Due to the ability of G4 ligands to induce replicative stress and DNA damage, we looked at a panel of proteins involved in DNA damage signaling, repair and checkpoint activation such as ATM, pATM, ATR, pATR, CHK1, pCHK1, CHK2, pCHK2, RAD51, PCNA, Ku80, DNA-Pk. Our data highlighted that RHPS4 activated the DNA damage response through both ATM and ATR kinases, which resulted phosphorylated at Ser1981

and Thr1989, respectively (**fig. 33A**). In particular, we observed that RHPS4 caused the activation of the ATR-CHK1 pathway (**fig. 33A, B**) as shown by the phosphorylation level of ATR and CHK1 observed in almost all the patient derived GSC lines. As previously observed, and reported above, RHPS4 in U251MG-Adh was able to induce ATR and CHK1 phosphorylation but concomitantly reduced also basal level of total CHK1 (**fig. 21**). Overlapping data were also obtained on GSC #1, #83, #163 and U251MG-Sph (**fig. 33C**). At the mRNA levels, we observed that *Chk1* was downregulated in U251MG-Adh and U251MG-Sph, in GSC line #1 and #83 but not in line #163 (the latter significantly upregulated). These data indicate that, in addition to transcriptional mechanisms, also post-translational regulation may be involved in protein levels reduction (**fig. 33D**). In contrast with the other cell lines, GSC line #61 modulates neither *Chk1* expression nor its protein level in response to RHPS4 (**fig. 33C, D**). Remarkably, also RAD51 protein levels were strongly reduced in response to RHPS4 treatment. In particular, we observed a 60 to 90% reduction of RAD51 levels in U251MG-Adh, U251MG-Sph, GSC #1, #83, and #163 treated cells compared to untreated ones; no significant reduction was observed in line #61 (**fig. 33E**). Expression profile of *Rad51* showed that protein depletion was determined by a reduced gene expression (**fig. 33F**), indicating *Rad51* (and *Chk1*) as a possible previously unidentified RHPS4 targets. As RAD51 and CHK1 are modulated in a cell cycle dependent manner with higher expression in S and G_2 phase, we checked also the S-phase specific protein PCNA to exclude that downregulation observed is due to accumulation in G_1 phase following treatments. We found that PCNA was increased after RHPS4 treatment in all the GSC, and hence indicating a strong blockage of cell cycle in S-phase and confirming that *Chk1* and *Rad51* reduction was not caused by blockage in G_1 (**figure S3**).

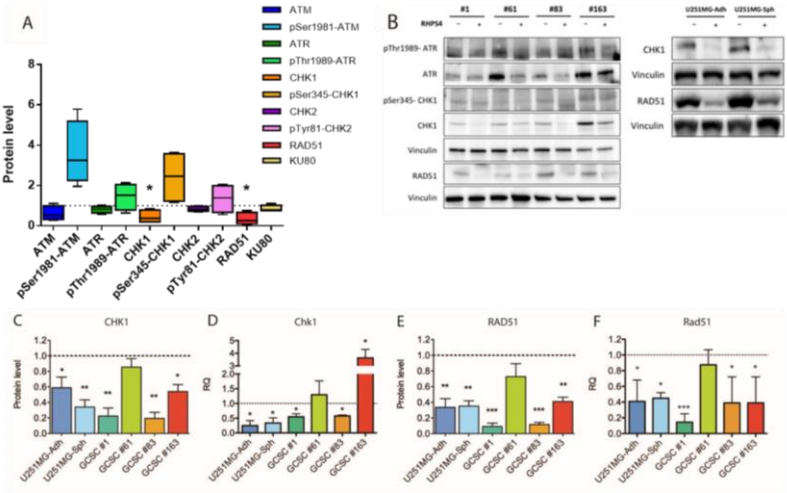

Figure 33: (A) Analysis of proteins involved in DNA damage response and checkpoint activation in patient derived-GSCs (B). Representative western immunoblotting showing protein amounts in GSCs and U251MG-Adh and -Sph RHPS4 treated cells. Vinculin was used to ensure for equal protein loading. Cropped image of the selected protein has been shown. (C, D, E, F) CHK1 and RAD51 protein level and gene expression in all the cell lines analyzed. Quantification of mRNA expression have been reported as relative quantity with respect to untreated cells, according to the $2^{-\Delta\Delta Ct}$ method. Data represent mean ± s.d. (n=3). * $P < 0.05$, ** $P < 0.01$, *** $P < 0.001$. Student's t-test.

Cell cycle deregulation and S-phase accumulation in RHPS4-treated GSC line #1 may explain quiescence observed *in vivo*

The patient-derived GSC line #1 was tested for basal proliferation and BrdU incorporation after RHPS4 treatment (**fig. 34**). Experiments of pulse and chase BrdU incorporation show that untreated glioma stem cells have a very slow S-phase progression as expected for cells with stemness characteristics. At 8h, after BrdU removal, most cell BrdU+ are predominantly at S/G_2 of cell cycle phases, at 24h appears a G_1 (BrdU+) population that has passed mitosis. Instead, in RHPS4 treated cells, not BrdU incorporation was observed (green square gate), probably indicating a lack of S phase progression. Furthermore, an evident sub-diploid peak appears after RHPS4 treatment as cell death induction (red square gate). Data on the other GSC (i.e. GSC lines #61, #83 and #163) could not be obtained because they failed to incorporate BrdU also after longer pulses (up to 6 h). This data could be explained by very long doubling times of GSC that are comprised between 48 and 96 h.

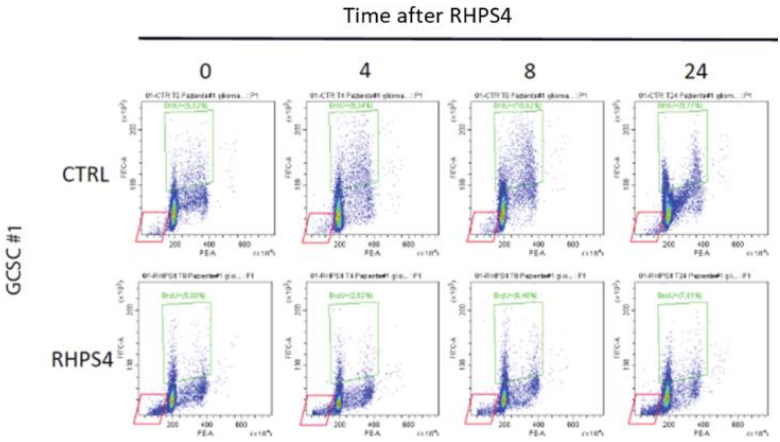

Figure 34: Detailed analysis of cell cycle progression after RHPS4 treatment in GSC #1. Assessment of BrdU incorporating cells over time upon a pulse and chase experiments within the first 24 h after RHPS4 wash out. BrdU incorporating-cell are indicated in the green square gate. Red square gate indicates apoptotic cells.

RHPS4 induction of replication stress in U251MG hBLM knockout cells

Protein level of cell cycle regulator CDK2, PCNA, and ATR-CHK1 S-phase checkpoint pathway is strongly modulated by RHPS4 treatment, in U251MG total cell line (as well in the staminal component). This correspond to a slowdown of the S-phase, which even 48 h after the washout of the ligand, remains depleted (as shown in **fig. 22**). Cells also show an increased telomeric fragility (as shown in **fig. 32**), suggesting that RHPS4 induces replication stress in S-phase, probably trough the stabilization of G4 structures within the telomere which interferes with the normal progression of the replication fork. RecQ helicase BLM has a prominent role in S-phase in the unwinding of G4s during telomere replication. It was appealing therefore to use a genomic approach to investigate RHPS4 replication effects in absence of hBLM helicase. First, we generated BLM$^{-/-}$U251MG clones by CRISPR/Cas9 genome editing (**fig. 35A**). The knockout or knockdown of the helicase was confirmed by analysis of protein levels with Western Blot using a specific BLM primary antibody (**fig. 35B**). We decide to use two clones: A9, where the protein was completely knockout, and the other C2, where the protein was present in very low levels (**fig. 35B**).

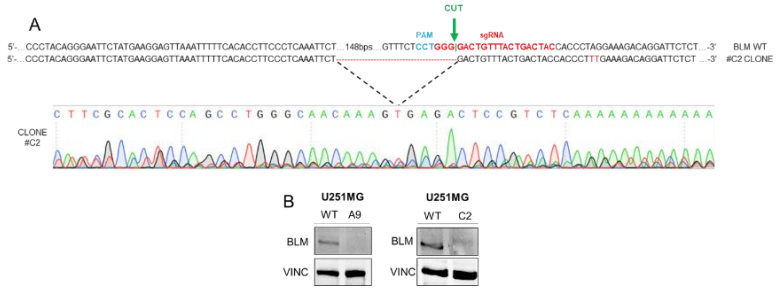

Figure 35: (A) CRISPR/Cas9 gene editing of hBLM in U251MG cells, a schematic of the BLM locus showing landmarks relevant to CRISPR editing, and DNA sequence of BLM in the C2 clone as an example. sgRNA target region, PAM sequences and the region of the cut are indicated (respectively in RED, BLU and GREEN) in the reference sequence and the deletions/insertions are highlighted in red in the clone sequence. (B) Western blot showing the protein level of BLM in the wild type and clones.

In order to verify if BLM is actually present in RHPS4 treated cells, the occurrence of telomeric-localized BLM foci was investigated after the exposure of U251MG cells to both IC_{25} and IC_{50} using a co-immunofluorescence with primary antibodies against BLM and shelterin protein TRF2, which localize at telomeres (**fig. 36A**). Data showed a significant increase in the presence of BLM with increasing concentration of the G4 ligand (**fig. 36B**), indicating probably that cells are facing a replication stress due to the physical impediment of G4s. Therefore, we decided to study RHPS4 replication defects on BLM KO clones.

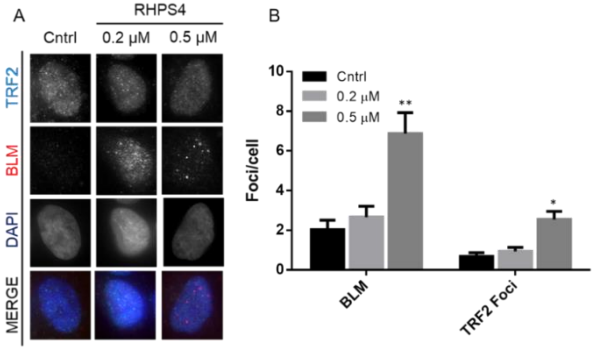

Figure 36: (A) Representative image of U251MG cells stained with antibodies against BLM and TRF2 to determine BLM telomeric localization. Scale bars, 5 μm. (B) Quantification of BLM foci and BLM colocalized with TRF2 in U251MG cells. U251MG cells were treated with both IC_{25} and IC_{50} of RHPS4. Data have been reported as number of foci per cell and represent mean values ± SD (n = 2). $*P < 0.05$, $**P < 0.01$, $***P < 0.001$ (Student's t-test).

We first assessed RHPS4 cytotoxicity in CRISPR/Cas9 U251MG BLM KO clones with SRB assay, treating cells with increasing concentrations of the G4 ligand, and comparing the results with the effect on the wild-type cell line. Interestingly we noticed that RHPS4 exerted a slightly higher inhibition on cell growth only in the C2 clone, whilst the effects on A9 clone are comparable to RHPS4 inhibition of wild-type cells, proficient for BLM, as revealed by the values of IC_{50} (**fig. 37A, B**).

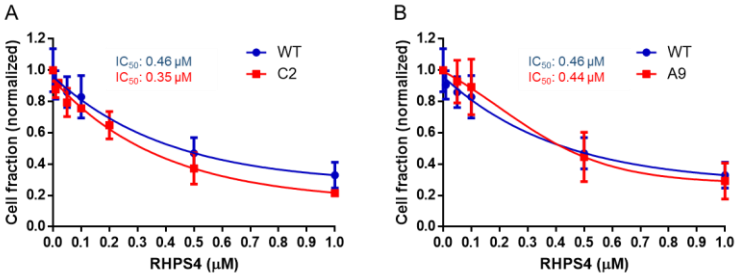

Figure 37: (A, B) Effect of increasing concentration of RHPS4 on the proliferation of U251MG wild type glioma cells and two BLM knock-out clones, C2 and A9. RHPS4 displayed a slightly higher growth inhibition potential on C2 cells. Data have been reported as cell fraction with respect to untreated cells and represent mean values ± SD (n = 3). The IC_{50} values have been reported on each graph (blue and red IC_{50} values for U251MG wild type and U251MG BLM KO clones, respectively)

We decide next to investigate telomere fragility induced by RHPS4 in cells that lacks totally or partially BLM, by the analysis of telomeric doublets (**fig. 38**). We used the IC_{50} values calculated from the U251MG wild type cell line. We fixed the cells after 5 days of treatment. We confirmed in the wild-type cells the induction of fragility after RHPS4 treatment. We also saw in the clone C2 a higher telomeric fragility without the ligand, but we could not find any statistically significance in the fragility induced by RHPS4. This effect is even more evident in clone A9, where cells completely lack BLM helicase; we did not find any increase after treatment with the G4 ligand, but the basal levels in untreated cells were much higher than the untreated wild type cells (**fig. 38**). We hypothesize that the absence of an increased telomeric fragility in treated cells lacking BLM could be ascribed to the fact that replication stress is already high in untreated cells with no BLM activity, making difficult to appreciate any variation after G4 ligand treatment.
To further elucidate the effects of RHPS4, it will be necessary to find a new strategy to visualize telomeric replication stress in BLM absence.

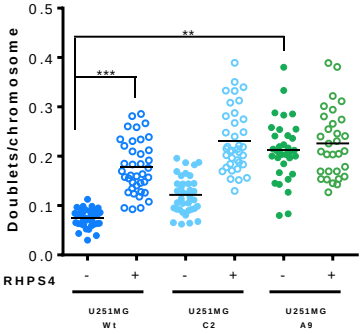

Figure 38: Frequency of fragile telomeres (doublets at telomeres) per chromosome in the U251MG wild type cells, and in C2 and A9 clones, respectively knockdown and knockout for BLM helicase, treated or not with RHPS4. Data represent the frequency of each chromosome scored and black bars denotes mean values (n=2) At least 50 metaphases were counted for each condition. $P < 0.05$, ** $P < 0.01$, *** $P < 0.001$ (Student's t-test).

DISCUSSION

TELOMERIC G4 LIGANDS, A NEW THERAPEUTIC APPROACH TO MODULATE CANCER CELLS RADIOSENSITIVY:

Targeting telomeres to sensitize cancer cells to DNA-damaging genotoxic treatments, including radiotherapy, has become of increasing interest since telomeric G4 have received particular attention, with the availability of new G4 stabilizing agents. Data from literature show that ligands able to stabilize telomeric G4s, besides affecting cell proliferation when administered as single agent, might display also radiosensitizing properties when combined with IR treatment. Since it was already proved the therapeutic potential of chemicals able to stabilize G4s within telomeric sequences in radioresistant cells (e.g. RHPS4 [187,194], we decide to use a chemical approach to investigate the relation between telomere and radiation sensitivity, and characterize in detail the cellular effects of three NDIs synthetized in collaboration with Mauro Freccero, from University of Pavia. Experiments were performed using U251MG radioresistant GBM cells, with the purpose of evaluating NDIs capacity to: (a) inhibit glioma growth in single treatment and (b) radiosensitize this highly radioresistant tumor type, using the previous data on RHPS4 to verify NDIs capability to induce both those effects. Proliferative effect of the three compounds were already visible at very low concentrations, with IC_{50} values in the nanomolar concentrations range (180, 75 and 33 nM for C1, C2 and C6, respectively) whereas the IC_{50} value calculated for RHPS4 was in the micromolar range [187]. In addition, as previously reported for RHPS4, also NDIs IC_{50} values were lower for tumor cells compared to primary fibroblasts, used as representative of human normal tissues. Hence, we assessed the telomeric effects of NDIs treatment. A panel of tests for telomere dysfunctionalization, ranging from TIF immunostaining to ChIP assay, showed that the telomere targeting effectiveness of NDIs was always lower compared to that of RHPS4. In particular, RHPS4 was the most effective ligand in the induction of DNA damage at telomeres and ChIP experiments indicated that both TRF2 and POT1 were significantly displaced from telomeres after treatment whereas γH2AX increased, indicating DDR activation. Interestingly, all the ligands induced the displacement of POT1 from telomeres. POT1 detachment from telomeric 30-overhang determines its degradation and may impair the telomerase docking to telomeres [202] suggesting that all the ligands may have a telomerase inhibitory potential by the targeting of the

telomerase docking site. Moreover, C1, C2 and RHPS4 determined also the reduction of *hTert* expression levels and telomerase activity indicating that at least two different mechanisms contributed to telomerase inactivation in U251MG cells. Downregulation of *hTert* gene was (very likely) determined by the direct stabilization of G4 at the *hTert* gene promoter [182]. Indeed, *hTert* promoter holds different G4-forming regions [203] and a direct binding has been shown for other ligands, such as Telomestatin and TMPyP4 [204]. Interestingly, we report that an additional mechanism of telomerase repression is caused by RHPS4 treatment. Indeed, analysis of PINX1, a telomerase repressor [205] frequently downregulated in cancer [206–208] and negatively associated with metastasis and prognosis, was upregulated after RHPS4 treatment, indicating that multiple mechanisms may cooperate to repress telomerase activity upon G4 ligands exposure. We next investigated if telomere and telomerase targeting by G4s stabilizing compound was coupled with an increase response to IR [144,158,209]. In contrast to RHPS4 [187], NDIs did not increase U251MG sensitivity to X-rays as shown by SF and long-term proliferation experiments. In this context, analysis of IR-induced DNA damage repair kinetic failed to show any difference between NDIs-treated and untreated samples, whereas RHPS4 determined a delay in DSB-rejoining [187,194]. The potent antiproliferative effect of NDIs accompanied by the moderate telomeric specificity and the absence of radiosensitization in U251MG cells opened the way to the search for additional NDIs targets others than telomeres. Of note, NDIs telomere specificity (C2 > C1 > C6) seems to be unlinked from the extent of proliferation inhibition (C6 > C2 > C1), supporting that factors other than telomeres were implicated in U251MG response to NDIs. In fact, it has been previously shown that C2 was able to differently modulate the expression of genes involved in telomere function and cancer-related mechanisms [191]. For this purpose, we evaluated the amounts of proteins encoded by genes involved in DNA repair, replication stress and cell cycle regulation, based on the fact that G4s are formed also in other regions of the genome. We did not find any significant modulation in the amounts of DNA repair factors including both DSBs sensing and repair (i.e., NBN, RAD50, MRE11, DNA-PK, Ku80, 53BP1, γH2AX, data not shown). Conversely, we found interesting variations in proteins involved in the signaling of replicative stress and in cell cycle regulation. The ATR-CHK1 mediated DNA damage response is generally thought to be the main replication-stress responsive pathway that mediates cellular DNA damage checkpoint responses in S-phase [210–212]. Our data indicated

increased levels of pATR and pCHK1 after treatment with both ligands thus suggesting that for both NDIs and RHPS4 a major mechanism for cytotoxicity is related to replication stress occurring during the S-phase. In line with this observation, NDIs prompted the increase in cyclin E and A, suggesting a slowdown of S-phase whereas RHPS4 induced the downregulation of CDK2 and PCNA, indicating an S-phase depletion. Interestingly, significant increase in p21/CDKN1A level after NDIs treatment may indicate that cells escaping S-phase blockage enter again in the cell cycle and then accumulate in G_1. Modulation of genes involved in cell cycle regulation and replicative stress signaling confirmed that the antiproliferative effect observed may be determined by an incorrect progression in the cell cycle and in particular into S-phase. Indeed, a stabilized G4 may represent a physical impediment to replication fork progression, determining critical cell cycle perturbations. In order to check cell cycle progression with particular attention to S and G_2/M phase, we performed BrdU incorporation experiments and M-phase analysis through the immunostaining of the phosphorylated form (phopspho-S10) of the histone H3, which is a specific marker of mitosis. We found a strong delay in S-phase for all the ligands analyzed that results in a significant G_1 accumulation. However, also in this case, NDIs and RHPS4 behaved differently: the NDI-mediated delay in S-phase was transient and cell recovered S-phase after 48 h from ligands wash-out, whereas RHPS4 treated cells showed a persistent block (up to 48 h) with a total depletion of S-phase cells. Also, analysis of M-phase cells underlines the difference between the two classes of compounds, showing a depletion of M-phase cells after RHPS4 but not after NDIs, indicating that the acridine salt determined a very strong blockage of cell cycle that persisted also after drug washout. In contrast, we observed a fraction of cells engaging PCC after NDIs but not after RHPS4 treatment. Interestingly, PCC correlated with a significant percentage of ipoG_1 cells in C2- and C6-treated samples that, of note, were also characterized by the downregulation of the anti-apoptotic factor BCL2 and increased levels of p21/CDKN1A. Overall, our results indicated that NDIs and RHPS4 induced distinct cellular effects. Indeed, analysis of protein levels and gene expression indicated a diametrically opposite behavior between the two classes of ligands and suggested a different G4 target spectrum. Our data confirmed the very interesting profile of RHPS4 as antiproliferative drug in glioblastoma. In addition to the well-known effects of this compound, we report also its remarkable ability to upregulate the telomerase inhibitor PINX1, which has been recently reported as a

suppressive gene in glioma through its ability to repress telomerase activity and cell invasion and migration [213]. We also confirmed the ability of RHPS4 to induce *in vitro* telomere dysfunction to enhance the outcome of IR treatment.

RHPS4 TELOMERIC EFFECTS AND RADIOSENSITIZATION IN *in vivo* AND IN THE STAMINAL COMPONENT OF GLIOMA:

We then decided to show if RHPS4 maintains its radiosensitizing ability, through telomeric dysfunction, also *in vivo*, in a U251MG heterotopic xenograft mouse model. Data indicated a very potent inhibition of tumor growth in mice treated with RHPS4 combined to IR, in contrast to tumor growth in controls and mice exposed only to RHPS4 or IR. Furthermore, inhibition was very durable in the combined treated mice, as we observed till the 65th day after drug administration. Notably, differently from most of the other studies that use human tumor cells xenografted on mice, we performed RHPS4 and IR combined treatment on 800 mm^3 tumor mass that are well visible and full-blown tumor. This choice was due to at least two different reasons: (a) in this way we were confident to treat mice harboring aggressive and fast-growing tumors; (b) we posed our model in a very disadvantageous condition mimicking the therapeutic treatment of rooted tumors. In addition to the RHPS4 radiosensitizing effect on glioma differentiated cells, the absence of tumor relapse in the combined treated mice let us to hypothesize that RHPS4 is also able to target glioma initiating cells (responsible for resistance to chemo- and radiotherapy and also for tumor recurrence) and prompted us to investigate *in vitro* the response of those stem-like cells. Therefore, in order to dissect the response of GSCs to RHPS4 and IR single and combined treatments, experiments were performed in two different models. The first one was represented by the isolation of U251MG stem-like compartment (U251MG-Sph) from the U251MG total cell line (U251MG-Adh): in this way, we were able to study the same cell line used for xenograft experiments. To assure the robustness of U251MG stem-like spheres isolation protocol, we firstly performed a very detailed molecular and cytogenetic characterization of the samples. The U251MG-derived spheres displayed increased levels of Nestin and decreased levels of GFAP as assessed in WB, qRT-PCR and IF experiments. Moreover, molecular cytogenetic karyotype analysis of U251MG-Adh and -Sph cells revealed a perfectly over-imposable ploidy level but a different frequency of chromosomal rearrangements. In particular, apart from conserved derivative chromosomes that are present with high frequency

in both U251MG and neurospheres, the latter displayed a very lower frequency of chromosomal rearrangements that indicates an enhanced control of genomic stability. The lower chromosomal instability of the stem-like population may be ascribed to more efficient DNA repair mechanisms evolved in stem and progenitor cells, whereas, upon differentiation, a certain degree of somatic mutations becomes more acceptable and, consequently, DNA repair is less active [214]. Moreover, telomere analysis revealed longer telomeres in U251MG-Sph than in -Adh, that is coupled with a lower telomerase activity, in accordance with published data that indicate that neural CSC have lower telomerase activity due to their lower replication rate in vivo [215]. Overall, the analysis of telomere status revealed significant differences between glioma derived stem-like cells and the whole adherent cell line that, as far as we know, was not previously characterized neither in the same type of tumor nor in other tumors. After the characterization of the U251MG derived stem-like model we performed experiments to determine the sensitivity of stem cells to RHPS4 and IR in single or combined treatments. Sensitivity to RHPS4 of U251MG-Adh and -Sph was very similar (about 0.5 μM for both). Strikingly, spheres were very resistant to a subsequent exposure to IR. Indeed, after 5 days from the exposure to 10 Gy of X-rays, data indicate only a 25% reduction in spheres number and no difference in spheres size when compared to irradiated controls not treated with RHPS4. Therefore, unexpectedly and contrastingly to data obtained in Adh cells, RHPS4 failed to radiosensitize stem-like cells. To further confirm data observed in the neurospheres model, similar experiments were carried out also in in a panel of 4 well-characterized primary GSCs obtained from GBM patients (WHO grade IV) [46,198,216]. The *in vivo* tumorigenic potential of these lines had been previously evaluated by intracranial cell injection in immunocompromised mice, where GSCs were able to recapitulate the patient tumor in terms of antigen expression and histological tissue organization. In line with data reported in literature [198,217,218] indicating high drug resistance, GSCs displayed a higher resistance to RHPS4 compared to U251MG differentiated cells with IC_{25} ranging from 0.5 to 1.2 μM as evaluated after 96 h. However longer treatments (i.e. 7 days) determined a massive cell death in GSCs with reduction of IC_{25} to 0.07, 0.05, 0.04 and 0.37 μM for cell line 1, 61, 83 and 163, respectively, pointing to a very potent effect of RHSP4 as single treatment. Longer times required for proliferation inhibition may be related to longer cell population doubling times of GSC, that were approximately two-fold greater than that reported in U251MG cells.

Despite the high sensitivity of GSCs to RHPS4, and in agreement to what observed in stem-like derived U251MG, we did not observe any radiosensitizing effect of RHPS4 as evaluated by cell viability assay 72 and 168 hours post 10 Gy γ-irradiation. As previously demonstrated by our lab, one of the mechanisms behind the RHPS4 radiosensitizing properties is the induction of telomere damage and hence lethal chromosome aberrations involving telomeres such as telomere fusions [187,194]. Interestingly, although it is largely documented the ability of RHPS4 to induce telomere fusions in different cell lines including U251MG-Adh, such kind of aberrations were not detected in U251MG-Sph cells and GSCs. We already proposed for NDIs and RHPS4 their potential to induce replication stress due to physical impediment to DNA polymerase during DNA replication, caused by stabilized G4, and this in turn activate a very well characterized DDR (at telomere as well) [188,219]. Telomeres act as common fragile site and preferentially form gaps or breaks on metaphase chromosomes under replication stress condition. Indeed, fragile telomeric sites or telomeric doublets represent a well-accepted marker of replication defects at telomeres [197]. In this context, RHPS4 determined a significant increase in doublets frequency in U251MG-Adh cells, whereas no differences were found comparing RHPS4 treated and untreated U251MG-sph and GSCs. Taken together these data point to a higher telomeric resistance of stem-like and GSCs to RHPS4 that ultimately influences also the radiosensitizing properties of the G4 ligand. This led us to speculate that other, non-telomeric targets also in GSCs might be responsible for the extensive inhibition of cell proliferation observed both *in vivo* and *in vitro*. With the aim of finding those alternative RHPS4 targets, we performed a screening of a panel of proteins involved in DNA DSBs repair and replication stress in U251MG-Sph and in GSCs. Notably, we found that RHPS4 markedly reduced the level of RAD51 and confirmed the reduction of CHK1 (that we obtained on U251MG-Adh cells while testing NDIs off-targets) in all the cell lines analyzed. Both genes displayed G4 putative binding sites in their promoter or gene bodies with G-scores higher than 37 for both and very close to G-score calculated for the telomere (Telomeric G-score: 42), thus representing possible novel RHPS4 target genes (G-Scores calculated using QGRS database). Notably, depletion of both CHK1 and RAD51 has been proposed in the literature as a strategy to radiosensitize GSCs [45,55,62]. Our data seem to be apparently in contrast with the absence of radiosensitization achieved in GSCs and stem-like cells after RHPS4 treatment. However, our opinion is that the mechanism by which RHPS4

reduced proliferation in GSCs may be linked to RAD51 and CHK1 reduction also in the absence of radiosensitization. Indeed, though CHK1 was normally phosphorylated after RHPS4 treatment, the level of total CHK1 was significantly lower in the RHPS4-treated cell lines compared to untreated controls. We believe that the downregulation of CHK1 (also if its ATR-mediated phosphorylation is proficient) determines a deficient replication stress response that increases the yield of replication fork stall in regions harboring stabilized G4. In normal conditions, stalled replication forks are repaired by HR, although this process has not completely characterized [220]. Furthermore, it was recently proposed that GSCs have higher basal levels of RS respect the bulk population, and this could be one possible explanation for the general upregulated DDR of the stem component. Constant perturbation of replication increased the probability of DSBs formation, with consequently activation of DDR mechanisms, including HR. As a matter of fact, GSCs showed high percentage of stalled replication forks [221]. The most accepted mechanism indicates that Mus81 endonuclease cleaves DNA at stalled fork and determines the formation of a one-ended DSB that in turn activate HR through the recruiting of RAD51 [222]. However, the concomitant RHPS4-induced depletion of RAD51 determined the failure of HR the stalled replication fork leading in turn, to replication fork collapse and DSBs induction. Even if RHPS4 induce a strong down-modulation of effector of the RS response, which are also implicated in DDR, at the same time increased the total RS of the stem component, making this a possible explanation for the lack of radiosensitization (even if affects greatly proliferation), since high RS was indicated as a possible cause of radioresistance. Sensitivity to RHPS4 BrdU incorporation analysis in GSCs line #1 sustains this hypothesis showing that RHPS4 not only determines a strong arrest of cells in early S-phase but is also accompanied by a significant presence of a sub-G1 cells population suggestive of cell death that was not detectable in U251MG-Adh cells. In agreement with our hypothesis, the sensitivity of GSCs to RHPS4 was proportional to the extent of RAD51 and CHK1 protein level reduction for 3 out 4 lines analyzed (line #61 excluded). However, line #61 is the only line that showed a strong reduction of ATR that may partially explain the high sensitivity observed.

RHPS4 AND HELICASES – HOW G4s AFFECT TELOMERE REPLICATION:

To fully understand the extent of RS induced by RHPS4 in glioblastoma cells, we focus on the possible effects of stabilized G4 at replication fork, and, with a genomic approach, we induce the knockout of a RecQ helicase, hBLM, already known to be involved in the unwinding of telomeric G4s to assure correct replication [223,224]. We demonstrated the presence of BLM that specifically localize at telomere, after RHPS4 treatment, indicating that stabilized G4 probably recall the unwinding action of the RecQ helicase during replication. We then assessed the proliferation inhibition induced by RHPS4 in U251MG-BLM$^{-/-}$ clones generated via CRIPSR/Cas9 genome editing. In absence of the helicase, RHPS4 seems to be effective in arresting the growth of those cells, with IC_{50} values slightly lower respect the wild type cell, with 0.35 µM for the clone C2. Instead, in the A9 clone, RHPS4 shown the same cytotoxicity of the wild-type cells, with IC_{50} values comparable. We then investigated the induction of replication stress in BLM deficient cells, in presence of RHPS4, by counting fragile telomeres. Interestingly, we noticed that cells lacking BLM already had basal levels of telomeric fragility higher respect the untreated wild type, despite the absence of significant increase after RHPS4 treatment. Since BLM exerts its role during S-phase of the cell cycle, by processing any possible structure that could impede correct progression of replication fork [224], it could be one possible explanation that the strong RS induced by RHPS4 lead to a complete block of the cell cycle. It will be necessary to study BLM cell cycle regulation in relation to RHPS4 treatment and S-phase progression. Nonetheless, this genomic approach allowed us to study replication in RHPS4 destabilized telomeres, and this open a new possible way to study telomeric G4 potential as therapeutic targets. However, we just began to approach this interesting project, which need more investigation, specially to study the replication stress in the stem component where the basal level of RS is already high [221], by generating BLM knock-out in GSCs. Indeed, the inhibition potential of G4 ligands on cancer cells probably relied also on their ability to perturb preferentially replication at telomeres. Their action could be enhanced with the inhibition of different helicases, to eventually increase selectively cancer cell killing and at the same time the sensitivity to IR.

CONCLUSIONS

NDIs AND RHPS4: TELOMERIC G4s STABILIZATION TO INDUCE SENSITIVY TO IR

With regard to the possibility to destabilize telomere through the stabilization of telomeric G4 structures, to induce a telomere-driven chromosomal instability, with the final aim to sensitize cancer cells to IR induced DNA damage, we decide to test different types of proposed telomeric G4 ligands: NDIs and RHPS4. We indicate both NDIs and RHPS4 as very potent antiproliferative agents as tested in U251MG GBM cells. Among NDIs, C2 was the most interesting agent, able to induce moderate telomere dysfunction, Bcl2 downregulation, ATR-CHK1 DNA damage response, cell cycle slowdown in S-phase coupled with PCC and apoptosis. However, only RHPS4 was confirmed as a potent radiosensitizer in GBM radioresistant cells, since it was the only ligand to induce a direct relationship between drug-mediated telomere dysfunction and radiosensitisation, confirming the role of telomere dysfunction-inducing compounds in radiotherapy. Furthermore, we report also its remarkable ability to upregulate the telomerase inhibitor PINX1, which has been recently reported as a suppressive gene in glioma through its ability to repress telomerase activity and cell invasion and migration [213].

G4s NON-TELOMERIC ABILITY

Since NDIs were able to inhibit cancer cells proliferation, in absence of telomeric effects, we highlight the ability of those compound to have very different target spectrum in G4s stabilization. Indeed, though NDIs and RHSP4 are both able to bind with high affinity G4 DNA, affinity constants obtained by surface plasmon resonance analyses (for htel22 are: $9x106\ M^{-}1$ for RHPS4 and from $7x106\ M^{-}1$ to $3.1x105\ M^{-}1$ for the NDIs [195,225,226]) suggested that the major difference between those compounds may be related to the G4 selectivity, and this could be linked to the presence of different G4 topologies.

RHPS4 *in vivo* RADIOSENSITIZATION

We provide evidence that RHPS4 maintains its ability to radiosensitize glioma cells also *in vivo* preventing tumor recurrence in xenograft model in mice, by the targeting and dysfunctionalization of telomeres.

RHPS4 in GLIOMA STEM CELLs

We showed in two different cancer stem cell models (neurospheres and GSCs from biopsy) strong sensitivity to RHPS4 in single treatment coupled with the lack of telomeric damage and radiosensitization. We believe that, the potent antiproliferative effect of the drug in GSCs is achieved by the induction of replicative stress and by the concomitant depletion of CHK1 and RAD51 that, in turn, lead to a massive RS, that enhanced the DNA damage (with no opportunity to counteract) and cell death. Our data confirm that multiple DNA damage signaling pathways contribute to GSC resistance to DNA damage and that combined inhibition of cell-cycle checkpoints and DNA repair targets provides the most effective means to overcome resistance of GSC to genotoxic insults.

RHPS4 AND TELOMERE REPLICATION

The strong replication stress induced by RHPS4 could possibly be coupled with the action of others players, such as helicases to cope with that. Fork blockage due to G4 stabilization could enhance the replication stress in absence of players needed for the unwinding such as BLM or other helicases. Indeed, telomeric fragility increased in cells that lack the RecQ helicases. However, treatment with RHPS4 does not induce any significant increase in fragility. We suppose that, since the G4 ligand is alone a strong element of replication stress, we could not appreciate the effect in fragility, but we need to design new experiments to visualize the exact effect during replication. Probably, impairment of BLM activity leads to loss of telomeric sequences due to G4 stabilized structure not correctly removed during replication. Nonetheless, we figure out a new possible genomic approach to study elements, which collaborate to the removal of secondary structure during replication, and this could be applied in combination of G4 stabilizing agents to enhance replication stress in tumors, to selectively disrupt cancer cells.

REFERENCES

1. Siegel, R. L., Miller, K. D. & Jemal, A. Cancer statistics, 2018. *CA. Cancer J. Clin.* **68,** 7–30 (2018).
2. Baskar, R., Lee, K. A., Yeo, R. & Yeoh, K. W. Cancer and radiation therapy: Current advances and future directions. *Int. J. Med. Sci.* **9,** 193–199 (2012).
3. Cleary, J., Gelband, H. & Wagner, J. Cancer: Disease Control Priorities. *Dis. Control Priorities 3rd Ed.* 1–363 (2015). doi:10.1017/CBO9781107415324.004
4. Shim, G., Ricoul, M., Hempel, W. M., Azzam, E. I. & Sabatier, L. Crosstalk between telomere maintenance and radiation effects: A key player in the process of radiation-induced carcinogenesis. *Mutat. Res. Rev. Mutat. Res.* (2014). doi:10.1016/j.mrrev.2014.01.001
5. Jackson, S. P. & Bartek, J. The DNA-damage response in human biology and disease. *Nature* **461,** 1071–1078 (2010).
6. Ward, J. F. DNA Damage Produced by Ionizing Radiation in Mammalian Cells: Identities, Mechanisms of Formation, and Reparability. *Prog. Nucleic Acid Res. Mol. Biol.* **35,** 95–125 (1988).
7. Baskar, R., Dai, J., Wenlong, N., Yeo, R. & Yeoh, K.-W. Biological response of cancer cells to radiation treatment. *Front. Mol. Biosci.* **1,** 1–9 (2014).
8. Seong, K. M. *et al.* Intrinsic radiosensitivity correlated with radiation-induced ROS and cell cycle regulation. *Mol. Cell. Toxicol.* **6,** 1–7 (2010).
9. Moding, E. J., Kastan, M. B. & Kirsch, D. G. Strategies for optimizing the response of cancer and normal tissues to radiation. *Nat. Rev. Drug Discov.* **12,** 526–542 (2013).
10. Haber, J. E. Partners and pathways - Repairing a double-strand break. *Trends Genet.* **16,** 259–264 (2000).
11. Takata, M. *et al.* Homologous recombination and non-homologous end-joining pathways of DNA double-strand break repair have overlapping roles in the maintenance of chromosomal integrity in vertebrate cells. *EMBO J.* **17,** 5497–5508 (1998).
12. Albertini, R. J. *et al.* IPCS guidelines for the monitoring of genotoxic effects of carcinogens in humans. *Mutat. Res. - Rev. Mutat. Res.* **463,** 111–172 (2000).
13. Rothkamm, K. & Lobrich, M. Misrepair of radiation-induced DNA double-strand breaks and its relevance for tumorigenesis and cancer treatment (review). *Int. J. Oncol.* **21,** 433–440 (2002).
14. Olive, P. The role of DNA single-and double-strand breaks in cell killing by ionizing radiation. *Radiat. Res.* **150,** S42-51 (1998).
15. Lim, Y. C. *et al.* Increased sensitivity to ionizing radiation by targeting the homologous recombination pathway in glioma initiating cells. *Mol. Oncol.* **8,** 1603–1615 (2014).

16. Uchida, N. *et al.* Direct isolation of human central nervous system stem cells. *Pnas* **97,** 14720–5 (2000).
17. Altaner, C. {Glioblastoma and stem cells - Minireview}. *{Neoplasma}* **{55},** 369–374 (2008).
18. Ohka, F., Natsume, A. & Wakabayashi, T. Current trends in targeted therapies for glioblastoma multiforme. *Neurol. Res. Int.* **2012,** (2012).
19. Thakkar, J. P. *et al.* Epidemiologic and molecular prognostic review of glioblastoma. *Cancer Epidemiol. Biomarkers Prev.* **23,** 1985–1996 (2014).
20. Hanif, F., Muzaffar, K., Perveen, K., Malhi, S. M. & Simjee, S. U. Glioblastoma Multiforme: A Review of its Epidemiology and Pathogenesis through Clinical Presentation and Treatment. *Asian Pac. J. Cancer Prev.* **18,** 3–9 (2017).
21. Somasundaram, K. *Advances in biology and treatment of Glioblastoma*. (2017).
22. Walker, M. D., Strike, T. A. & Sheline, G. E. An analysis of dose-effect relationship in the radiotherapy of malignant gliomas. *Int. J. Radiat. Oncol. Biol. Phys.* **5,** 1725–1731 (1979).
23. Lara-Velazquez, M. *et al.* Advances in brain tumor surgery for glioblastoma in adults. *Brain Sci.* **7,** 1–16 (2017).
24. Ferrandon, S. *et al.* Cellular and molecular portrait of eleven human glioblastoma cell lines under photon and carbon ion irradiation. *Cancer Lett.* **360,** 10–16 (2015).
25. Pasi, F. *et al.* Uptake of 18F-FET and 18F-FCH in Human Glioblastoma T98G Cell Line after Irradiation with Photons or Carbon Ions. *Contrast Media Mol Imaging* **2017,** 6491674 (2017).
26. Berardinelli, F. *et al.* The G-quadruplex-stabilizing ligand RHPS4 enhances sensitivity of U251MG glioblastoma cells to clinical carbon ion beams. *FEBS J.* (2018). doi:10.1111/febs.14415
27. Orecchia, R., Krengli, M., Jereczek-Fossa, B. A., Franzetti, S. & Gerard, J. P. Clinical and research validity of hadrontherapy with ion beams. *Crit. Rev. Oncol. Hematol.* **51,** 81–90 (2004).
28. Mannino, M. & Chalmers, A. J. Radioresistance of glioma stem cells: Intrinsic characteristic or property of the 'microenvironment-stem cell unit'? *Mol. Oncol.* **5,** 374–386 (2011).
29. Lapidot, T. *et al.* A cell initiating human acute myeloid leukaemia after transplantation into SCID mice. *Nature* **367,** 645–648 (1994).
30. Ignatova, T. N. *et al.* Human cortical glial tumors contain neural stem-like cells expressing astroglial and neuronal markers in vitro. *Glia* **39,** 193–206 (2002).
31. Dick, J. E. Looking ahead in cancer stem cell research. *Nat. Biotechnol.* **27,** 44–46 (2009).
32. Foo, J., Leder, K. & Michor, F. Stochastic dynamics of cancer initiation. *Phys. Biol.* **8,** (2011).
33. Nowell, P. C. The clonal evolution of tumor cell populations. *Science*

(80-.). **194,** 23–28 (1976).
34. Greaves, M. & Maley, C. C. Clonal evolution in cancer. *Nature* **481,** 306–313 (2012).
35. Tannishtha, R., Morrison, S. J., Clarke, M. F. & Weissman, I. L. Stem cells, cancer, and cancer stem cells. *Nature* **414,** 105–111 (2001).
36. Sheila K. Singh, Ian D. Clarke, Mizuhiko Terasaki, Victoria E. Bonn, Cynthia Hawkins, Jeremy Squire, A. *et al.* Identification of a cancer stem cell in human brain tumors. *Cancer Res* **63,** 5821–5828 (2003).
37. Climate, B., Dyck, V., Phylogenies, T. F. & Compare, E. P. Identification of human brain tumour initiating cells. **432,** (2004).
38. Kreso, A. & Dick, J. E. Evolution of the Cancer Stem Cell Model. *Cell Stem Cell* **14,** 275–291 (2014).
39. Sanai, N., Alvarez-Buylla, A. & Berger, M. S. Neural Stem Cells and the Origin of Gliomas. *N. Engl. J. Med.* **353,** 811–822 (2005).
40. Cho, D. *et al.* Targeting cancer stem cells for treatment of glioblastoma multiforme. *Cell Transplant.* **22,** 731–9 (2013).
41. Galli, R. *et al.* Isolation and Characterization of Tumorigenic , Stem-like Neural Precursors from Human Glioblastoma Isolation and Characterization of Tumorigenic , Stem-like Neural Precursors from Human Glioblastoma. *Cancer Res.* **64,** 7011–7021 (2004).
42. Beier, D. *et al.* CD133+ and CD133- glioblastoma-derived cancer stem cells show differential growth characteristics and molecular profiles. *Cancer Res.* **67,** 4010–4015 (2007).
43. Ogden, Alfred T, Waziri, Allen E, Lochhead, RA, Fusco, D, Lopez, K, Ellis, JA, Kang, J, Assanah, M, Sisti, MB, McCormick, PC, Canoll, P, Bruce, J. Identification of a2B5+Cd133– Tumorinitiating Cells in Adult Human Gliomas. *Neurosurgery* **62,** 505–515 (2008).
44. Liu, G. *et al.* Analysis of gene expression and chemoresistance of CD133+ cancer stem cells in glioblastoma. *Mol. Cancer* **5,** 1–12 (2006).
45. Bao, S. *et al.* Glioma stem cells promote radioresistance by preferential activation of the DNA damage response. *Nature* **444,** 756–760 (2006).
46. Pallini, R. *et al.* Cancer stem cell analysis and clinical outcome in patients with glioblastoma multiforme. *Clin. Cancer Res.* **14,** 8205–8212 (2008).
47. Gangemi, R. M. R. *et al.* SOX2 Silencing in Glioblastoma Tumor-Initiating Cells Causes Stop of Proliferation and Loss of Tumorigenicity. *Stem Cells* **27,** 40–48 (2009).
48. Ligon, K. L. *et al.* Olig2-Regulated Lineage-Restricted Pathway Controls Replication Competence in Neural Stem Cells and Malignant Glioma. *Neuron* **53,** 503–517 (2007).
49. Kim, J., Woo, A. J., Chu, J. & Snow, J. W. A Myc rather than core pluripotency module accounts for the shared signatures of embryonic stem and cancer cells. *Cell* **143,** 313–324 (2010).
50. Tunici, P. *et al.* Genetic alterations and in vivo tumorigenicity of neurospheres derived from an adult glioblastoma. *Mol. Cancer* **3,** 1–5 (2004).

51. Sherry, M. M., Reeves, A., Wu, J. K. & Cochran, B. H. STAT3 is required for proliferation and maintenance of multipotency in glioblastoma stem cells. *Stem Cells* **27,** 2383–2392 (2009).
52. Hemmati, H. D. *et al.* Cancerous stem cells can arise from pediatric brain tumors. *Proc. Natl. Acad. Sci.* **100,** 15178–15183 (2003).
53. Ben-Porath, I. *et al.* An embryonic stem cell-like gene expression signature in poorly differentiated aggressive human tumors. *Nat. Genet.* **40,** 499–507 (2008).
54. Suvà, M. L. *et al.* Reconstructing and reprogramming the tumor-propagating potential of glioblastoma stem-like cells. *Cell* **157,** 580–594 (2014).
55. Ahmed, S. U. *et al.* Selective inhibition of parallel DNA damage response pathways optimizes radiosensitization of glioblastoma stem-like cells. *Cancer Res.* **75,** 4416–4428 (2015).
56. Cheng, L. *et al.* L1CAM regulates DNA damage checkpoint response of glioblastoma stem cells through NBS1. *EMBO J.* **30,** 800–813 (2011).
57. Bartkova, J. *et al.* Replication stress and oxidative damage contribute to aberrant constitutive activation of DNA damage signalling in human gliomas. *Oncogene* **29,** 5095–5102 (2010).
58. Galia, A. *et al.* PARP-1 protein expression in glioblastoma multiforme. *Eur. J. Histochem.* **56,** 9 (2012).
59. Fouse, S. D., Nakamura, J. L., James, C. D., Chang, S. & Costello, J. F. Response of primary glioblastoma cells to therapy is patient specific and independent of cancer stem cell phenotype. *Neuro. Oncol.* **16,** 361–371 (2014).
60. Welsh, J. W. *et al.* Rad51 Protein Expression and Survival in Patients with Glioblastoma Multiforme. *Int. J. Radiat. Oncol. Biol. Phys.* **74,** 1251–1255 (2009).
61. Balbous, A. *et al.* A radiosensitizing effect of RAD51 inhibition in glioblastoma stem-like cells. *BMC Cancer* **16,** 1–13 (2016).
62. King, H. O. *et al.* RAD51 Is a Selective DNA Repair Target to Radiosensitize Glioma Stem Cells. *Stem Cell Reports* **8,** 125–139 (2017).
63. Ruíz, G. *et al.* Inhibition of RAD51 by siRNA and resveratrol sensitizes cancer stem cells derived from hela cell cultures to apoptosis. *Stem Cells Int.* **2018,** (2018).
64. Stupp, R., Hegi, M. E., Gilbert, M. R. & Chakravarti, A. Chemoradiotherapy in malignant glioma: Standard of care and future directions. *J. Clin. Oncol.* **25,** 4127–4136 (2007).
65. Ahn, G. O. & Brown, J. M. Influence of bone marrow-derived hematopoietic cells on the tumor response to radiotherapy: experimental models and clinical perspectives. *Cell Cycle* **8,** 970–976 (2009).
66. Jain, R. K. Normalization of tumor vasculature : An emerging concept in angiogenic therapy. *Science (80-.).* **307,** 58–62 (2005).
67. Vredenburgh, J. J. *et al.* Bevacizumab plus irinotecan in recurrent glioblastoma multiforme. *J. Clin. Oncol.* **25,** 4722–4729 (2007).

68. Vredenburgh, J. J. *et al.* The Addition of Bevacizumab to Standard Radiation Therapy and Temozolomide Followed by Bevacizumab, Temozolomide and Irinotecan for Newly Diagnosed Glioblastoma. *Clin. Cancer Res.* **17,** 4119–4124 (2011).
69. Chinot, O. L. *et al.* AVAglio: Phase 3 trial of bevacizumab plus temozolomide and radiotherapy in newly diagnosed glioblastoma multiforme. *Adv. Ther.* **28,** 334–340 (2011).
70. Ohgaki, H. & Kleihues, P. Genetic alterations and signaling pathways in the evolution of gliomas. *Cancer Sci.* **100,** 2235–2241 (2009).
71. Rich, J. N. *et al.* Phase II trial of gefitinib in recurrent glioblastoma. *J. Clin. Oncol.* **22,** 133–142 (2004).
72. Van Den Bent, M. J. *et al.* Randomized phase II trial of erlotinib versus temozolomide or carmustine in recurrent glioblastoma: EORTC brain tumor group study 26034. *J. Clin. Oncol.* **27,** 1268–1274 (2009).
73. Schmidt, J. C. & Cech, T. R. Human telomerase : biogenesis , trafficking , recruitment , and activation. 1095–1105 (2015). doi:10.1101/gad.263863.115.GENES
74. McClintock, B. The Stability of Broken Ends of Chromosomes in Zea Mays. *Genetics* **26,** 234–282 (1941).
75. Blackburn, E. H. Structure and function of telomeres. *Nature* **350,** 569–573 (1991).
76. Lu, W., Zhang, Y., Liu, D., Songyang, Z. & Wan, M. Telomeres-structure, function, and regulation. *Exp. Cell Res.* **319,** 133–141 (2013).
77. Sfeir, A. Telomeres at a glance. *J. Cell Sci.* **125,** 4173–8 (2012).
78. Blasco, M. a. Mammalian telomeres and telomerase: why they matter for cancer and aging. *Eur. J. Cell Biol.* **82,** 441–6 (2003).
79. De Lange, T. Shelterin: The protein complex that shapes and safeguards human telomeres. *Genes Dev.* **19,** 2100–2110 (2005).
80. Marion, R. M. *et al.* Telomeres Acquire Embryonic Stem Cell Characteristics in Induced Pluripotent Stem Cells. *Cell Stem Cell* **4,** 141–154 (2009).
81. Blasco, M. A. Telomerase beyond telomeres. *Nat. Rev. Cancer* **2,** 627–632 (2002).
82. Griffith, J. D. *et al.* Mammalian telomeres end in a large duplex loop. *Cell* **97,** 503–514 (1999).
83. Grandin, N. & Charbonneau, M. Protection against chromosome degradation at the telomeres. *Biochimie* **90,** 41–59 (2008).
84. Sundquist, W. I. & Klug, A. Telomeric DNA dimerizes by formation of guanine tetrads between hairpin loops. *Nature* **342,** 825–829 (1989).
85. Gellert, M., Lipsett, M. N. & Davies, D. R. Helix Formation By Guanylic Acid. *Proc. Natl. Acad. Sci.* **48,** 2013–2018 (1962).
86. Zimmerman, S. B., Cohen, G. H. & Davies, D. R. X-ray fiber diffraction and model-building study of polyguanylic acid and polyinosinic acid. *J. Mol. Biol.* **92,** 181–192 (1975).
87. Arnott, S., Chandrasekaran, R. & Marttila, C. M. Structures for

polyinosinic acid and polyguanylic acid. *Biochem. J.* **141,** 537–543 (1974).
88. Howard, F. B., Frazier, J. & Miles, H. T. Stable and Metastable Forms of Poly (G). *Biopolymers* **16,** 791–809 (1977).
89. Williamson, J. R. G-Quartet Structures I N Telomeric Dna. *Annu.Rev.Biophys.Biomol.Sruct* **23,** 703–730 (1994).
90. Ambrus, A. *et al.* Human telomeric sequence forms a hybrid-type intramolecular G-quadruplex structure with mixed parallel/antiparallel strands in potassium solution. *Nucleic Acids Res.* **34,** 2723–2735 (2006).
91. Burge, S., Parkinson, G. N., Hazel, P., Todd, A. K. & Neidle, S. Quadruplex DNA: Sequence, topology and structure. *Nucleic Acids Res.* **34,** 5402–5415 (2006).
92. Lane, A. N., Chaires, J. B., Gray, R. D. & Trent, J. O. Stability and kinetics of G-quadruplex structures. **36,** 5482–5515 (2008).
93. Paeschke, K., Simonsson, T., Postberg, J., Rhodes, D. & Lipps, H. J. Telomere end-binding proteins control the formation of G-quadruplex DNA structures in vivo. **12,** 847–854 (2005).
94. Lam, E. Y. N., Beraldi, D., Tannahill, D. & Balasubramanian, S. G-quadruplex structures are stable and detectable in human genomic DNA. *Nat. Commun.* **4,** 1796 (2013).
95. Zahler, A. M., Williamson, J. R., Cech, T. R. & Prescott, D. M. Inhibition of telomerase by G-quartet DMA structures. *Nature* **350,** 718–720 (1991).
96. Rhodes, D. & Lipps, H. J. Survey and summary G-quadruplexes and their regulatory roles in biology. *Nucleic Acids Res.* **43,** 8627–8637 (2015).
97. Huppert, J. L. & Balasubramanian, S. Prevalence of quadruplexes in the human genome. **33,** 2908–2916 (2005).
98. Todd, A. K., Johnston, M. & Neidle, S. Highly prevalent putative quadruplex sequence motifs in human DNA. **33,** 2901–2907 (2005).
99. Palm, W. & de Lange, T. How Shelterin Protects Mammalian Telomeres. *Annu. Rev. Genet.* **42,** 301–334 (2008).
100. Zhong, Z., Shiue, L., Kaplan, S. & de Lange, T. A mammalian factor that binds telomeric TTAGGG repeats in vitro. *Mol. Cell. Biol.* **12,** 4834–4843 (1992).
101. Chong, L. *et al.* A human telomeric protein. *Science (80-.).* **270,** 1663–1667 (1995).
102. Van Steensel, B. & De Lange, T. Control of telomere length by the human telomeric protein TRF1. *Nature* **385,** 740–743 (1997).
103. Richter, T. *et al.* TRF2 overexpression diminishes repair of telomeric single-strand breaks and accelerates telomere shortening in human fibroblasts. *Mech. Ageing Dev.* **128,** 340–345 (2007).
104. Lazzerini-Denchi, E. & Sfeir, A. Stop pulling my strings [mdash] what telomeres taught us about the DNA damage response. *Nat Rev Mol Cell Biol* **17,** 364–378 (2016).
105. Lei, M., Podell, E. R. & Cech, T. R. Structure of human POT1 bound to

telomeric single-stranded DNA provides a model for chromosome end-protection. *Nat. Struct. Mol. Biol.* **11,** 1223–1229 (2004).
106. Bryan, T. M., Englezou, A., Dalla-Pozza, L., Dunham, M. A. & Reddel, R. R. Evidence for an alternative mechanism for maintaining telomere length in human tumors and tumor-derived cell lines. *Nat. Med.* **3,** 1271–1274 (1997).
107. O'Sullivan, R. J. & Karlseder, J. Telomeres: Protecting chromosomes against genome instability. *Nat. Rev. Mol. Cell Biol.* **11,** 171–181 (2010).
108. Harley, C. B. Telomere loss: mitotic clock or genetic time bomb? *Mutat. Res. DNAging* **256,** 271–282 (1991).
109. Dahse, R., Fiedler, W. & Ernst, G. Telomeres and telomerase: biological and clinical importance. *Clin. Chem.* **43,** 708–14 (1997).
110. Wright, W. E. & Shay, J. W. Historical claims and current interpretations of replicative aging. *Nat. Biotechnol.* **20,** 682–688 (2002).
111. Harley, C. B., Futcher, A. B. & Greider, C. W. Telomeres shorten during ageing of human fibroblasts. *Nature* **345,** 458–460 (1990).
112. Smith, J. R. & Hayflick, L. Variation in the life-span of clones derived from human diploid cell strains. *J. Cell Biol.* **62,** 48–53 (1974).
113. Shay, J. W., Pereira-Smith, O. M. & Wright, W. E. A role for both RB and p53 in the regulation of human cellular senescence. *Exp. Cell Res.* **196,** 33–39 (1991).
114. He, S. & Sharpless, N. E. Senescence in Health and Disease. *Cell* **169,** 1000–1011 (2017).
115. Kim, S. H., Kaminker, P. & Campisi, J. Telomeres, aging and cancer: In search of a happy ending. *Oncogene* **21,** 503–511 (2002).
116. Wright, W. E., Pereira-Smith, O. M. & Shay, J. W. Reversible cellular senescence: implications for immortalization of normal human diploid fibroblasts. *Mol. Cell. Biol.* **9,** 3088–3092 (1989).
117. Verdun, R. E. & Karlseder, J. Replication and protection of telomeres. *Nature* **447,** 924–931 (2007).
118. Artandi, S. E. & Attardi, L. D. Pathways connecting telomeres and p53 in senescence, apoptosis, and cancer. *Biochem. Biophys. Res. Commun.* **331,** 881–890 (2005).
119. Counter, C. M. *et al.* Telomere shortening associated with chromosome instability is arrested in immortal cells which express telomerase activity. *EMBO J.* **1,** 921–1929 (1992).
120. Maciejowski, J. & de Lange, T. Telomeres in cancer: tumour suppression and genome instability. *Nat. Rev. Mol. Cell Biol.* (2017). doi:10.1038/nrm.2016.171
121. And, G. A. & Lansdorp, P. M. Telomeres and Aging in Mammals. *Physiol. Rev.* 557–579 (2008). doi:10.1152/physrev.00026.2007.
122. Denchi, E. L. & de Lange, T. Protection of telomeres through independent control of ATM and ATR by TRF2 and POT1. *Nature* **448,** 1068–1071 (2007).
123. Kirk, K. E. *et al.* Block in Anaphase Chromosome Separation Caused by

a Telomerase Template Mutation. **275,** 1478–1481 (1997).
124. Hinchcliffe, E. H. *et al.* Chromosome missegregation during anaphase triggers p53 cell cycle arrest through histone H3.3 Ser31 phosphorylation. *Nat. Cell Biol.* **18,** 668–675 (2016).
125. Lengauer, C., Kinzler, K. W. & Vogelstein, B. Genetic instabilities in human cancers. *Nature* **396,** 643–649 (1998).
126. Londoño-Vallejo, J. A., Der-Sarkissian, H., Cazes, L., Bacchetti, S. & Reddel, R. R. Alternative Lengthening of Telomeres Is Characterized by High Rates of Telomeric Exchange. *Cancer Res.* **64,** 2324–2327 (2004).
127. Greider, C. W. & Blackburn, E. H. Identification of a specific telomere terminal transferase activity in tetrahymena extracts. *Cell* **43,** 405–413 (1985).
128. Collins, K. & Mitchell, J. R. Telomerase in the human organism. *Oncogene* **21,** 564–579 (2002).
129. Ducrest, A. L., Szutorisz, H., Lingner, J. & Nabholz, M. Regulation of the human telomerase reverse transcriptase gene. *Oncogene* **21,** 541–552 (2002).
130. Blackburn, E. H., Greider, C. W. & Szostak, J. W. Telomeres and telomerase: The path from maize, Tetrahymena and yeast to human cancer and aging. *Nat. Med.* **12,** 1133–1138 (2006).
131. Wong, J. M. Y. & Collins, K. Telomerase RNA level limits telomere maintenance in X-linked dyskeratosis congenita. *Genes Dev.* **20,** 2848–2858 (2006).
132. Armanios, M. & Blackburn, E. H. The telomere syndromes. *Nat. Rev. Genet.* **13,** 693–704 (2012).
133. Shay, J. W. & Wright, W. E. Telomeres and telomerase in normal and cancer stem cells. *FEBS Lett.* **584,** 3819–25 (2010).
134. Stewart, S. A. & Weinberg, R. A. Telomerase and human tumorigenesis. *Semin. Cancer Biol.* **10,** 399–406 (2000).
135. Artandi, S. E. & DePinho, R. A. Telomeres and telomerase in cancer. *Carcinogenesis* **31,** 9–18 (2009).
136. Horn, S. *et al.* TERT Promoter Mutations in Familial and Sporadic Melanoma. *Science (80-.).* **339,** 959–961 (2013).
137. Huang, F. W., Hodis, E., Xu, M. J., Kryukov, G. V & Garraway, L. A. Highly recurrent TERT promoter mutations in human melanoma. *Science (80-.).* **339,** 957–959 (2013).
138. Kim, N. W. *et al.* Specific association of human telomerase activity with immortal cells and cancer. *Science (80-.).* **226,** 2011–2015 (1994).
139. Pickett, H. A. & Reddel, R. R. Molecular mechanisms of activity and derepression of alternative lengthening of telomeres. *Nat. Struct. Mol. Biol.* **22,** 875–880 (2015).
140. Cesare, A. J. & Reddel, R. R. Alternative lengthening of telomeres: Models, mechanisms and implications. *Nat. Rev. Genet.* **11,** 319–330 (2010).
141. Dunham, M. a, Neumann, A. a, Fasching, C. L. & Reddel, R. R.

Telomere maintenance by recombination in human cells. *Nat. Genet.* **26,** 447–450 (2000).
142. Reddel, R. Telomere Maintenance Mechanisms in Cancer: Clinical Implications. *Curr. Pharm. Des.* **20,** 6361–6374 (2014).
143. Gaspar, T. B. *et al.* Telomere maintenance mechanisms in cancer. *Genes (Basel).* **9,** (2018).
144. Genescà, A. *et al.* Telomere dysfunction: A new player in radiation sensitivity. *BioEssays* **28,** 1172–1180 (2006).
145. Soler, D., Pampalona, J., Tusell, L. & Genescà, A. Radiation sensitivity increases with proliferation-associated telomere dysfunction in nontransformed human epithelial cells. *Aging Cell* **8,** 414–425 (2009).
146. Ayouaz, A., Raynaud, C., Heride, C., Revaud, D. & Sabatier, L. Telomeres: Hallmarks of radiosensitivity. *Biochimie* **90,** 60–72 (2008).
147. Hande, M. P., Balajee, a S., Tchirkov, a, Wynshaw-Boris, a & Lansdorp, P. M. Extra-chromosomal telomeric DNA in cells from Atm(-/-) mice and patients with ataxia-telangiectasia. *Hum. Mol. Genet.* **10,** 519–528 (2001).
148. Callén, E. & Surrallés, J. Telomere dysfunction in genome instability syndromes. *Mutat. Res. - Rev. Mutat. Res.* **567,** 85–104 (2004).
149. Ranganathan, V. *et al.* Rescue of a telomere length defect of Nijmegen breakage syndrome cells requires NBS and telomerase catalytic subunit. *Curr. Biol.* **11,** 962–966 (2001).
150. Callén, E. *et al.* Breaks at telomeres and TRF2-independent end fusions in Fanconi anemia. *Hum. Mol. Genet.* **11,** 439–444 (2002).
151. Cabuy, E. *et al.* Accelerated telomere shortening and telomere abnormalities in radiosensitive cell lines. *Radiat. Res.* **164,** 53–62 (2005).
152. Hernández, L. *et al.* Aging and radiation: bad companions. *Aging Cell* **14,** 153–161 (2015).
153. Lange, T. de. Telomere biology and DNA repair: Enemies with benefits. *FEBS Lett.* **584,** 3673–3674 (2010).
154. Verdun, R. E., Crabbe, L., Haggblom, C. & Karlseder, J. Functional human telomeres are recognized as DNA damage in G2 of the cell cycle. *Mol. Cell* **20,** 551–561 (2005).
155. Zhu, X. D., Küster, B., Mann, M., Petrini, J. H. J. & De Lange, T. Cell-cycle-regulated association of RAD50/MRE11/NBS1 with TRF2 and human telomeres. *Nat. Genet.* **25,** 347–352 (2000).
156. Latre, L. *et al.* Shortened telomeres join to DNA breaks interfering with their correct repair. *Exp. Cell Res.* **287,** 282–288 (2003).
157. Goytisolo, F. A. *et al.* Short telomeres result in organismal hypersensitivity to ionizing radiation in mammals. *J. Exp. Med.* **192,** 1625–36 (2000).
158. Wong, K. K. *et al.* Telomere dysfunction impairs DNA repair and enhances sensitivity to ionizing radiation. *Nat. Genet.* **26,** 85–88 (2000).
159. Mcilrath, J. *et al.* Telomere Length Abnormalities in Mammalian Radiosensitive Cells Advances in Brief Telomere Length Abnormalities

in Mammalian Radiosensitive Cells 1. *Cancer Res.* 912–915 (2001).
160. Sprung, C. N., Davey, D. S. P., Goh, S. K., Radford, I. R. & McKay, M. J. Uncoupling of telomere length and radiosensitivity in mouse lymphoma cell lines of similar genetic background. *Int. J. Radiat. Biol.* **83,** 515–521 (2007).
161. Fairlie, J. & Harrington, L. Enforced telomere elongation increases the sensitivity of human tumour cells to ionizing radiation. *DNA Repair (Amst).* **25,** 54–59 (2015).
162. Zhong, Y. H. *et al.* Telomere length inversely correlates with radiosensitivity in human carcinoma cells with the same tissue background. *Biochem. Biophys. Res. Commun.* **367,** 84–89 (2008).
163. Berardinelli, F., Coluzzi, E., Sgura, A. & Antoccia, A. Targeting telomerase and telomeres to enhance ionizing radiation effects in in vitro and in vivo cancer models. *Mutat. Res. - Rev. Mutat. Res.* **773,** 204–219 (2017).
164. Puri, N. & Girard, J. Novel therapeutics targeting telomerase and telomeres. *J. Cancer Sci. Ther.* **5,** 1–3 (2013).
165. Folini, M., Venturini, L., Cimino-Reale, G. & Zaffaroni, N. Telomeres as targets for anticancer therapies. *Expert Opin. Ther. Targets* **15,** 579–593 (2011).
166. Strahl, C. & Blackburn, E. H. The effects of nucleoside analogs telomeres in Tetrahymena telomerase and. **22,** 893–900 (1994).
167. Strahl, C. & Blackburn, E. H. Effects of reverse transcriptase inhibitors on telomere length and telomerase activity in two immortalized human cell lines. *Mol. Cell. Biol.* **16,** 53–65 (1996).
168. Datta, A. *et al.* Persistent inhibition of telomerase reprograms adult T-cell leukemia to p53-dependent senescence. *Blood* **108,** 1021–1029 (2006).
169. Damm, K. *et al.* A highly selective telomerase inhibitor limiting human cancer cell proliferation. *EMBO J.* **20,** 6958–6968 (2001).
170. Pascolo, E. *et al.* Mechanism of human telomerase inhibition by BIBR1532, a synthetic, non-nucleosidic drug candidate. *J. Biol. Chem.* **277,** 15566–15572 (2002).
171. Asai, A. *et al.* A novel telomerase template antagonist (GRN163) as a potential anticancer agent. *Cancer Res.* **63,** 3931–3939 (2003).
172. Marian, C. O. *et al.* The telomerase antagonist, imetelstat, efficiently targets glioblastoma tumor-initiating cells leading to decreased proliferation and tumor growth. *Clin. Cancer Res.* **16,** 154–163 (2010).
173. Takai Hiroyuki, Smogorzewska Agata, de L. T. DNA Damage Foci at Dysfunctional Telomeres. *Curr. Biol.* **13,** 1549–1556 (2003).
174. Goldkorn, A. & Blackburn, E. H. Assembly of mutant-template telomerase RNA into catalytically active telomerase ribonucleoprotein that can act on telomeres is required for apoptosis and cell cycle arrest in human cancer cells. *Cancer Res.* **66,** 5763–5771 (2006).
175. Folini, M., Gandellini, P. & Zaffaroni, N. Targeting the telosome:

therapeutic implications. *Biochim. Biophys. Acta* **1792,** 309–16 (2009).
176. Yang, Q. *et al.* POT1 and TRF2 Cooperate To Maintain Telomeric Integrity. *Mol. Cell. Biol.* **25,** 1070–1080 (2005).
177. Sarraf, S. A. & Harper, J. W. Telomeric TuRF1 Wars. *Dev. Cell* **18,** 167–168 (2010).
178. Neidle, S. & Read, M. A. G-quadruplexes as therapeutic targets. *Biopolymers* **56,** 195–208 (2000).
179. Riou, J. F. *et al.* Cell senescence and telomere shortening induced by a new series of specific G-quadruplex DNA ligands. *Proc. Natl. Acad. Sci.* **99,** 2672–2677 (2002).
180. Cian, A. De *et al.* Action R ?? valuation of telomerase inhibition by quadruplex ligands and their mechanisms of action. (2016). doi:10.1073/pnas.0707365104
181. Sun, D. *et al.* Inhibition of Human Telomerase by a G-Quadruplex-Interactive Compound. **2623,** 2113–2116 (1997).
182. Gowan, S. M., Heald, R., Stevens, M. F. & Kelland, L. R. Potent inhibition of telomerase by small-molecule pentacyclic acridines capable of interacting with G-quadruplexes. *Mol. Pharmacol.* **60,** 981–988 (2001).
183. Salvati, E. *et al.* Telomere damage induced by the G-quadruplex ligand RHPS4 has an antitumor effect. *J. Clin. Invest.* **117,** 3236–3247 (2007).
184. Leonetti, C. *et al.* G-Quadruplex Ligand RHPS4 Potentiates the Antitumor Activity of Camptothecins in Preclinical Models of Solid Tumors G-Quadruplex Ligand RHPS4 Potentiates the Antitumor Activity umors. 7284–7291 (2008). doi:10.1158/1078-0432.CCR-08-0941
185. Phatak, P. *et al.* Telomere uncapping by the G-quadruplex ligand RHPS4 inhibits clonogenic tumour cell growth in vitro and in vivo consistent with a cancer stem cell targeting mechanism. *Br. J. Cancer* **96,** 1223–33 (2007).
186. Merle, P. *et al.* Telomere Targeting with a New G4 Ligand Enhances Radiation-Induced Killing of Human Glioblastoma Cells. *Mol. Cancer Ther.* **10,** 1784–1795 (2011).
187. Berardinelli, F. *et al.* The G-quadruplex-stabilising agent RHPS4 induces telomeric dysfunction and enhances radiosensitivity in glioblastoma cells. *DNA Repair (Amst).* **25,** 104–115 (2015).
188. Rizzo, A. *et al.* Stabilization of quadruplex DNA perturbs telomere replication leading to the activation of an ATR-dependent ATM signaling pathway. *Nucleic Acids Res.* **37,** 5353–5364 (2009).
189. Siddiqui-Jain, A., Grand, C. L., Bearss, D. J. & Hurley, L. H. Direct evidence for a G-quadruplex in a promoter region and its targeting with a small molecule to repress c-MYC transcription. *Proc. Natl. Acad. Sci. U. S. A.* **99,** 11593–8 (2002).
190. Salvati, E. *et al.* Evidence for G-quadruplex in the promoter of vegfr-2 and its targeting to inhibit tumor angiogenesis. *Nucleic Acids Res.* **42,**

2945–2957 (2014).
191. Nadai, M. *et al.* Assessment of gene promoter G-quadruplex binding and modulation by a naphthalene diimide derivative in tumor cells. *Int. J. Oncol.* **46,** 369–380 (2015).
192. Soohoo, C. Y. *et al.* Telomerase inhibitor PinX1 provides a link between TRF1 and telomerase to prevent telomere elongation. *J. Biol. Chem.* **286,** 3894–3906 (2011).
193. Li, H.-L. *et al.* PinX1: structure, regulation and its functions in cancer. *Oncotarget* **7,** 66267–66275 (2016).
194. Berardinelli, F. *et al.* The G-quadruplex-stabilizing ligand RHPS4 enhances sensitivity of U251MG glioblastoma cells to clinical carbon ion beams. *FEBS J.* **285,** 1226–1236 (2018).
195. Doria, F. *et al.* Hybrid ligand–alkylating agents targeting telomeric G-quadruplex structures. *Org. Biomol. Chem.* **10,** 2798 (2012).
196. Strahl, B. D. & Allis, C. D. The language of covalent histone modifications. *Nature* **403,** 41–45 (2000).
197. Sfeir, A. *et al.* Mammalian Telomeres Resemble Fragile Sites and Require TRF1 for Efficient Replication. *Cell* **138,** 90–103 (2009).
198. Eramo, A. *et al.* Chemotherapy resistance of glioblastoma stem cells [2]. *Cell Death Differ.* **13,** 1238–1241 (2006).
199. Milano, M. T. *et al.* Single- and Multi-Fraction Stereotactic Radiosurgery Dose Tolerances of the Optic Pathways. *Int. J. Radiat. Oncol. Biol. Phys.* (2018). doi:10.1016/j.ijrobp.2018.01.053
200. Perner, S. *et al.* Quantifying telomere lengths of human individual chromosome arms by centromere-calibrated fluorescence in situ hybridization and digital imaging. *Am J Pathol* **163,** 1751–1756 (2003).
201. Berardinelli, F. *et al.* Transient activation of the ALT pathway in human primary fibroblasts exposed to high-LET radiation. *Radiat. Res.* **174,** 539–49 (2010).
202. Choi, K. H. *et al.* The OB-fold domain 1 of human POT1 recognizes both telomeric and non-telomeric DNA motifs. *Biochimie* **115,** 17–27 (2015).
203. Chaires, J. B. *et al.* An improved model for the hTERT promoter quadruplex. *PLoS One* **9,** 1–13 (2014).
204. Palumbo, S. M. L., Ebbinghaus, S. W. & Hurley, L. H. Formation of a unique end-to-end stacked pair of G-quadruplexes in the hTERT core promoter with implications for inhibition of telomerase by G-quadruplex-interactive ligands. *J. Am. Chem. Soc.* **131,** 10878–10891 (2009).
205. Zhou, X. Z. & Lu, K. P. The Pin2/TRF1-interacting protein PinX1 is a potent telomerase inhibitor. *Cell* **107,** 347–359 (2001).
206. Kondo, T. *et al.* Loss of heterozygosity and histone hypoacetylation of the PINX1 gene are associated with reduced expression in gastric carcinoma. *Oncogene* **24,** 157–164 (2005).
207. Cai, M. Y. *et al.* Decreased expression of PinX1 protein is correlated with tumor development and is a new independent poor prognostic factor

in ovarian carcinoma. *Cancer Sci.* **101,** 1543–1549 (2010).
208. Shi, R. *et al.* The role of PinX1 in growth control of breast cancer cells and its potential molecular mechanism by mRNA and lncRNA expression profiles screening. *Biomed Res. Int.* **2014,** (2014).
209. Yang, L. *et al.* Telomere-binding protein TPP1 modulates telomere homeostasis and confers radioresistance to human colorectal cancer cells. *PLoS One* **8,** 1–11 (2013).
210. Abraham, R. T. cell cycle checkpoint signaling therough the ATM an ATR kinases.pdf. *Genes Dev.* **15,** 2177–2196 (2001).
211. McGowan, C. H. & Russell, P. The DNA damage response: Sensing and signaling. *Curr. Opin. Cell Biol.* **16,** 629–633 (2004).
212. Durocher, D. & Jackson, S. P. DNA-PK, ATM and ATR as sensors of DNA damage: Variations on a theme? *Curr. Opin. Cell Biol.* **13,** 225–231 (2001).
213. Chen, P. M. Y. & Du, Y. PinX1 inhibits cell proliferation, migration and invasion in glioma cells. *Med. Oncol.* **32,** 73 (2015).
214. Frosina, G. The bright and the dark sides of DNA repair in stem cells. *J. Biomed. Biotechnol.* **2010,** (2010).
215. Shervington, A., Lu, C., Patel, R. & Shervington, L. Telomerase downregulation in cancer brain stem cell. *Mol. Cell. Biochem.* **331,** 153–9 (2009).
216. Ricci-Vitiani, L. *et al.* Mesenchymal differentiation of glioblastoma stem cells. *Cell Death Differ.* **15,** 1491–1498 (2008).
217. Pecchia, I. *et al.* Glioblastoma Stem Cells: Radiobiological Response to Ionising Radiations of Different Qualities. *Radiat Prot Dosim.* 1–5 (2015). doi:10.1093/rpd/ncv299
218. D'Alessandris, Q. G. *et al.* The clinical value of patient-derived glioblastoma tumorspheres in predicting treatment response. *Neuro. Oncol.* **19,** 1097–1108 (2017).
219. Vannier, J. B., Pavicic-Kaltenbrunner, V., Petalcorin, M. I. R., Ding, H. & Boulton, S. J. RTEL1 dismantles T loops and counteracts telomeric G4-DNA to maintain telomere integrity. *Cell* **149,** 795–806 (2012).
220. Shi, W. *et al.* The role of RPA2 phosphorylation in homologous recombination in response to replication arrest. *Carcinogenesis* **31,** 994–1002 (2010).
221. Carruthers, R. D. *et al.* Replication stress drives constitutive activation of the DNA damage response and radioresistance in glioblastoma stem-like cells. *Cancer Res.* **78,** canres.0569.2018 (2018).
222. Osman, F. & Whitby, M. C. Exploring the roles of Mus81-Eme1/Mms4 at perturbed replication forks. *DNA Repair (Amst).* **6,** 1004–1017 (2007).
223. Drosopoulos, W. C., Kosiyatrakul, S. T. & Schildkraut, C. L. BLM helicase facilitates telomere replication during leading strand synthesis of telomeres. *J. Cell Biol.* **210,** 191–208 (2015).
224. Barefield, C. & Karlseder, J. The BLM helicase contributes to telomere maintenance through processing of late-replicating intermediate

structures. *Nucleic Acids Res.* **40,** 7358–7367 (2012).
225. Rizzo, A. *et al.* Identification of novel RHPS4-derivative ligands with improved toxicological profiles and telomere-targeting activities. *J. Exp. Clin. Cancer Res.* **33,** 1–8 (2014).
226. Lopergolo, A. *et al.* Targeting of RET oncogene by naphthalene diimide-mediated gene promoter G-quadruplex stabilization exerts anti-tumor activity in oncogene-addicted human medullary thyroid cancer. *Oncotarget* **7,** (2014).

APPENDIX A – Materials and Methods

Cell lines and culture conditions

U251MG (-Adh) cell line was purchased from Banca Biologica and Cell Factory (Banca Biologica and Cell Factor y, Genoa, Italy). AG01522 normal human primary fibroblasts (PD 18–25) were purchased from Coriell Institute (Camden, NJ, USA). U251MG was routinely maintained in minimum essential medium with Earle's balanced salt solution (MEM/EBSS) supplemented with 10% fetal bovine serum (FBS), 2 mM L-glutamine, 1 mM sodium Pyruvate, 1% non-essential aminoacids, 100 units/mL^{-1} penicillin and 100 µg/mL^{-1} streptomycin. AG01522 were maintained in EMEM/EBSS with 15% FBS, 2 mML-glutamine,1% non-essential aminoacids, 100 units/mL^{-1} penicillin and 100 µg/mL^{-1} streptomycin. For neurospheres generation (U251MG-Sph), U251MG cell line was cultured in NeuroCult™ Proliferation NS-A Basal Medium (Stemcell Technologies, Vancouver, Canada), complemented with NeuroCult™ NS-A Proliferation Supplement (Human), 20 ng/ml of recombinant human epidermal growth factor (EGF), 10 ng/mL of fibroblast growth factor-basic (b-FGF) and 2 µg/mL of heparin solution. GSCs were obtained from adult GBM patients (WHO grade IV), who had undergone complete or partial surgical resection at the Institute of Neurosurgery, Catholic University School of Medicine in Rome. Informed consent was obtained from the patients before surgery. The tumor tissue was mechanically dissociated and single cell suspension was cultured in a serum-free medium supplemented with epidermal growth factor and basic fibroblast growth factor, as previously described [1,2]. The *in vivo* tumorigenic potential of GSCs was evaluated by intracranial cell injection in immunocompromised mice, where GSCs were able to recapitulate the patient tumor in terms of antigen expression and histological tissue organization. All the aforementioned cell lines were maintained at 37°C in a 5% CO_2 95% air atmosphere. Unless otherwise specified, media and supplements for cell culture were purchased from Euroclone (Euroclone, Pero, MI, Italy) and the plasticware was purchased from Corning (Corning Life Sciences, NY, USA).

Subcutaneous xenograft model

Female (n=30) athymic mice (CD1 nude) were obtained from Charles River S.r.l. (Lecco, Italy), and housed in sterilized filter-topped cages kept in laminar flow isolators, fed with autoclaved food and water ad libitum and maintained in 12 h light/dark cycle. At 5-weeks of age all mice

received 0.25 ml subcutaneous injection of $7.5x10^6$ U251MG cells in 50% Matrigel (BD Biosciences, San Diego, CA) into one or both flanks. Inoculated animals were daily monitored and tumors measured with a caliper three times a week. Tumor dimension was estimated using the formula: Tumor volume = length x $width^2/2$. When tumor mass reached the volume of 800 mm^3, mice were randomized in four experimental groups: mice with double tumor mass for vehicle and RHPS4 groups while mice with single tumor mass for vehicle + 10Gy and RHPS4 + 10 Gy groups. RHPS4 (10 mg/kg per day) or PBS (vehicle) were administered through intravenous injection for 5 days, then mice were irradiated with a single dose of 10 Gy of X-rays. During the delivery time of 10 Gy, mice were lightly anesthetized with 35 mg/Kg of pentobarbital sodium and the body was shielded with 4 mm thick lead plates in order to irradiate only the tumor mass. After treatments, mice were daily monitored and tumor dimension recorded as described above. To evaluate differences in efficacy between treatment groups, the percentage of tumor growth inhibition (TGI) was calculated as follows: TGI(%) = (Vc-Vt)/(Vc-Vo)*100, where Vc, Vt are the median of control and treated groups at the end of the study and Vo at the start [3]. At necropsy, all tumors were removed and collected for histology and immunoblot analysis. Animal studies were performed according to the European Community Council Directive 2010/63/EU, approved by the local Ethical Committee for Animal Experiments of the ENEA and authorized by the Italian Ministry of Health (n° 690/2015-PR).

Chemical compounds

Tri- and tetra-substituted naphthalene diimide (NDI) ligands, namely H-NDI-NMe1 (C1), H-NDI-NMe2 (C2) and H-NDI-NMe6 (C6), were dissolved in dimethyl sulfoxide (DMSO), as also pentacyclic acridine, 3,11-difluoro-6,8,13-trimethyl-8Hquino[4,3,2-kl]acridinium methosulfate (RHPS4) (kindly provided by Malcolm Stevens, University of Notthingham, Notthingham, UK). The drugs were always added to the cells at least 8 h after plating. An appropriate volume of DMSO was employed as the negative control. For the *in vivo* study, RHPS4 was dissolved in PBS and administered intravenously (10 mg/kg per day) in nude mice. PBS only was administrated as negative control. Drugs were freshly prepared from frozen aliquots for each set of experiments.

Sulforhodamine B (SRB) assay

Exponential growing cells were harvested with trypsin-EDTA counted and seeded in 96-well plates at a density of 4000 cells/well. Optimal seeding density was determined to ensure exponential growth during a 5-day assay (120 h). The SRB assay was performed as previously described [4], with minor modifications. Cell were fixed in 10% cold trichloroacetic acid, incubated at 4°C for 1 h and then washed with deionized water. Cells were stained with 200 µL/well^{-1} of 0.1% SRB (ICN, Asse, Belgium) for 30 min and washed four times with 1% acetic acid. Plates were air dried at room temperature (RT) and stained proteins were solubilized with 200 µL of 10 mM unbuffered Tris base (tris(hydroxymethyl) aminomethane). Optical density was read at 530 nm with a Victor plate-reader (VICTOR X3 Multilabel plate reader, PerkinElmer, Waltham, MA, USA). Experiments were repeated four times.

γH2AX, 53BP1, TRF1 (TIFs), TRF2 and BLM immunofluorescence staining

Cells were seeded on glass slides until the time of fixation. Slides were fixed with 4% paraformaldehyde (Sigma Aldrich, St. Louis, USA), then permeabilized with 0.2% Triton X-100 and blocked in BSA 1% dissolved in PBS (w/v). Samples were then co-immunostained overnight (ON) at 4 °C, using a rabbit telomeric protein TRF1 antibody (Santa Cruz Biotechnology, Santa Cruz, CA, USA) in combination with a mouse monoclonal anti-phospho-histone H2AX antibody (Millipore, Temecula, CA, USA) or an anti-53BP1 antibody (Novus Biologicals, Littleton, CO, USA) for TIFs immunostaining, and mouse telomeric protein TRF2 antibody (Santa Cruz Biotechnology, Dallas, TX, USA) in combination with a rabbit polyclonal BLM antibody (Bethyl Laboratories, Montgomery, TX, USA). After washes in PBS/BSA 1% samples were incubated with the secondary antibody (anti-mouse Alexa 546 and anti-rabbit Alexa 488, Invitrogen, Life Technologies, Carlsbad, CA, USA) for 1 h at 37 °C. Finally, slides were washed in PBS/BSA 1%, counter-stained with DAPI and analyzed with an Axio-Imager Z2 fluorescent microscope equipped with automatic nucleus capture system (Metacyte, Metasystems, Milano, Italy). The frequency of DNA damage marker foci and TRF1/53BP1 (or γH2AX) colocalization dots per cell, or TRF2/BLM colocalization dots per cell were scored in 100 nuclei in at least two independent experiments.

Collection of chromosome spreads

Chromosome spreads were obtained following incubation in 30 nM calyculin-A (Wako, Osaka, Japan) a protein phosphatase inhibitor that induces chromosome condensation in a cell cycle phase independent manner [5]. Spreads of prematurely condensed chromosomes (PCC) were prepared by a standard procedure consisting of treatment with a hypotonic solution (75 mM KCl) for 28 min at 37°C, followed by fixation in freshly prepared Carnoy solution (3:1 v/v methanol/acetic acid). Cells were then dropped onto slides, air dried, and utilized for cytogenetic analysis.

Quantitative fluorescence in situ hybridisation (Q-FISH) and pancentromeric and telomeric FISH

The Q-FISH technique was based on the use of peptide nucleic acid (PNA) telomere oligonucleotides, that generate stronger and more specific hybridization signals than the same DNA oligonucleotides. The resolution of Q-FISH was in the region of about 200 bp [6]. The Q-FISH allowed: (1) precise measurement of individual telomeres at every single chromosome arm (2) to detect even small differences in telomere length. Centromere calibrated Q-FISH staining was performed as previously described [7]. Briefly, 48 h after the seeding, slides were rinsed with PBS at pH 7.5, and fixed in 4% formaldehyde for 2 min. After two rinses in PBS, the slides were incubated in acidified pepsin solution for 10 min, rinsed, and dehydrated through graded alcohols. Slides and probes (Cy3 linked telomeric and chromosome 2 centromeric PNA probe; DAKO Cytomation, Denmark) were co-denatured at 80 °C for 3 min and hybridized for 2 h at room temperature in a humidified chamber. After hybridization, slides were washed twice for 15 min in 70% formamide, 10 mM Tris at pH 7.2, and 0.1% BSA, followed by three 5-min washes in 0.1 M Tris at pH 7.5, 0.15 M NaCl, and 0.08% Tween 20. Slides were then dehydrated with an ethanol series, and finally air dried. Slides were counterstained with 4,6-diamidino-2-phenylindole (Sigma Aldrich, St. Louis, MO) in Vectashield (Vector Laboratories, Burlingame, CA, USA). Images were captured at 63X magnification with an Axio Imager Z2 equipped with an automatic metaphase capture system (Metafer, Metasystems) and the telomere size was analyzed with ISIS software (MetaSystems). The software calculates telomere lengths as the ratio between the fluorescence of each telomere signal and the fluorescence of the centromere of chromosome 2, used as the internal reference in each metaphase analyzed. Data were expressed as a percentage (telomere/centromere x 100 - T/C%) [8,9]. For each experiment, at least 30

metaphases were analyzed in two independent experiments. Telomeric/pancentromeric FISH experiments were performed following the aforementioned procedure described for Q-FISH staining with one notable difference; in addition to the Cy3-linked telomeric peptidic nucleic acid (PNA) probe, an Alexa 488-linked pancentromeric PNA probe (Panagene, Korea) was used to label all the centromeres of the cells. A total of 200 metaphases were analyzed for each sample in two independent experiments.

Multicolor FISH (M-FISH)

Fixed cells were dropped onto glass slides and hybridized with the 24XCyte Human Multicolour FISH Probe Kit (MetaSystems, Altlussheim, Germany), following the manufacturer's instructions. Briefly, the slides were denatured in 0.07N NaOH and then rinsed in a graded ethanol series. Meanwhile, the probe mix was denatured using a MJ mini personal thermal cycler (Bio-Rad laboratories, Hercules, CA, USA) with the following program: 5 min at 75 ◦C, 30 s at 10 ◦C, and 30 min at 37 ◦C. The probe was added to the slides and a coverslip was added and sealed using rubber cement. The Samples were then hybridized in a humidified chamber at 37 ◦C for 48 h, washed in saline-sodium citrate (SSC) buffer for 5 min at 75 ◦C and counterstained with DAPI. Finally, metaphases were visualized and captured using an Axio-Imager M1 microscope (Zeiss, Jena, Germany). The karyotyping and cytogenetic analysis of each single chromosome was performed using the ISIS software (MetaSystems).

ChIP assay and telomere dot-blot ChIP

ChIP analysis was performed as previously described [10]. Briefly $4x10^6$ cells were used for each experimental point. Formaldehyde, at a final concentration of 1%, was added directly to the medium for 15 min at room temperature on a shaking platform. Glycine, to a final concentration of 0.150 M, was added to the medium to stop the cross-link. Cells were then washed twice in cold PBS containing protease inhibitors, collected and lysed at the density of 20 x 106/ml for 10 min at 4°C in 1% SDS, 50 mM Tris-HCl pH 8.0 and 10 mM EDTA containing protease inhibitors. Lysate were sonicated (Bandelin SONOREX RK 100H) to obtain chromatin fragments < 1 kb and centrifuges for 15 min a room temperature. Chromatin was diluted 1:10 in a buffer containing 1.1% Triton X-100, 2 mM EDTA, 150 mM NaCl, 20 mM Tris-HCl pH 8.0, protease inhibitors and salmon sperm DNA-Protein A-50% agarose slurry (Santa Cruz

Biotechnology, Inc, Dallas, Texas, USA). Chromatin fragments were incubated O.N. at 4 °C on a rotating platform with different antibodies: anti-TRF2 (Cell Signaling Technology, Danvers, MA, USA), anti-γH2AX (Millipore), anti-POT1 (Abcam, Cambridge, UK), anti-H3 (Abcam), preimmune serum (Jackson ImmunoResearch Laboratories Inc., Baltimore Pike, PA, USA). Salmon sperm DNA-protein A agarose beads were then added and the incubation continued for 1 h at 4°C. Immunoprecipitated pellets were washed one time with different buffers: Low salt buffer (0.1% SDS, 1% Triton X-100, 2 mM EDTA, 20 mM Tris-HCl (pH 8.0) and 150 mM NaCl); high salt buffer (0.1% SDS, 1% Triton X-100, 2 mM EDTA, 20 mM Tris-HCl (pH 8.0) and 500 mM NaCl); LiCl Buffer (0.25 M LiCl, 1% Nonidet P-40, 1% sodium deoxycholate, 1 mM EDTA and 10 mM Tris-HCl, pH 8.0); and two washes whit TE (10 mM Tris-HCl (pH 8.0) and 1 mM EDTA). Chromatin was eluted from the beads twice by incubation with 250 ml of 1% SDS/0.1 M NaHCO3 for 15 min at room temperature with rotation. After adding 20 ml of 5 M NaCl, cross-links were reversed by incubation o.n. at 65°C. Samples were supplemented with 20 ml of 1 M Tris-HCl (pH 6.5), 10 ml of 0.5 M EDTA, 20 mg of RNase A and 40 g of proteinase K and were incubated for 1 h at 45°C. DNA was then recovered by phenol-chloroform extraction and ethanol precipitation, slot-blotted into a Hybond N+ membrane (Amersham Pharmacia Biotech, Milano, Italy) and hybridized with a telomeric probe (kindly provided by Maria Blasco, Spanish National Cancer Research Centre-CNIO) obtained from a plasmid containing 1.6 kb of TTAGGG repeats labeled with α-32P. The signal was quantified using the IMAGEJ software. For total DNA samples, aliquots corresponding to a 1:250 dilution of the amount of lysate used in the immunoprecipitations were processed along with the rest of the samples during the crosslink reversal step. The amount of telomeric DNA immunoprecipitated in each ChIP was calculated based on the signal relative to the corresponding total telomeric DNA input signal, instead for cH2AX data were normalized on the telomeric H3 signal. The ChIP values were presented as the percentage of the total input telomeric DNA, corrected for differences in the number of telomere repeats [11]. Experiments were performed at least in triplicate.

Evaluation of telomerase activity (RTQ-TRAP assay)

Telomerase activity was measured on 1 µg of protein by the SYBR green real-time quantitative telomerase repeat amplification protocol (RTQ-TRAP) assay, which was conducted as described elsewhere [12] with minor

modifications. The reaction was performed with protein extracts and anchored return primer mixed with SYBR Green PCR Master Mix (Biorad, Hercules, CA, USA). The reaction was performed using the Agilent AriaMx Real-Time PCR system (Agilent Technologies, Palo Alto, CA, USA). The threshold cycle values (Ct) were determined from semi-log amplification plots (log increase in fluorescence as a function of cycle number) and compared with standard curves generated from serial dilutions of telomerase-positive (tel+) U251MG cell extracts. Each sample was analyzed in triplicate in at least three independent experiments. Telomerase activity was expressed relative to the telomerase-positive (tel+) sample.

Irradiation conditions and combined treatments

X-ray irradiations on U251MG and neuroshperes cells were conducted at RT using a Gilardoni apparatus (Gilardoni S.p.A., Mandello del Lario, Lecco, Italy) (250 kV, 6 mA) with a dose rate of 0.53 Gy/min. Cells were seeded as monocellular suspension treated with NDIs or RHPS4 (concentrations depend on cell line and experiment) and then exposed to 10 Gy X-rays after 120 h. Mice irradiation was performed using a Gilardoni CHF 320 G X-ray generator (Gilardoni S.p.A., Mandello del Lario, Lecco, Italy) operated at 250 kVp, 15 mA (dose rate: 0.89 Gy/min), with filters of 2.0 mm Al and 0.5 mm Cu (HVL=1.6 mm Cu). GSCs were exposed to single dose of acute cesium-137 (137Cs) γ-irradiation with a dose rate of 0.8 Gy/min. RHPS4 and γ-ray combined treatments were performed by treating cells for 96h with RHPS4 (concentrations depend on cell line and experiment), then irradiating with 10 Gy dose, and the cell viability was assessed 72h and 168h after irradiation. Combined treatments were performed following different procedures accordingly with the different biological models used. Protocols for combined G4 ligands and IR treatments used in the present work are resumed in **Table 1**.

Target (biological model)	Drug administration	IR exposure
U251MG AG01522	NDIs were added in the culture medium at IC_{50} concentration for 5 days	At day 5 cells were irradiated with doses comprised between 0.5 and 6 Gy of X-rays (250 kV, 6 mA) with a dose rate of 0.53 Gy/min
U251MG-Adh U251MG-SC-Sph	RHPS4 0.2, 0.5 or 1 μM was added in the culture medium and maintained for 5 days	At day 5 cells were exposed to 10 Gy of X-rays (250 kV, 6 mA) with a dose rate of 0.53 Gy/min
Xenograft GBM tumors in mice	Intravenous injection in caudal vein of 10mg/kg/die RHPS4 for 5 days or 10 days	At day 5 or 10 tumors were exposed to 10 Gy of X-rays (mice were schermed using appropriate lead plates)
Patient derived GSCs	RHPS4 was added in the culture medium and maintained for 4 or 8 days	At day 4 cells were exposed to graded dose 10 Gy of γ-rays (cesium-137 γ-irradiation) with a dose rate of 0.8 Gy/min

Table 1: Experimental protocols for the combined G4 ligands treatment and IR in the different biological models used in this work.

Colony-forming assay

To evaluate clonogenic survival, untreated and NDI-treated U251MG cells were irradiated with 0.5–6 Gy of X-ray and then plated at appropriate concentrations in T25 culture flasks in triplicate. After 15 days, cells were fixed/stained with an aqueous solution containing 0.25% (w/v) crystal violet, 70% (v/v) methanol and 3% (v/v) formaldehyde, and they were counted. Only colonies comprised of > 50 cells were included in the quantification. For each treatment, the SF was assessed according to the following formula: SF = number of colonies formed/number of cells seeded. Plating efficiency was represented by the SF in untreated conditions. Results were reported as the mean of three independent experiments.

Long-term proliferation assessment

Cells treated with NDIs for 120 h (5 days) and then exposed to IR, were grown for 21 days with three intermediate passages after 7, 14 and 21 days of culture. At each time point, cells were harvested and counted using a Scepter handheld automated cell counter (Millipore). cPDL after 7, 14 and 21 as calculated as follows: cPDL = log2(Nf/N0), where Nf is the final cell number and N0 is the initial number of seeded cells.

Assessment of cell viability in GSCs

To assess cell viability after RHPS4 exposure, GSCs were mechanically dissociated and plated at a density of $2x10^4$ cells/ml in 96-well microtiter plates. After 16 hours, RHPS4 was added to the cells. ATP levels were measured at different time points as a surrogate of cell viability using CellTiter-Glo™ (Promega Inc., Madison, WI) following the

manufacturer's instructions. The mean of the raw luminescence values from triplicate wells treated with vehicle alone (mean Luminescence control), was used as reference to interpolate percent viability from wells treated with drugs (Viability with drugs), using the following formula: Viability with drugs = (Luminescence with drugs/mean Luminescence control)*100.

Real Time Quantitative PCR

FOR NDIs and RHPS4 off-target analysis:

U251MG cells either untreated or exposed to IC_{50} of NDIs or RHPS4 were subjected to RNA extraction by the RNeasy® Mini kit (Qiagen, Hilden, Germany) according to the manufacturer's instructions. Total RNA (0.5 µg) was randomly primed and reverse-transcribed using the GeneAmp RNA PCR Core kit (Applied Biosystems, Foster City, CA, USA), according to the manufacturer's instructions. The expression levels of individual genes were assessed as previously described [13]. Briefly, cDNA amplification was performed on the 7900HT Fast Real-Time PCR system (Applied Biosystems) using the following TaqMan® Assays (Applied Biosystems): Hs99999018_m1 (*Bcl2*), Hs00153408_m1 (*Myc*) and Hs00972656_m1 (*hTert*). Data analysis was carried out by SDS 2.2.2 software (Applied Biosystems). Data have been reported as relative quantity (RQ) vs. untreated cells (calibrator) upon normalization with respect to Ribonuclase P (RNaseP control reagent, Applied Biosystems), according to the $2^{-\Delta\Delta Ct}$ method [14]. Experiments were performed in duplicate.

For U251-Sph and GSCs gene expression and off-target analysis:

Total RNA was extracted using TRIzol® (Life Technologies) according to the manufacturer's instructions. RNA was reverse transcribed using an oligo-dT primer to prime the reverse transcription and the SuperScript™ II Reverse Transcriptase system (Invitrogen, California, USA). The RT reaction was carried out under the following conditions: at 65 °C for 5 min and quick chill on ice, then at 50 °C for 50 min, followed by 70 °C for 15 minutes. Gene expression levels were analyzed by RT-qPCR using SYBR Green PCR Master Mix (Biorad, California, USA). The reaction was performed using the Agilent AriaMx real-time PCR system (Agilent Technologies, California, USA). The analytic primers for RT-qPCR are following:

Sox2 Fw: 5'GGCAGCTACAGCATGATGCAGGAGC3'
Sox2 Rev: 5'CTGGTCATGGAGTTGTACTGCAGG3'
Cd44 Fw: 5'CCACGTGGAGAAAAATGGTC3'

Cd44 Rev: 5'CATTGGGCAGGTCTGTGAC3'
Gfap Fw: 5'GTGGGCAGGTGGGAGCTTGATCT3'
Gfap Rev: 5'CTGGGGCGGCCTGGTATGACA3'
Nestin Fw: 5'AGGATGTGGAGGTAGTGAGA3'
Nestin Rev: 5'TGGAGATCTCAGTGGCTCTT3'
Rad51 Fw: 5'GCATAAATGCCAACGATGTG3'
Rad51 Rev: 5'GGCGTTTGGAGTGGTAGAAA3'
Chk1 Fw: 5' CGGTGGAGTCATGGCAGTGCCC3'
Chk1 Rev: 5' TCTGGACAGTCTACGGCACGCTTCA3'
Data were reported as relative quantity (RQ) with respect to a calibrator sample (i.e. Actin or GADPH) according to the $2^{-\Delta\Delta Ct}$ method [14]. Experiments were performed in duplicate.

Immunoblotting

Total protein extracts were prepared according to standard methods. Protein extracts (20-30 µg) were fractionated by SDS/PAGE and transferred onto Hybond nitrocellulose membranes (RPN 303D; GE Healthcare, Milan, Italy). Filters were blocked for 40 min at RT with either 3% BSA/PBS (w/v) and 0.1% Tween-20 (v/v) or with 3% nonfat dry milk/PBS (w/v) and 0.1% Tween-20 (v/v) and then incubated O.N. at 4 °C with the following primary antibodies: ATR, BCL2, CDK2, Cyclin A, Cyclin E, PCNA, RAD51 (Santa Cruz Biotechnology, Dallas, TX, USA), CHK1, DNA-PK, Ku80, phosphoThr1989-ATR, phosphoSer345-CHK1 (Cell Signaling Technology, Danvers, MA, USA), PINX1 (Abcam, Cambridge, UK), KIT (mouse monoclonal, #3308; Cell Signaling Technology), MYC (mouse monoclonal, ab32; Abcam), 53BP1 (rabbit polyclonal, Ab21083, Abcam), BLM (rabbit polyclonal, Ab2179, Abcam), WRN (rabbit polyclonal; A300-239A; Bethyl Laboratories Inc., Montgomery, TX, USA), p27kip1 (rabbit polyclonal, ab7961; Abcam),/CDKN1A (rabbit polyclonal, ab7960; Abcam), CD44 (BD Bioscience, Franklin Lakes, NJ, USA), SOX2 (Abcam), GFAP (DAKO, Santa Clara, CA, USA), NESTIN (Novus Biologicals, Littleton, CO, USA). Vinculin (Sigma-Aldrich) and b-Actin (Abcam) were used on each blot to ensure equal protein loading. Filters were then incubated 1 h at RT with the appropriate secondary peroxidase-linked antibody (GE Healthcare, Chalfont St. Gile, UK). Proteins were visualized by the supersignal West Pico Chemiluminescent detection system (Thermo-Fisher Scientific, Rockford, IL, USA). Experiments were repeated at least three times.

Flow cytometric analysis

S-phase progression in different models, was evaluated by two different approaches: pulse and chase and pulse and fix methods. The first is aimed to understanding the progression of cells in S-phase at the time of treatment and their possible delay over time, and it was used to study NDIs and RHPS4 treatment in U251MG cells and also in line #1 of GSCs. For this purpose, after treatments cells were pulsed 30 min with 10 μM BrdU, then washed and grown in fresh medium and harvested at 2, 4, 6, 8 and 24 h. The second method is aimed to understanding if NDIs have an effect in terms of reduction or block in cell proliferation at longer times from drugs wash-out. To do this, after treatment, NDIs and RHPS4 were washed-out and cells were incubated in fresh medium for 48 h. In the last 30 min, BrdU was added to the medium and then cells were fixed and analyzed. For both the protocols, each sample was fixed, permeabilized, and the histones were dissociated with 2 M HCl as previously described [15]. BrdU-positive cells were detected with an anti-BrdU primary antibody diluted 1:100 (DAKO Cytomatation) and with an anti-mouse-Alexa488 conjugated diluted 1:100 (Invitrogen). Both antibodies were incubated for 1 h RT in the dark. All samples were counterstained with propidium iodide (PI) for DNA/BrdU biparametric analysis. The percentage of cells in mitosis was assessed using a cytometric biparametric analysis of phospho-histone H3 (S10) (Cell Signaling Technology) vs. DNA content. Briefly, cells were detached, washed with PBS, and fixed for 15 min at RT with PFA 4% dissolved in PBS (w/v). Subsequently, cells were permeabilized with 90% methanol and left at ?20 °C for at least 30 min. After rehydratation with 0.5% BSA/PBS (w/v) and 0.1% Triton, cells were incubated with an Alexa 488-conjugated anti-p-H3 (S10) antibody for 1 h at RT. Finally, cells were counterstained with a solution of propidium iodide/RNaseA as well as for the cell cycle analysis. The p-H3 positive cells were gated and the relative percentage was calculated by CYTEXPERT software (Beckman Coulter, Inc., San Diego, CA, USA).

CRISPR/Cas9 genome editing

hBLM knockout cells were generated using CRISPR/Cas9 gene targeting of U251MG cells via NHEJ and HR mediated repair. sgRNA was cloned into pCDNA5-H1-sgRNA (Addegene, Cambridge, MA, USA) and co-transfected with the plasmid pSpCas9(BB)-2A-Puro (PX459) (Addgene) encoding the Cas9-nuclease from *S. pyogenes*. Cells efficiently edited were selected with puromycin. Targeting of hBLM in U251MG cells was carried out with the following sgRNA: GGGGACTGTTTACTGACTAC

(Exon 7). To introduce stop codons in U251MG cells by HR-mediated repair, a donor cassette was used with the following sequence: GTCGGATCCTTTAAACCTTAATTAAGCTGTTGTAG. Clones derived from single cell lines were genotyped to determine successful targeting. hBLM knockout in single clones was then confirmed by quantification of protein levels by Western blotting.

Statistical analysis

Statistical analyses were performed using GraphPad Prism version 5.0 for Windows (GraphPad Software, San Diego, CA). The statistical tests vary according to the technique used. Linear correlation value for neurospheres growth effect of RHPS4 treatment was also obtained using GraphPad Prism. We used the student's t-test for the analysis of telomerase activity, for the analysis of telomeric damage, for the comparisons among multiple group in cell growth and viability assay, for the analysis of the density of telomeric marks in ChIP and for the analysis of foci and TIFs. Two-tailed Student's t-tests were applied to compare tumor growth between treated and control groups in mice. Significance was accepted for value $p<0.05$.

REFERENCES

1. Pallini, R. *et al.* Cancer stem cell analysis and clinical outcome in patients with glioblastoma multiforme. *Clin. Cancer Res.* **14,** 8205–8212 (2008).
2. D'Alessandris, Q. G. *et al.* The clinical value of patient-derived glioblastoma tumorspheres in predicting treatment response. *Neuro. Oncol.* **19,** 1097–1108 (2017).
3. Bai, L. *et al.* Targeted degradation of BET proteins in triple-negative breast cancer. *Cancer Res.* **77,** 2476–2487 (2017).
4. Vichai, V. & Kirtikara, K. Sulforhodamine B colorimetric assay for cytotoxicity screening. *Nat. Protoc.* **1,** 1112–1116 (2006).
5. Durante, M., Furusawa, Y. & Gotoh, E. A simple method for simultaneous interphase-metaphase chromosome analysis in biodosimetry. *Int. J. Radiat. Biol.* **74,** 457–462 (1998).
6. Slijepcevic, P. Telomere length measurement by Q-FISH. *Methods Cell Sci.* **23,** 17–22 (2001).
7. Berardinelli, F. *et al.* Telomere alterations and genomic instability in long-term cultures of normal human fibroblasts irradiated with X rays and protons. *Radiat. Prot. Dosimetry* **143,** 274–278 (2011).
8. Perner, S. *et al.* Quantifying telomere lengths of human individual chromosome arms by centromere-calibrated fluorescence in situ hybridization and digital imaging. *Am J Pathol* **163,** 1751–1756 (2003).
9. Nieri, D. *et al.* Cyogenetics effects in AG01522 human primary fibroblasts exposed to low doses of radiations with different quality. *Int. J. Radiat. Biol.* **89,** 698–707 (2013).
10. Benetti, R., García-Cao, M. & Blasco, M. A. Telomere length regulates the epigenetic status of mammalian telomeres and subtelomeres. *Nat. Genet.* **39,** 243–250 (2007).
11. Benetti, R. *et al.* Suv4-20h deficiency results in telomere elongation and derepression of telomere recombination. *J. Cell Biol.* **178,** 925–936 (2007).
12. Berardinelli, F. *et al.* Transient activation of the ALT pathway in human primary fibroblasts exposed to high-LET radiation. *Radiat. Res.* **174,** 539–49 (2010).
13. Nadai, M. *et al.* Assessment of gene promoter G-quadruplex binding and modulation by a naphthalene diimide derivative in tumor cells. *Int. J. Oncol.* **46,** 369–380 (2015).
14. Livak, K. J. & Schmittgen, T. D. Analysis of Relative Gene Expression Data Using Real-Time Quantitative PCR and the $2^{-\Delta\Delta CT}$ Method. *Methods* **25,** 402–408 (2001).
15. Darzynkiewicz, Z. & Juan, G. Analysis of DNA content and BrdU incorporation. *Curr. Protoc. Cytom.* 7.7.1-7.7.9 (1997). doi:10.1002/0471142956.cy0707s02

APPENDIX B – Supplementary Figures

Figure S1:

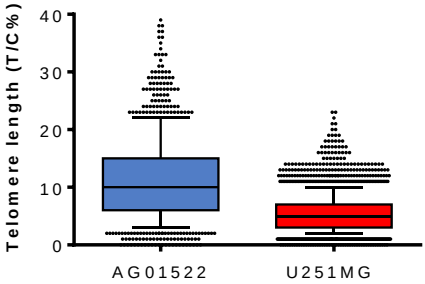

The mean basal values of telomere length were showed as T/C% in AG01522 and U251MG, respectively. Data represent mean values ± s.d. (n=2).

Figure S2:

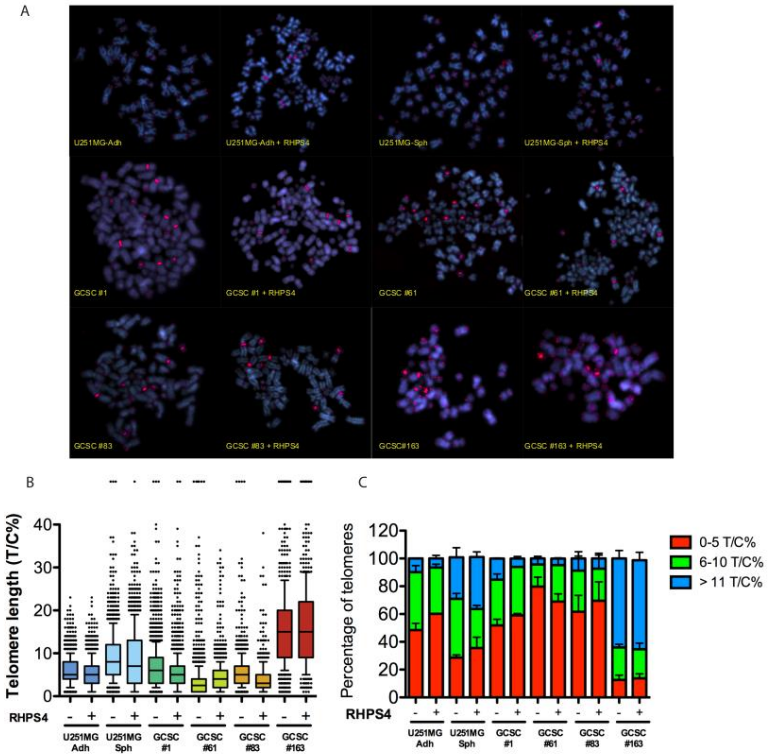

(A) Representative images of a U251MG-Adh, U251MG-Sph and GSCs metaphase spread stained with telomeric and centromere 2 PNA probes (RED) and counterstained with DAPI (BLUE), of untreated and RHPS4 treated cells. GSCs line 1, 61 and 83 shown near-to-tetraploid modal number. (B) The mean basal values of telomere length were showed as T/C% in U251MG-Adh, U251MG-Sph and GSCs with or without RHPS4 treatment. Data have been reported as mean values ± SD (n = 2). (C) Quantification of telomere length in U251MG-Adh, U251MG-Sph and GSCs in untreated and treated cells. RHPS4 was used at the IC_{50} value for each cell line. Telomeres length was grouped in 3 different classes (0–5, 6–10 and > 11 T/C%). Data have been reported as fraction of the total number of telomeres analyzed and represent mean values ± SD (n = 2). **P* < 0.05, ** *P* < 0.01, *** *P* <0.001 (Student's t-test).

Figure S3:

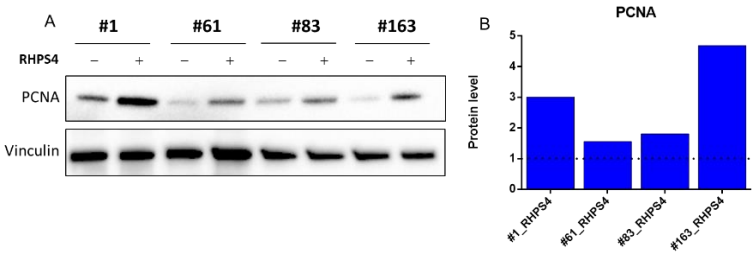

(A) Representative western immunoblotting showing PCNA protein amounts in GSCs RHPS4 treated cells. Vinculin was used to ensure for equal protein loading. Cropped image of the selected protein has been shown. (B) Quantification of PCNA protein amounts after RHPS4 treatment. Data have been reported as relative protein levels with respect to untreated cells (n = 1).